SCUOLA DI DOTTORATO

UNIVERSITÀ DEGLI STUDI DI MILANO-BICOCCA

School of Medicine and Surgery

PhD program in Molecular and Translational Medicine

XXXII Cycle

STUDY OF THE INTERACTIONS AMONG ARG/ABL2, TGF-β1 AND LOX IN CLEAR CELL RENAL CELL CARCINOMA PROGRESSION

Dr.ssa Sofia De Marco
Matr. No. 787177
Tutor: Prof. Roberto Perego
Co-tutor: Dr.ssa Cristina Bianchi
Supervisor: Dr.ssa Barbara Torsello
Coordinator: Prof. Andrea Biondi

ACADEMIC YEAR 2018/2019

To my family

Table of contents

Chapter 1

General Introduction

RENAL CELL CARCINOMA

Renal carcer is a relatively rare disease, which accounts for around 3% of all adult malignancies and is the twelfth most common cancer in the world. Renal cell carcinoma (RCC) accounts for 80-85% of kidney cancers (Petejova N, 2016), and it's the seventh most common cancer in men and the ninth in women. It is more common in men than in women (2:1 ratio), and generally occurs in the sixth to eighth decade of life (Nabi S, 2018).

Patients with RCC can present with local or systemic symptoms, although most renal masses are sometimes identified during a radiographic examination. The classical triad of RCC comprises flank-pain, gross haematuria and palpable abdominal mass, all of which have negative prognostic implications (Escudier B, 2019; Rühle A, 2019). Other common presenting features may not be specific, such a fatigue, weight loss or anemia. Smoking, obesity, hypertension, and chronic kidney disease are risk factors for RCC (Capitanio U, 2019; Rühle A, 2019). Surgery, including partial and radical nephrectomy, is the gold standard therapy for non-metastatic RCC; however, medical comorbidities may rule out surgical excision in a significant number of patients. Despite the advances in precocious diagnosis, cosiderably improved by imaging techniques, mortality has increased, and about 20-30% of all patients are diagnosed with metastatic disease. Most common metastasis in RCC occurs

in the lung, followed by bone in 20-35% of patients, lymph nodes, liver, adrenal gland and brain (Umer M, 2018). Furthermore, about 20% of patients undergoing nephrectomy will develop metastasis during follow-up (Cohen HT, 2005; Petejova N, 2016). For those with metastatic disease, the prognosis is extremely poor, around 12 months, despite advances in multimodal treatment. Therapeutic options for RCC are limited due to resistance to chemotherapy and radiotherapy and to the low efficiency and toxicity of immunotherapy (Belldegrun AS, 2008; McDermott DF, 2005; Petejova N, 2016). For this reason, kinase pathway inhibitors have been developed (Motzer RJ, 2007; Hudes GR, 2007). The most important and generally used is sunitinib, a drug approved as the preferred therapy to treat metastatic RCC; it inhibits cellular signal transduction by blocking various tyrosine kinase receptors (RTKs) including PDGFR and VEGFR, which play a role in both angiogenesis and tumor proliferation. Other drugs used in the treatment of RCC are everolimus, mTOR inhibitor; nivolumab, immunotherapeutic agent that inhibits the T cell PD-1 death receptor (Motzer RJ, 2015); and cabozantinib, a multikinase inhibitor that targets VEGFR, MET, RET and AXL, factors that favor angiogenesis, tumor progression and the survival of tumor cells. However, the efficacy of these drugs is limited over time, the average disease-free survival in treated patients does not exceed 7.4 months. Metastasectomy remains the only curative option in

most patients with metastatic RCC, but the decision of a metastasectomy depends on the site of the disease and on a case-by-case basis. There is some evidence of effectiveness of neoadjuvant targeted therapy before metastasectomy, that however induces an increase in surgical complications in tissue healing due to the effects of these new drugs (Alonso AH, 2015).

Key information on the prognosis of RCC is given by the TNM classification which combines anatomical factors and the Fuhrman grading system. This is based on morphological parameters (Ljungberg B, 2015; Boguslawska J, 2016) like the simultaneous assessment of nuclear size, nuclear irregularity and nucleolar prominence. Incorporation of these parameters resulted in tumors being classified into four grades. Nowadays, the Fuhrman grading system has been replaced by World Health Organization/International Society of Urological Pathology (WHO/ISUP) grading system (Dagher J, 2017). According to the WHO/ISUP grading system, grade 1-3 tumors are based on nucleolar prominence. Grade 4 is defined by the presence of the pronounced nuclear pleomorphism, tumor giant cells, rhabdoid and/or sarcomatoid differentiation. This grading system is applicable to clear cell RCC and papillary RCC, but should not be used for chromophobe RCC because of its innate nuclear atypia (Mikami S, 2016).

Recently, individualized protocols and clinical scoring

algorithms have been developed that aid in determining which RCC patients will progress and die after nephrectomy (Frank I, 2002; Leibovich BC, 2003; Parker AS, 2007). However, these predictive methods are based entirely on clinical and pathologic indices and do not include molecular characteristics of the tumor itself. In fact, to date no molecular markers have been recomended for routine clinical use (Ljungberg B, 2015; Boguslawska J, 2016). Identification of specific molecular markers within tumor tissue that correlate with RCC outcome would not only have the potential to improve ability to predict which patients require more aggressive surveillance and therapy but could also help to better stratify patients for clinical trials as well as inform on targets for novel adjuvant therapies (Atkins MB, 2004; Lam JS, 2005; Parker AS, 2007).

The RCC classification system originally proposed by Heidelberg in 1997, identifies the following histological subtypes in order of frequency: conventional or clear cells (RCC-cc) 70-80%, papillary (RCC-P) 10-15%, chromophobe (RCC-Ch) 4-5% and carcinoma of the collecting duct 1%. This classification organizing the different subtypes is based on cellular origins, different histological morphologies and distinct genetic characteristics (Störkel S, 1997; Kovacs G, 1997). Each histological subtype could be described by a typical gene expression profile (Higgins JP, 2003) and the characterization of the gene expression profile may not only

provide a new sub-classification of these tumors, but could also help to identify new tumor markers and new potential therapeutic targets (Takahashi M, 2001; Rogers CG, 2005). The incorporation of these new markers into future staging systems could revolutionize the current diagnosis and prognosis approach and also lead to the development of targeted therapies for each different RCC subtype.

Clear Cell Renal Cell Carcinoma: histology and genetic characteristics

Clear cell RCC (ccRCC) is the most frequent subtype and primarily responsible for mortalities among renal epithelial tumors (Hsieh JJ, 2017). It originates from an alteration of the cells of the proximal tubule. At the microscopic level, it is composed of large and uniform cells with an abundant and visibly clear cytoplasm, rich in lipids and glycogen and a compact-alveolar or acinar growth pattern interspersed with intricate, arborizing vasculature (Figure 1). In some cases it is possible to observe a mixture of clear cells and cells with a more eosinophilic cytoplasm. A small portion of clear cell tumors are cystic (Kovacs G, 1997; Störkel S, 1997; Cheville JC, 2003).

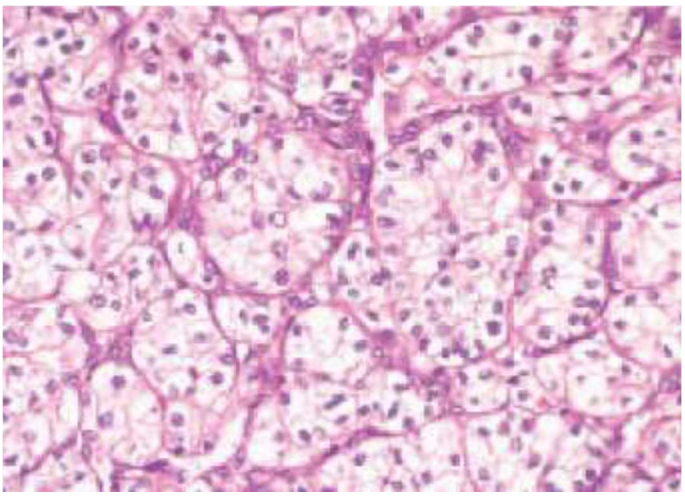

Figure 1: Histological section of a clear cell renal cell carcinoma. Hematoxylin eosine staining. The clear cytoplasm is the result of the removal of lipids during histological staining procedures.

At a genetic level ccRCC is characterized by complex chromosomal alterations. The most important loss in this tumor type involves 2p, 4q, 6q, 13q, 14q and Xq chromosome, but the most common genetic aberration involves 3p chromosome. This alteration is seen in approximately 95% of cases of ccRCC (Nabi S, 2018).

The hereditary form of ccRCC is almost always linked to the Von Hippel-Lindau syndrome (VHL) caused by alterations affecting and inactivating the VHL gene, located on the short arm of chromosome 3 (3p25). This gene has the typical characteristics of the tumor suppressor gene. The functional inactivation of the gene occurs following mutation of the two gene alleles in two distinct and successive moments: individuals with the Von Hippel-Lindau disease inherit a

defect on one of the alleles of the gene and RCC arise from the inactivation or silencing of the remaining VHL allele (Nabi S, 2018). A close causal relationship has been demonstrated in the tumor suppressor gene VHL and the occurrence of sporadic ccRCC. A somatic inactivation of VHL has been found in almost 90% of sporadic cases (Dondeti VR, 2012) and hypermethylation of the VHL promoter region was observed in over 19% of cases (Yoshida M, 2002). The identification of this gene as responsible for most of ccRCC has been really useful not only for the diagnosis and prognosis of this tumor, but in particular for the study of its pathogenesis. The protein product of the VHL gene is a component of the E3 ubiquitin-ligase complex that helps in the proteasomic degradation of several intracellular proteins. (Barry RE, 2004; Kaelin WG, 2002) Due to its role as component of this complex, loss of VHL leads to stabilization and activation of the hypoxia-inducible factor HIF-1α and HIF-2α proteins that control angiogenesis, glycolysis, and apoptosis (Kaelin WG, 2007; Bleu M, 2019).

The regulation of HIFs-α by the E3-ubiquitin ligase complex is critical for normal cellular functioning. HIF is a heterodimeric transcription factor that mediates cellular responses to hypoxia. It consists of an oxygen-sensitive α subunit and a constitutively expressed β subunit. Under normal oxygen conditions, the α subunit of HIF is hydroxylated on proline residues so as to be able to bind to

the VHL protein of the E3 ubiquitin-ligase complex, from which it will be ubiquitinated for the consequent degradation (Kim WY, 2004; Pugh CW, 2003). Under hypoxic conditions or in the absence of pVHL, the lack of hydroxylation of HIF-α prevents the recognition by the VHL protein. In this way the HIF-α subunit, which is not degraded, translocates into the nucleus and with constitutively expressed β (HIF-β) subunit will form the HIF heterodimer which will activate the transcription of different genes, including VEGF, PDGF-β, TGF-α, erythropoietin, glycolytic and metabolic enzymes and extracellular matrix proteins (Maxwell PH, 2001; Barry RE, 2004) (Figure 2).

The HIF-dependent upregulation of these gene products plays a key role in the development of a highly vascular tumor, such as ccRCC, characterized by metabolic alterations. Transcriptomic, proteomic and metabolomic profiling of ccRCC tissues support the involvement of the metabolism in ccRCC progression revealing metabolic reprogramming characterized by upregulation of aerobic glycolysis (Warburg effect), the pentose phosphate pathway, fatty acid synthesis, glutamine and glutathione metabolism, and by downregulation of the tricarboxylic acid (TCA) cycle, fatty acid β oxidation (FAO), and oxidative phosphorylation. Several patients revealed specific metabolic alterations, in particular the downregulation of the TCA cycle and the upregulation of the pentose phosphate pathway and fatty

acid synthesis, which may correlate with tumor aggressiveness and poor survival in ccRCC patients (Gatto F, 2014). The association between metabolic shifts and ccRCC clinical stages reveal an increase of fatty acid biosynthesis and a decrease of oxidative phosphorylation in early-stage tumors, whereas these metabolic patterns reversed and glutathione metabolism increased in late-stage tumors (Hakimi AA, 2016). A decrease of specific FAO enzyme expression has also been found to correlate with an increase of tumor stage, size and grade and a conseguent decrease in survival (Zhao Z, 2016). Furthermore, it has been revealed that grade-dependent metabolic reprogramming occurs in ccRCC tissues with the Warburg effect, relatively more prominent in higher grade tumors at the expense of the TCA cycle and oxidative metabolism. Grade-dependent alterations were also shown in fatty acid, glutamine and glutathione metabolisms (Wettersten HI, 2015).

In our study we showed that ccRCC primary cell cultures maintained the cytological (Bianchi C, 2010), genomic, transcriptomic (Cifola I, 2011; Di Stefano V, 2016) and metabolic features of the original tissues in early passages as described in chapter 2 (Bianchi C, 2017), confirming the upregulation of aerobic glycolysis/lactate fermentation. Our primary cultures also showed a grade-dependent modulation of lipid and glycogen storage and of aerobic glycolysis/lactate fermentation, according to the grade-dependent metabolic

reprogramming described in ccRCC tissues (Wettersten HI, 2015).

The transcription activity of HIF-1 induces the expression of metabolic enzymes as well as enzymes involved in rearrangement of extracellular matrix like lysyl oxidase (Lox).

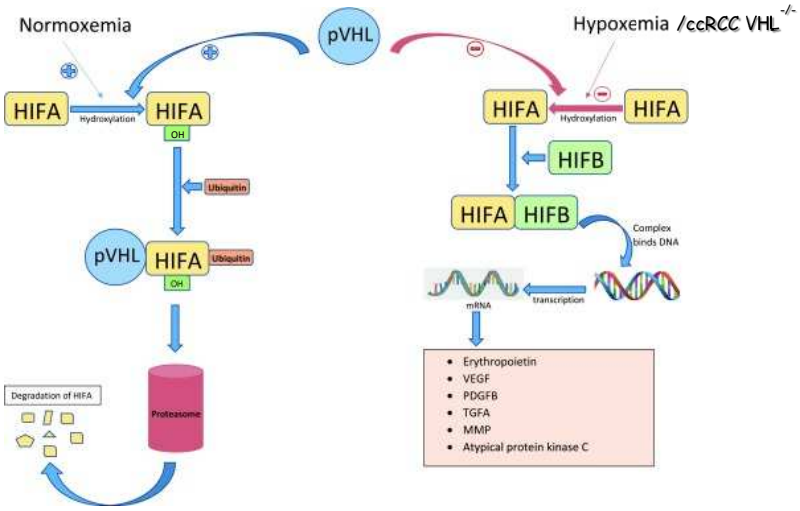

Figure 2: VHL pathway. The VHL pathway in the normal renal cell, in which the VHL protein conveys the ubiquitinated HIF-α protein to the proteasome for degradation and in the hypoxemia or in the ccRCC cells ($VHL^{-/-}$), where the failure of the VHL protein causes the constitutive activation of HIF-α (Nabi S, 2018).

LYSYL OXIDASE (LOX)

Lox: structure and functions

Lysyl oxidase (Lox) is a copper-dependent monoamine oxidase of the extracellular matrix (ECM) (Li T, 2018; Barker HE, 2012), which is an important player in tumor progression and metastasis formation. The LOX family (LOXs) contains

four other additional members, Lox protein 1-4, which show similarity (95%) in the carboxyl (C)-terminus, and whose amino (N)-terminal regions are variable and unique to each family member, so may contribute to their individual biological functions and cellular localization (Cai L, 2017; Li T 2018).

Lox is most commonly expressed in the heart and it is also highly expressed in the lung, kidney, testis, uterus, and placenta, but only marginally in the brain and liver.

After intracellular post-translational modifications, LOX gene product results in an inactive 50-kDa proenzyme of 417 amino acids (Pro-Lox) (Trackman PC, 1992). Once secreted in the extracellular matrix (ECM), Pro-Lox is proteolyzed by the bone morphogenetic protein 1 (BMP1) and cleaved into the 32-kDa active enzyme (Lox) and the 18-kDa propeptide domain (Lox-PP) (Perryman L, 2014). The extracellular active Lox enzyme catalyzes the covalent crosslinking of collagen and elastin in the ECM, increasing tensile strength and structural stability and integrity of tissues, while producing hydrogen peroxide as a by-product (Cox TR, 2016; Barker HE, 2012; Di Stefano V, 2016). The Lox action can increase stiffness of cancer ECM and promote cellular adhesion and migration, favoring progression, invasion, and metastasis as shown using tumor cell lines of breast, brain and colon (Payne SL, 2005; Laczko R, 2007; Baker AM, 2013; Cox TR, 2015).

Although Lox was first described as an ECM protein, it also

performs intracellular functions and both active 32-kDa enzyme and 18-kDa propeptide can re-enter the cells by still unknown mechanisms. Active 32-kDa Lox, through reactive oxygen species by-products and integrin stimulation, promotes cell proliferation and invasion of colorectal carcinoma cell lines by activating phosphatidylinositol 3-kinase PI3K and the downstream FAK and Src signaling cascades (Baker AM, 2013; Baker AM, 2011). Otherwise, the 18-kDa Lox-PP acts as a tumor suppressor, having Ras recision activity (Palamakumbura AH, 2004) and apoptotic activity by blocking the mitogen-activated protein kinases/extracellular signal-related kinases (MAPK/ERK) pathways (Bais MV, 2012) or impairing DNA repair pathways in the nucleus (Bais MV, 2015). It has also been reported that in colon carcinoma cell lines Lox and HIF-1α potentiate each other to sustain tumor progression (Pez F, 2011). All these findings suggest that Lox may have complex and different roles in tumorigenesis, depending on the transformation status of the cells (Friesenhengst A, 2014), the molecular network, the cellular location and the cell type in which it is active (Barker HE, 2012; Erler JT, 2006).

Lox in ccRCC

In our laboratory it has been demonstrated that human ccRCC primary cell cultures and in particular the HIF-1α positive cells, Lox is overexpressed, confirming that in

ccRCC LOX gene is a direct target of HIF-1α. Matched primary cell cultures of normal cortex and ccRCC expressing HIF-1α were analyzed by Western blot. The 50-kDa Pro-Lox proenzyme had an exclusive localization in the nuclear-free fraction. The 32-kDa Lox active enzyme had a nuclear localization and a weak localization in the nuclear-free fraction. Both proteins, Pro-Lox and Lox, were prevalent in ccRCC cells compared to normal cells. The 18-kDa Lox-PP propeptide had an exclusive nuclear localization with a significantly stronger signal in normal cortex cells compared to ccRCC cells. The immunofluorescence analysis also supported these results. Lox enzyme was more abundant in the ccRCC primary cell culture media than in those of cortex. We confirmed the key role of Lox in promoting tumor cell migration and adhesion. ccRCC primary cultures, after Lox silencing by siRNA, migrated less than control samples and we also observed a decrease in cell adhesion on both plastic and fibronectin-coated plates. Furthermore, Lox silencing reduced the invasion capability of cancer cells compared to control cells using an invasion assay with collagen-coated membrane, suggesting the role of Lox in the invasion process. Tumor progression has been correlated with Lox capacity to crosslink collagen and increase ECM stiffness. We quantified the mechanical effects of secreted Lox on collagen-coated gels using the atomic force microscopy technique and calculating the values of the Young modulus.

The active Lox constitutively produced by ccRCC increased the collagen matrix stiffness. As indicated by our data, it seems that Lox plays an important role in ccRCC progression (Di Stefano V, 2016).

It has been recently demonstrated that Lox expression shows no correlation with intratumoral fibrosis (ITF) or any other clinicopathologic parameters (Joung JW, 2018).

Various miRNAs are deregulated in RCC and are thought to play a central role in tumor formation and progression by altered regulation of their targets. It has been demonstrated that miR-141-3p and miR-145-5p were downregulated in ccRCC, whereas Lox expression was enhanced in ccRCC compared to non-malignant tissue and it was higher in metastatic ccRCC than in non-metastatic ccRCC. A strong negatively directed correlation was observed between the expression of Lox and of both miR-141-3p and miR-145-5p. The two miRNAs miR-141-3p and miR-145-5p, as well as their target Lox, have prognostic and diagnostic potential and might be used as new biomarkers (Liep J, 2016).

Lox and premetastatic niche formation

During tumor progression, cells can acquire the capability to escape the primary tumor mass and colonize nutrient-rich new organs (Gupta GP, 2006; Hanahan D, 2000). The development of metastasis in distant organs is a multistep process that begins with the detachment of cancer cells from

the primary tumor, via their invasion of the extracellular matrix entry into the blood stream and the eventual colonisation and outgrowth at secondary sites (Allocca G, 2019). However, only a small proportion of the cells which escape from the primary tumor will successfully colonize a distant organ. The majority of circulating tumor cells (CTCs) are recognised and eliminated by the immune system, undergoing spontaneous apoptosis, return to the circulation and entry into a quiescent or dormant state. It is hypothesised that during bone metastasis formation disseminated tumor cells (DTCs), colonize specialized regions of bone microenvironment the “metastatic niche" (Allocca G, 2019).

The metastatic niche, site of the future metastasis, consists of cells derived from bone marrow (BMDCs). These BMDCs are thought to create an environment that is permissive for the subsequent invasion and growth of tumor cells (Condeelis J, 2006). This bone region is characterized by a complex milieu of cytokines, hormones and soluble factors produced by the different components of the surrounding niches, creating a rich soil for seeding of the tumor cells. This metastatic niche strongly influences the fate of DTCs which arrive in bone, driving them towards either dormancy or proliferation and development of overt bone metastasis (Kan C, 2016). It is a well-established concept that the microenvironment plays an important role in all the stages of bone metastasis, however the precise cellular composition of

the metastatic niche must still be defined (Allocca G, 2019). It is also known that a tumor can modulate not only the behavior of local cells and the resulting microenvironment at the primary site to facilitate its progression, but also at distant secondary sites prior to tumor cell arrival. Thus secreted factors (secretome) from cancer cells are capable of modulating the behavior of host cells resident in secondary organs in the absence of tumor cells. This leads to remodeling of the local environment to create permissive niches (premetastatic niches) for tumor cells to subsequently colonize and form overt secondary metastasis (Cox TR, 2016). The term secretome was first coined in 2000 in a study on bacterial secretory processes and was later re-defined as the global group of proteins secreted into the extracellular space by a cell, tissue, organ, or organism through known and unknown mechanisms involving constitutive and regulated secretory organelles. Secreted proteins, including non-protein cargos such as lipids, microRNAs (miRNA), and messenger RNAs (mRNA) can be released into the extracellular space through at least two mechanisms: the classical (endoplasmic reticulum and Golgi apparatus) and nonclassical secretory pathways (exosomes and ectosomes) (Liu Y, 2016).

The concept of the premetastatic niche comes from the idea of the “seed and soil” hypothesis that defines the seed as cells from the primary tumor that colonize the soil, or specific

organs, that have been prepared to support their growth (Liu Y, 2016)

Erler et al. (2006) showed that inhibition of Lox activity reduces invasion and formation of lung metastasis in an orthotopic model of breast cancer. It has been shown that in an orthotopic model of breast cancer with MDA-MB-231 cells (human breast cancer cell line) much more lung metastasis were formed compared to an orthotopic model with MDA-MB-231 cells transfected with a specific Lox-shRNA. Therefore they studied the role of Lox in the recruitment and invasion of BMDCs in premetastatic sites and in the formation of the premetastatic niche (Erler JT, 2009). The immonohistochemical analysis of pulmonary metastasis in MDA-MB-231 orthotopic model has identified the presence of a high concentration of the Lox protein and fibronectin, both produced by tumor cells. In the same area, which coincides with terminal bronchioles and distal alveoli, cells of myeloid origin (BMDCs $CD11b^+$/F4/80) and tumor cells were found. Lox crosslinked collagen IV in the basement membrane of the metastatic neoformation niche, and increased adhesion of $CD11b^+$ cells. Adherent $CD11b^+$ cells produced MMP-2, which degraded collagen IV, increasing $CD11b^+$ cell invasion into the lung tissue and releasing chemoattractive collagen IV peptides. The collagen IV peptides enhanced further recruitment of $CD11b^+$ cells, generating a positive feed-forward loop for increased accumulation of BMDCs,

increased extracellular matrix remodeling, and the creation of the premetastatic niche permissive to the formation of metastasis. Together, these data demonstrate a crucial role for Lox secreted mainly by tumor cells in the formation of the premetastatic niche and in the enhancement of metastatic tumor growth and suggest that Lox protein could be a potential therapeutic target for the treatment and prevention of metastasis (Erler JT, 2009).

It has been recently demonstrated that Lox also induces bone premetastatic niche in breast and colon cancer (Cox TR, 2015; Reynaud C, 2017). In particular, tumor hypoxia drives the expression and secretion into the circulation of Lox, which travels to the bone and acts to disrupt the delicate balance between osteoblasts (bone building cells) and osteoclasts (bone degrading cells) in favor of bone destruction, leading to the generation of focal premetastatic osteolytic lesions. Tumor-secreted Lox inhibited osteoblast differentiation and induced a robust production of IL6 in colorectal cancer cells. In turn, both Lox and IL6 were acting in concert to promote RANKL-dependent osteoclast differentiation, thereby creating an imbalance between bone resorption and bone formation with generation of premetastatic osteoclastic lesions (Reynaud C, 2017). These subsequently act to enhance metastatic colonization of circulating tumor cells. It has been demonstrated that the treatment with anti-Lox antibodies or bisphosphonates (osteoclastic activity

inhibitors) eliminated premetastatic niche formation and reduced metastatic colonization. However, further studies are required to confirm the role of Lox or its downstream inhibitors as preventive treatment for patients at a higher risk of bone metastasis (Cox TR, 2016).

Lox and transforming growth factor-β1 (TGF-β1)

It has been noted that in rat lung fibroblasts both HIF-1 activation and TGF-β stimulation induced the upregulation of Lox transcript, protein and secreted active form, but it has no effect on proenzyme processing (Boak AM, 1994; Roy R, 1996).

Moreover, TGF-β1 upregulates the production of Lox by tubular epithelial cells in a mouse model of glomerulonephritis (ICGN). In this model the upregulated Lox catalyzes the crosslinking formation on the collagens, which are produced by the activated myofibroblasts deriving from TGF-β induced differentiation of tubulointerestitial cells and located in the tubulointerstitial space. The crosslinked interstitial collagens are resistant to degradation by proteolytic enzymes and accumulate around the renal tubules. Thus, the authors propose a relationship between the TGF-β1-mediated upregulation of Lox production and the progression of chronic renal fibrosis (Goto Y, 2005).

More recently, it has been demonstrated that TGF-β pathways are also involved in Lox transcription in cardiac

fibroblasts (Voloshenyuk TG, 2011) and trabecular meshwork cells (Sethi A, 2011; Sethi A, 2013). In particular, the increase of Lox mRNA, protein expression and activity induced by TGF-β1 in adult rat cardiac fibroblasts was mediated by the activation of PI3K/protein kinase B (Akt), Smad3, and MAPKs pathways (Voloshenyuk TG, 2011). In addition, TGF-β1-mediated increase in the expression of BMP1, involved in extracellular Lox processing, may activate Lox as well as TGF-β1 and provide a positive feedback to generate more Lox involved in ECM reorganization and fibrosis (Cai L, 2017) (Figure 3).

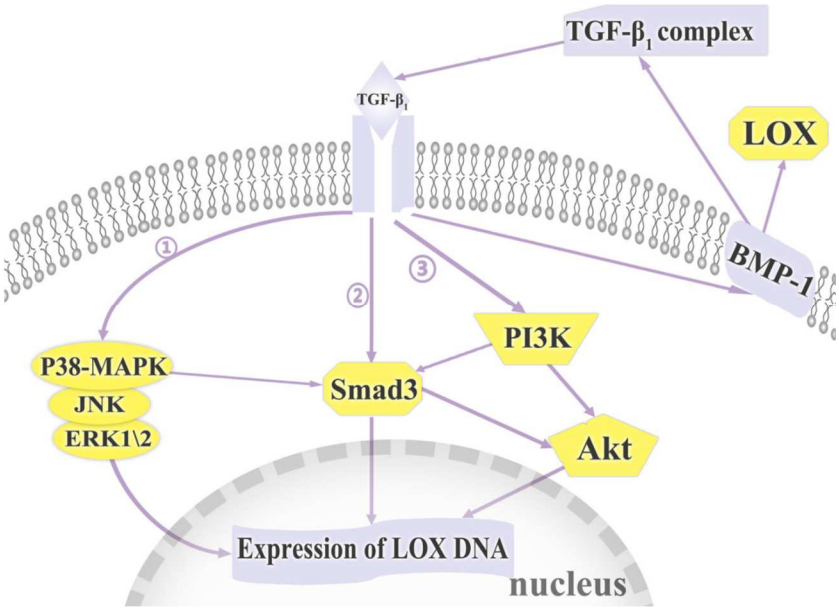

Figure 3: TGF-β1 pathways involved in Lox expression modulation in cardiac fiboblasts (Cai L, 2017).

TRASFORMING GROWTH FACTOR-β (TGF-β)

TGF-β: stucture and functions

The TGF-β superfamily is a large family of growth and differentiation factors that regulate a wide variety of cellular processes in many different cell types and biological contexts.

Different family members regulate cell proliferation, migration, apoptosis, extracellular matrix elaboration, adhesion, survival and differentiation, in both developing embryos and adult organisms (Inman GJ, 2002). TGF-β pathway is also involved in tissue repair and inflammation. Aberrant signaling by TGF-β has been implicated in a number of human diseases, including cancer, hereditary hemorrhagic telangiectasia, atherosclerosis, and fibrotic disease of the kidney, liver, and lung. In addition, low levels of TGF-β signaling have been implicated in compromised wound healing, and inappropriately high levels of TGF-β signaling are associated with excessive scarring (Inman GJ, 2002).

Five different TGF-β isoforms are known and in mammals only three of these isoforms, TGF-β1, TGF-β2, and TGF-β3, are expressed, each encoded by a specific gene and expressed either in a tissue-specific manner or regulated during development. TGF-β1 is expressed mainly in endothelial, hematopoietic and connective tissue cells; the TGF-β2 in neuronal and epithelial cells; while TGF-β3 is expressed in mesenchymal cells (Massagué J, 1990). The

three isoforms have highly conserved sequences with a homology of 70-80%.

TGF-β1, like the other two isoforms, is initially synthesized as a 75-kDa homodimer known as pro-TGF-β. Pro-TGF-β is then cleaved in the Golgi to form the 25-kDa mature TGF-β homodimer (Annes JP, 2003). These homodimers interact through a disulfide bond with latency-associated proteins to form in the endoplasmic reticulum the large latent complex, allowing for targeted export to the extracellular matrix (Rifkin DB, 2005; Horiguchi K, 2009). After export, the large latent complex interacts with fibronectin fibrils and heparin sulfate proteoglycans on the cell membrane. Eventually, the large latent complex localizes to fibrillin-rich microfibrils in the extracellular matrix, where it is stored until its activation (Isogai Z, 2003; Taipale J, 1994). Latent TGF-β1 is activated by several factors, including proteases (Taipale J, 1994; Ge G, 2006), thrombospondin 1 (Schultz-Cherry S, 1993), reactive oxygen species (Barcellos-Hoff MH, 1996), and integrins (Munger JS, 1999; Wipff PJ, 2008). These factors release mature TGF-β1 by freeing it from the microfibril-bound large latent complex.

Once activated, the TGF-β isoforms can regulate cellular processes, by binding to three types of highly affine surface receptors: the type I receptor (TβRI), the type II receptor (TβRII), the type III receptor (TβRIII).

The canonical TGF-β1 signaling pathway is initiated when

TGF-β1 ligand binds to TβRII which in turn recruits and through its kinase activity phosphorylates and activate TβRI. Through its active kinase activity TβRI phosphorylates Smad2 and Smad3, which form a complex with Smad4. The Smad complex is traslocated into the nucleus where, together with other transcription factors and co-factors, regulates the transcription of target genes involved in phisiological and phatological aspects, such as ECM maturation and deposition, cell proliferation, migration, invasion, apoptosis, adhesion, survival, differentiation, epithelial to mesenchymal transition (EMT) and senescence (Moustakas A, 2009). Canonical TGF-β1 signalling is negatively regulated by inhibitory Smads, including Smad6 and Smad7 (Principe DR, 2013). Through the interaction with TβRII TGF-β1 also signals through a number of non-canonical pathways, including PI3K/Akt, p38 MAPK, JNK MAPK, p42/p44 MAPK, c-Src, m-TOR, RhoA GTPases, Cdc42 and RAS (Principe DR, 2013; Zhang L, 2013). TGF-β receptors associating with TRAF4/6 are able to activate TAK1, leading to activation of the MKK4-JNK MAPK, MKK3/6-p38 MAPK, or IKK-NFκB signaling cascades. Phosphorylation of the adaptor protein ShcA by activated TβRI enables the ShcA-Grb2-SOS complex formation and Ras activation, thereby stimulating the ERK MAPK activity. Furthermore, there is evidence of a SMAD-independent rapid induction of AKT phosphorylation by TGF-β, which has

suggested a direct involvement of PI3K in TGF-β-receptor-initiated intracellular signaling. The PI3K subunit p85 was found to associate constitutively with TβRII. Upon TGF-β stimulation, TβRI interacts with p85 and drives downstream inhibition of the tuberous sclerosis complex (TSC) and activation of the mammalian target of rapamycin complex (mTORC) (Zhang L, 2013). PI3K catalyzes the conversion of phosphatidylinositol-4,5-bisphosphate (PIP_2) to phosphatidylinositol-3,4,5-triphosphate (PIP_3), that provides a docking site for pleckstrin homology domain containing AKT, which thereby becomes activated. Activated AKT mediates the phosphorylation of much effectors that mediate its antiapoptotic/pro-survival function and induces cell growth and protein translation (Zhang L, 2013). These non-Smad signaling pathways are highly context-dependent and contribute to the complex and versatile functions of TGF-β (Yan X, 2018).

TGF-β1 role in tumorigenesis

The involvement of TGF-β1 signaling pathway in human malignancies is complex and furthermore TGF-β1 shows contradictory roles in tumorigenesis. At early stages of cancer TGF-β acts as a tumor suppressor through activation of cell cycle inhibitors and induction of apoptosis, while in advanced stages, TGF-β contributes to the creation of a microenvironment that stimulates cancer growth and

metastasis (Kajdaniuk D, 2013; Boguslawska J, 2016). The pro-oncogenic activities of TGF-β are exerted both on the microenvironment and tumor cells, making the tumor more aggressive and prone for dissemination (Massagué J, 2006; Padua D, 2009, Boström AK, 2013). In fact, TGF-β has been shown to facilitate immunosuppressive functions, enhance the invasiveness and angiogenesis, and initiate the process of EMT, in which epithelial cells lose many of their epithelial characteristics and take on properties that are typical of mesenchymal cells, which require complex changes in cell architecture and behavior. It is believed that central events in tumor progression, such as local spread, intravasation and extravasation at the site of metastasis, are achieved through the EMT mechanism. Today, the EMT process, although still debated, is associated with distinct transcriptional changes in conjunction with morphological changes into a fibroblastoid phenotype (Boström AK, 2012). EMT, the embryonic program that loosens cell-cell adherence complexes and endows cells with enhanced migratory and invasive properties, can be co-opted by cancer cells during metastatic progression. Cancer cells that have undergone EMT are more aggressive, displaying increased invasiveness, stem-like features, and resistance to apoptosis. EMT programs can also stimulate the production of proinflammatory factors by cancer cells (Suarez-Carmona M, 2017).

TGF-β promotes angiogenesis through direct effects on

endothelial cells, stimulating the expression, secretion and activation of matrix metalloproteinases that permit the migration of endothelial cells. TGF-β effects can also be indirect when inducing the expression of the proangiogenic factors, vascular endothelial growth factor (VEGF) and connective-tissue growth factor (CTGF) in fibroblastic and epithelial cells (Juàrez P, 2011). TGF-β expression is increased in microvasculature of breast cancer and lung carcinoma, and TGF-β levels correlate with angiogenesis, tumor progression, and prognosis of these patients (de Jong JS, 1998; Hasegawa Y, 2001). Inhibition of TGF-β signaling decreased angiogenesis in human breast and prostate cancer (Tuxhorn JA, 2002).

Tumor-derived TGF-β contributes to an immunosuppressive environment by suppressing T-lymphocytes and natural killer cells, which allow cancer cells to escape cytotoxic T lymphocyte clearance (Thomas DA, 2005). TGF-β regulates T-cell function by many mechanisms, including inhibition of IL-2 production and the subsequent T-cell activation, induction of peripheral T-cell apoptosis and inhibition of cytotoxic T lymphocytes (Juàrez P, 2011).

Several studies show that TGF-β1 signaling contributes to the aggressiveness of ccRCC (Ananth S, 1999; Miyajima A, 2003; Copland JA, 2003; Sitaram RT, 2016). In particular, in ccRCC, elevated expression of TGF-β1 is correlated to poor prognosis and the loss of VHL has been associated with

modulations of the TGF-β1 expression (Hegele A, 2002; Mitropoulos D, 2004; Ananth S, 1999; Sjölund J, 2011). Primary ccRCC cells treated with TGF-β1 acquires a mesenchymal phenotype with characteristics of EMT, thus corroborating the oncogenic influence of TGF-β on ccRCC (Boström AK, 2012; Tretbar S, 2019).

Interestingly, elevated levels of TGF-β1 in serum from ccRCC patients are correlated with unfavorable outcome of the disease (Sjölund J, 2011). The tumor microenvironment in ccRCC is rich in TGF-β1 (Sjölund J, 2011). These observations therefore suggest that ccRCC cells might have acquired the capacity to evade the cytostatic effects imposed by the presence of TGF-β1. It has been postulated that structural alterations of TGF-β pathway components, such as mutations of TβRII render tumor cells insensitive to TGF-β cytostatic effects (Parker AS, 2007). Low tumor expression of TβRII is associated with a less aggressive tumor phenotype at time of surgery. Moreover, those patients with lower levels of TβRII expression experience better cancer-specific survival than patients with higher levels of TβRII expression, suggesting that evaluation of TβRII expression as a potential prognostic biomarker should involve careful analysis of tumors stratified by early and late disease phases (Parker AS, 2007).

An extensive cross-talk between Notch and TGF-β signaling cascades is present in ccRCC and the functional properties

of these two pathways are associated with the aggressiveness of this disease (Sjölund J, 2011).

TGF-β1 has a profound influence on the expression of adhesion related genes and it induced the expression of extracellular matrix related genes in Caki2 RCC cell line, suggesting an involvement of TGF-β1 in processes related to the development of metastasis (Boguslawska J, 2016).

Hegele et al. demonstrated that TGF-β1 in plasma is not a suitable tumor marker for diagnosis of localized RCC, but they described significantly higher plasma levels of TGF-β1 in metastatized RCC in comparison to localized disease (Hegele A, 2002).

However, it has been shown an enhanced expression of TGF-β1 mRNA and protein in tumor samples and increased serum TGF-β1 levels in RCC patients. The correlation of TGF-β1 expression intensity with tumor stage and nuclear grade indicates its possible role in the development of metastatic potential as well as in modulating the host's immune response (Mitropoulos D, 2004).

The canonical Smad-dependent TGF-β pathway significantly activated in ccRCC than in the kidney cortex, and was significantly associated with nuclear grade, tumor stage, and size. Through 2D invasion assay it has been demonstrated that the invasive capacity of ccRCC cells increased after TGF-β stimulation, suggesting that the Smad-dependent pathway of TGF-β significantly promotes tumor progression,

metastasis, and survival in ccRCC (Sitaram RT, 2016).

In ccRCC both TGF-β signaling and hypoxia have been associated with tumor aggressiveness and it has been shown that hypoxia augments TGF-β signaling through up regulation of the ligand TGF-β1 (Boström AK, 2013). Recently, we demonstrated a new specific regulation of TGF-β1 expression and secretion in tubular cells by the non-receptor tyrosine kinase Arg/Abl2. In paticular, we evidenced in tubular primary cell cultures grown in high glucose concentration that Arg tyrosine kinase downregulation by silencing with siRNA, or treatment with the tyrosine kinase inhibitor Imatinib, induced upregulation of TGF-β1 (Torsello B, 2016). We also demonstrated that Arg-modulated TGF-β1 production was not mediated by an Arg-dependent inhibition of proteasome activity. By contrast, in our cellular model Arg downregulation might induce upregulation of TGF-β1 through the activation of RhoA-ROCK signaling. In fact, in high-glucose-treated tubular cells, we documented that Arg downregulation increased TGF-β1 production, decreased p190RhoGAPA specific phosphorylation and increased the RhoA-GTP level. Therefore, Arg kinase downregulation could activate the RhoA-ROCK signaling by reducing RhoA inhibition induced by p190RhoGAPA. The activation of this signaling that modulates cytoskeleton activity would explain the increase of TGF-β1 secretion (Gu L, 2013).

In another work, reported in chapter 3 (Torsello B, 2019) we

show that the absence of Arg induced the increase of TGF-β1 production even in murine fibroblasts. In particular, the TGF-β1-mediated effects, carried out in wt MEF, were restored by 1BLCTL but not completely by 1ALCTL isoforms.

Role for TGF-β1 in bone homeostasis and in bone metastasis

Bone is a mineralized tissue continuously remodelled by the balanced processes of resorption and consecutive bone formation. Formation, deposition, and mineralization of bone tissue are due to osteoblasts deriving from mesenchymal precursor cells (Janssens K, 2005). The mesenchymal precursor cells differentiate into osteoblast lineage through various signaling pathways, such as BMP1, Wnt, Hedgehog (Hn) and Notch. Runt-related transcription factor 2 (Runx2) is a primary transcription factor, implicated in those pathways as a focal point for signaling integration and is involved in proliferation, migration, commitment and differentiation to the osteogenic lineage (Yi SJ, 2019). Osteoblasts are cuboidal cells harboring abundant rough endoplasmic reticulum and prominent Golgi apparatus, as well as secretory vesicles. They accumulate in larger groups of cells to simultaneously produce the extracellular matrix of bone, which is initially unmineralized. This matrix primarily consists of type I collagen, but also contains several additional proteins. During the process of matrix mineralization, which is still not

fully understood at the molecular level, a subset of osteoblasts is embedded into the mineralized bone matrix to terminally differentiate into osteocytes, another bone cell type (Brylka LJ, 2019). Bone resorption is performed by the osteoclasts and involves demineralization of the inorganic matrix by acidification followed by enzymatic degradation of the organic matrix by cathepsin K and matrix metalloproteinases (Teitelbaum SL, 2003). Osteoclasts are large, multinucleated cells (MNCs) of hematopoietic origin that differentiate from monocyte/macrophage precursor cells within the bone environment. Osteoclast differentiation requires the presence of marrow stromal cells and osteoblasts; and notably two osteoblast-derived factors are essential and sufficient to promote osteoclastogenesis: the macrophage-colony stimulating factor (M-CSF) and receptor activator of nuclear factor-kB ligand (RANKL).

Upon binding of M-CSF and RANKL to their respective receptors on the osteoclast precursor cell surface, the signaling cascades leading to activation of two prominent transcription factor complexes, the NF-kB and AP-1, are induced with consequent activation of osteoclast differentiation, fusion, function, motility and survival (Janssens K, 2005).

TGF-β1 affecting both bone resorption and formation has a pivotal role in the bone remodeling process. TGF-β1 is secreted in a latent form by both osteoblasts and osteoclasts

and is stored in the ECM. Active resorbing osteoclasts are capable of activating TGF-β1, which in turn attenuates bone resorption by impairing osteoclastogenesis and promotes bone formation through chemotactic attraction, proliferation and differentiation of osteoblast precursors (Janssens K, 2005).

Therefore, it is possible that TGF-β plays a role in premetastatic bone niche formation and in metastatic tumor growth within the bone (Mundy GR, 2002; Roodman GD, 1993; Weber K, 2007). In fact, the bone microenvironment consists of a rich store of multiple growth factors linked to ECM, including TGF-β. Metastatic cells that reach the bone activate osteoclasts that degrade the bone matrix and release the stored TGF-β. TGF-β can stimulate the cancer cells to release several osteolytic cytokines, including parathyroid hormone-related protein (PTHrP) and IL-11, which in turn stimulates the production of RANKL and inhibits osteoprotegerin (OPG) expression by osteoblasts promoting the differentiation of osteoclast precursors and bone resorption. TGF-β is released by osteoclast bone resorption and increases tumor cell production of osteolytic and osteoblastic factors. TGF-β also has direct effects on bone to stimulate osteoclast activity and inhibit osteoblastic differentiation. Collectively, these effects of TGF-β perpetuate the feed-forward cycle to increase tumor growth in bone (Ikushima H, 2010; Juárez P, 2011). Notably, an indirect

involvement of TGF-β1 in promoting bone metastasis in ccRCC patients was also described. In fact, Kominsky et al. showed that TGF-β1 may stimulate the cells derived from a bone metastasis of RCC to produce soluble factors that initiate growth-promoting paracrine interactions between tumor cells and bone microenvironment, suggesting the potential value of TGF-β1 signaling inhibitors in treating RCC patients (Kominsky SL, 2007).

The metastatic osteolytic lesions are particularly resistant to standard therapies and, despite diagnostic and therapeutic advances, treatment remains palliative. Maita et al. demonstrated that Sunitinib, a multitarget tyrosine kinase inhibitor, may be a potential anticancer for the treatment of patients with metastatic RCC, because it may also inhibit osteoclast maturation and thus bone metastasis growth as described in mouse model (Maita S, 2011).

ABELSON RELATED GENE (ARG/ABL2)

Arg: structure

Abelson related gene (Arg/Abl2) together with Abelson (Abl1) are members of the Abelson subfamily of non-receptor tyrosine kinases. They are involved in regulation of several biological processes that include cell motility and morphogenesis, development and maintenance of the nervous and immune systems, response to oxidative and genotoxic stress and apoptosis. ARG gene maps on

chromosome 1, in band 1q24-25 which spanning a fragile constitutional site (Kruh GD, 1986). ARG is expressed as a 12-kilobase (kb) transcript; the nucleotide sequence contains an open reading frame of 3546 base pairs coding for a protein composed of 1182 amino acids (Kruh GD, 1990) of 145 kDa with tyrosine kinase activity (Perego R, 1991). Like Abl1, Arg is an ubiquitous protein expressed with the highest levels in nervous tissue (Perego R, 1991). Following alternative splicing, the ARG gene gives rise to several transcripts. Initially two isoforms have been described that differed only in the 5' end and that, by analogy with Abl, have been defined 1A and 1B (Kruh GD, 1990). However, studies conducted in our laboratory have shown the existence in several human cell lines of four different isoforms of the 5'-terminal end of ARG transcript, produced for alternative splicing events on the second exon (II) of 1A and 1B isoforms and named 1AS, 1BS, 1AL, 1BL, and two further isoforms at the 3'-terminal end, produced by alternative deletion of a region (ΔCT) of the last exon and named CTS and CTL (Perego RA, 2005). The combination of these splicing events is responsible for the synthesis of eight different Arg isoforms (1ALCTL, 1ALCTS, 1BLCTL, 1BLCTS, 1ASCTL, 1ASCTS, 1BSCTL and 1BSCTS) demonstrated in the ccRCC Caki 1 cell line (Bianchi C, 2008). The eight different Arg isoforms are expressed in normal and neoplastic cells, such as cells derived from leukemia, colon and renal cancer, with different

ratios (Perego RA, 2005).

The Abl1 and Arg proteins present a high degree of structural and sequence homology. 1B isoforms of Arg, like 1B Abl1 isoform, present a residue of glycine in position 2 at the N-terminal, whose myristoylation facilitates its anchoring to the cell membrane, allowing its participation in signal transduction. Instead, 1A isoforms show a shorter N-terminal region consisting of the "cap" region only. This "cap" domain, common to the 1A and 1B isoforms, is composed of 80 amino acid residues and is involved in the regulation of kinase activity by interacting directly with the kinase domain (Hantschel O, 2004). In the N-terminal region of Abl1 and Arg, the Src-homology functional domains, SH2 and SH3, which in the two proteins present a 90% homology, are found sequentially and both are involved in the regulation of kinase activity. The tyrosine kinase domain of Arg and Abl has a 94% sequence homology, with difference of only 16 amino acids (Kruh GD, 1990). In the C-terminal region of Arg, that shows a sequence identity of 29% with Abl1, significant regions of the Abl structure are maintained, such as some proline-rich sequences (PXXP), which represent potential binding sites for SH3 domains of other proteins (Pendergast AM, 2002). Furthermore, in C-terminal region of Arg the three NLS (nuclear localization sequence) sequences of Abl1 are lacking. Similarly, the nuclear export sequence (NES) rich in leucine and also present in Arg is functional only in Abl1,

allowing the Abl1 protein a continuous movement from the nucleus to the cytoplasm and vice versa, in response to signals such as cellular adhesion to ECM proteins (Pendergast AM, 2002). A unique feature of Abl1 is also the presence of a DNA-binding site in the C-terminal region lacking in Arg. In fact, studies conducted by cell fractionation and immunofluorescence analysis have indicated that the two initially identified isoforms of Arg have cytoplasmic localization in the different cell types analyzed (Wang JY, 1993; Wang Y, 2001).

However, our more recent data confirmed that all the protein isoforms of Arg are present only at the cytoplasmic level, except for the 1BSCTS isoform, which localizes at the nuclear level (Bianchi C, 2013).

Abl1 and Arg are distinguished from other non-receptor tyrosine kinases by the presence at the C-terminal of actin-binding domains (Hernandez SE, 2004a). In Arg are present two F-actin binding domains, one common to Abl1 and one present only in Arg, downstream of the proline-rich region. This second F-actin binding domain, which has a 28% identity with the I/LWEQ motif of the talin protein (Wang Y, 2001), is partially lost in Arg CTS isoforms (Perego RA, 2005). In the C-terminal region of Arg, a microtubule-binding domain is also present (Miller AL, 2004). The described structural differences and the different cellular compartmentalization between Abl1 and Arg can account for

both overlapping and distinct functional role into the cells and in modulation of intracellular signaling.

Activation and functional role of Arg kinase

Abelson kinases, when stimulated and then activated, phosphorylate different substrates in tyrosine, controlling different cellular activities. The tyrosine kinase activity of Arg must be strictly regulated since a constitutive activity of the protein would activate some mitogenic and antiapoptotic signaling pathways that could lead to a transformation in the neoplastic sense of the cell (Ren R, 2005; Okuda K, 2005).

Arg can be activated by mechanisms of autophosphorylation or phosphorylated by other kinases, such as Src kinase family. Self-inhibiting mechanisms regulate its activity, ensuring an inactive conformation when the cell does not require its functionality.

Arg are also regulated by a variety of external stimuli that include: growth factors (Furstoss O, 2002; Plattner R, 1999; Plattner R, 2003; Plattner R, 2004), adhesion proteins of ECM, proteins of cell-cell adhesion (Hernandez SE, 2004b; Huang Y, 2008; Lewis JM, 1996; Renshaw MW, 2000; Zandy NL, 2007), DNA damage (Kharbanda S, 1995), oxidative stress (Cao C, 2001; Sun X, 2000) and invasion of microorganisms (Backert S, 2008; Burton EA, 2003; Newsome TP, 2006; Poppe M, 2007; Tammer I, 2007). These stimuli activated specific receptors that, in turn, activated

Abelson kinases as downstream signaling molecules (Hernandez SE, 2004a). Many receptor proteins (growth factor receptors and integrin receptors) and soluble factors that increase the kinase activity of Abl and Arg have been identified (Bradley WD, 2009).

With regard to growth factors, PDGFβ (platelet derived growth factor β) induces activation of Abl kinases by binding to its receptor which, in the intracellular portion, is autophosphorylated in tyrosine residues. Phosphotyrosines become binding sites for Src and the phospholipase C-γ1 that are activated. Abelson kinases are activated by the combined action of phospholipase C-γ1, which hydrolyzes the PIP_2 inhibitor in DAG and IP_3, and by the non-receptor kinase Src which, on the other hand, phosphorylates them in their activation loop (Hernandez SE, 2004b).

Furthermore, Plattner et al. (2004) showed that Abelson kinases can bind directly to the phosphotyrosine residues of PDGFRβ via the SH2 domain. Therefore PDGFRβ and Abelson kinases undergo mutual phosphorylation. In particular the phosphorylation of Abelson kinases by PDGFRβ has important functional consequences; in fact the receptor phosphorylates Abl in the tyrosine residues Y245 and Y412 and Arg in the tyrosine residue Y272 required for their activation. It has also been observed that PDGFRβ phosphorylates Arg also in two further tyrosine residues of the SH3 domain (Y419 and Y481) whose function is not

known (Srinivasan D, 2009). In contrast, the phosphorylation of PDGFRβ by Abelson kinases increases its catalytic activity in vitro, while its ability to induce chemotaxis in vivo decreases. These results indicate that Abl kinases are not only activated by PDGFRβ with consequent promotion of cell proliferation and migration, but also downregulate the chemotaxis mediated by PDGFRβ (Srinivasan D, 2009).

Other growth factor receptors, such as the ErbB family receptors (EGFR or Her2) or the insulin-like growth factor receptor (IGFR), have been implicated in the activation of the Abl family kinases. In fact, it has been shown that the dysregulation of these receptors leads to a constitutive activation of these kinases in invasive breast carcinoma cell lines (Srinivasan D, 2008). The hepatocyte growth factor receptor (HGF/Met) that is dysregulated in several solid tumors, is involved in the activation of kinases of the Abl family and their inhibition suppresses the mechanisms of cell diffusion, tubulogenesis, migration and invasion induced from HGF (Li R, 2015).

Integrin receptors can also activate Abelson kinases. Integrins are α-β etherodimeric receptors of adhesion to ECM proteins such as fibronectin, laminin and collagen, which physically couple to the actin cytoskeleton and regulate kinase signaling pathways that control cytoskeletal remodeling and the formation and disassembly of complexes of adhesion. The Arg kinase domain interacts with the β1

integrin at the level of a segment rich in lysine proximal to the membrane present in the cytoplasmic tail. This interaction is thought to promote allosteric activation of Arg kinase, altering conformation of the active site directly, or indirectly by interaction with the SH2 domain or with the hydrophobic pocket present in the C terminal lobe of the kinase domain which, in the inactive conformation, binds the myristolic residue of the "cap" region. Arg phosphorylates the integrin tail exclusively in the residue of tyrosine 783, this creates a second binding interface for interaction with the SH2 domain which further amplifies Arg kinase activity. The interaction of Arg with β1 integrin positions Arg at the cellular periphery where kinase activity is required to phosphorylate proteins such as p190RhoGAP or cortactin that control the structure and dynamics of the cytoskeleton, essential for cell motility and morphogeny (Simpson MA, 2015).

Other receptor molecules implicated in the activation of Abl family kinases have been identified, but the biochemical mechanisms that mediate these interactions still need to be clarified (Bradley WD, 2009).

Arg is involved in cytoskeleton rearrangement, in modulation of cell morphology, in the regulation of cell proliferation, survival, cell adhesion, cell migration and cell invasion.

In fact, in our recent work, reported in chapter 3 (Torsello B, 2019) we analyzed the role of 1ALCTL and 1BLCTL Arg isoforms transfected in $Arg^{-/-}$ murine embryonal fibroblasts

(MEF) cell line and we showed that 1BLCTL isoform has a major role in proliferation, migration/invasion of fibroblasts and in inducing a milieu able to modulate tumor cell morphology, while 1ALCTL isoform has a role in MEF adhesion maintaining active focal adhesions. On the whole, the presence of Arg in MEF supports the proliferation, activation, adhesion, ECM contraction and stiffness, while the absence of Arg affected these myofibroblast features (Torsello B, 2019).

Moreover, Arg is involved in axonogenesis, growth cone motility, nuerite extension and membrane protusion. It is also involved in tumor progression, not only in leukemias but also in several solid tumors, such as melanoma, breast, ovarian, gastric, colorectal, pancreatic, lung, renal and bladder tumors (Greuber EK, 2013; Wang J, 2015).

Role of Arg in cancer cell invasion and metastasis

The progression of solid tumors, a complex multistep process, require invasion of primary tumor cells into the surrounding tissue, followed by intravasation, migration, extravasation, and formation of metastasis at distant sites (Fidler IJ, 2003). The various steps of this process require dynamic remodeling of the actin cytoskeleton. Arg kinase has been shown to engage the actin polymerization machinery to promote formation in different cell types of membrane protrusions, morphological changes, altered cell adhesion,

migration and invasion (Bradley WD, 2009). Arg tyrosine kinase is required for cell motility and invasion induced by IGF-1, EGF, serum and chemokines in breast, hepatocellular carcinoma, and melanoma cells (Srinivasan D, 2006; Yoon CH, 2010; Ganguly SS, 2012). Moreover, Arg localizes to invadopodia, which are actin-rich protrusive membrane structures that promote remodeling of the extracellular matrix during tumor invasion (Smith-Pearson PS, 2010; Mader CC, 2011). Within invadopodia, Arg acts downstream of EGF receptor and Src kinases to phosphorylate cortactin which is required for actin polymerization (Mader CC, 2011). In addition to cortactin, other actin regulatory proteins required for invadopodia formation, maturation and matrix degradation are targeted by Arg. Consistent with its ability to positively regulate invadopodia formation and function, knockdown of Arg decreased cancer cell invasion and intravasation following implantation of breast cancer MDA-MB-231 cells in the mammary fat pad. Otherwise, Arg knockdown in these tumor cells improves their proliferation (Gil-Henn H, 2013). Even invasion and metastasis of melanoma cells require ABL kinases. In fact active ABL kinases induced cathepsin-dependent lysosomal degradation of the NM23-H1 metastasis suppressor in melanoma as well as in breast cancer cells (Fiore LS, 2014).

AIM OF THE THESIS

Renal cell carcinoma (RCC) represents approximately 3% of all human adult malignancies (Petejova N, 2016). Since it is resistant to chemotherapy and radiotherapy, partial and radical nephrectomy may be curative, but only in the early disease stages (Petejova N, 2016). It is estimated that approximately 25-30% of RCC patients have metastasis at the time of diagnosis (Song W, 2018; Motzer RJ, 2017), and another 30% of patients ultimately develop metastasis after initial nephrectomy (Petejova N, 2016). Most common metastasis in RCC occurs in the lung and bone (Umer M, 2018). The prognosis of metastatic RCC is generally considered poor (Raimondi A, 2019), emphasizing the importance of early detection and prompt treatment of primary lesion in its early stage. The progress of targeted therapy in recent decades has brought some improvement in the treatment of RCC and has contributed to improving the quality of life of patients, but better understanding the molecular mechanisms underlying the tumor progression might represent a useful tool for developing new therapeutic approaches to control the metastatic disease. This aspect is particularly important in ccRCC, the most common and aggressive RCC subtype (Voung L, 2019). Notably, about 30% of metastasis in ccRCC patients affect bones and the involvement of TGF-β1 in promoting ccRCC aggressiveness,

invasion and bone metastasis has been described (Kominsky SL, 2007; Sitaram RT, 2016). Moreover, even the extracellular matrix modifying enzyme Lysyl oxidase (Lox) has been described in breast and colon cancer to have a key role in the formation of premetastatic bone lesions through the activation of osteoclasts and the inhibition of osteoblasts (Cox TR, 2015; Reynaud C, 2017). In addition, Lox promotes cell migration and invasion through cytoskeleton rearrangement (Payne SL, 2005). Our previous data evidenced, in an *in vitro* model of primary cell cultures established from ccRCC and normal cortex tissue samples, that Lox is overexpressed in ccRCC (Di Stefano V, 2016) and that TGF-β1 production is modulated in human renal tubular cells by Arg/Abl2 tyrosine kinase (Torsello B, 2016). Notably, even Arg is known to modulate invasion and metastasis of breast and prostate cancer through cytoskeleton rearrangement (Beaty BT, 2013; Gil-Henn H, 2013).

As described in chapter 3 (Torsello B, 2019), we have also evidenced a differential role of two Arg isoforms, 1ALCTL and 1BLCTL, in the modulation of fibroblast activation, an important aspect of tumor microenvironment involved in modulation of invasion and progression. Using a cell model of $Arg^{-/-}$ murine embryonal fibroblasts (MEF), we showed how the transfection of 1BLCTL Arg isoform modulates proliferation, migration/invasion of MEF and induces a milieu able to modulate ccRCC tumor cell morphology, while

1ALCTL isoform transfection modulates MEF adhesion maintaining active focal adhesions.

All these data suggested that TGF-β1, Lox and Arg might interact to modulate invasion and formation of bone premetastatic lesions in ccRCC.

Based on these premises, the specific aims of experiments described in chapter 4 were:

- to evaluate the existence of molecular interactions among TGF-β1, Lox and Arg in ccRCC, by dissecting the role of each molecule on the modulation of the expression of the other two, and investigating the molecular pathways involved in these putative modulations;
- to study the functional effects of these interactions on two aspects of ccRCC tumor progression:
    1. invasion, by using an *in vitro* 3D invasion assay in a collagen matrix,
    2. formation of premetastatic bone lesion, by analyzing the effect of ccRCC cell secretome on *in vitro* osteoclast and osteoblast behavior.

To develop this project, we used an *in vitro* model of ccRCC primary cell cultures and cell lines. Thus it has been important to complete the characterization of the primary cell cultures routinelly obtained in our labotatory from ccRCC and normal cortex tissue specimens. These primary cultures were already well characterized in their cellular composition

(Bianchi C, 2010), and maintained the genomic and transcriptomic profile of the original tissues in the early passages (Cifola I, 2011; Di Stefano V, 2016). More recently, as described in chapter 2 (Bianchi C, 2017), these ccRCC primary cultures have been metabolically characterized and they showed the upregulation of aerobic glycolysis/lactate fermentation that was modulated in a grade-dependent manner, such as lipid and glycogen storage. Notably, these metabolic alterations were typical of corresponding tissues (Wettersten HI, 2015). These extensive characterizations have been instrumental in using these ccRCC primary cell cultures as a reliable in vitro model to study some aspects of the molecular interactions among TGF-β1, Lox and Arg and of their involvement in ccRCC progression.

REFERENCES

Allocca G, Hughes R, Wang N, Brown HK, Ottewell PD, Brown NJ and Holen I. The bone metastasis niche in breast cancer-potential overlap with the haematopoietic stem cell niche *in vivo. J Bone Oncol.* (2019); 17:100244.

Alonso AH, García MC and Enguita CG. Is there a role for systemic targeted therapy after surgical treatment for metastases of renal cell carcinoma? *World J Nephrol.* (2015); 4:254-262.

Ananth S, Knebelmann B, Grüning W, Dhanabal M, Walz G, Stillman IE and Sukhatme VP, Transforming growth factor beta1 is a target for the von Hippel-Lindau tumor suppressor and a critical growth factor for clear cell renal carcinoma. *Cancer Res.* (1999); 59(9):2210-2216.

Annes JP, Munger JS and Rifkin DB. Making sense of latent TGFbeta activation. *J Cell Sci.* (2003); 116(Pt2):217-224.

Atkins MB, Avigan DE, Bukowski RM, Childs RW, Dutcher JP, Eisen TG, Figlin RA, Finke JH, Flanigan RC, George DJ, Goldberg SN, Gordon MS, llipoulos O, Kaelin WG Jr, Linehan WM, Lipton A, Motzer RJ, Novick AC, Stadler WM and The BT. Innovations and challenges in renal cancer: consensus statement from the first international conference. *Clin Cancer Res.* (2004); 10(18 Pt 2):6277S-6281S.

Backert S, Feller SM and Wessler S. Emerging roles of Abl family tyrosine kinases in microbial pathogenesis. *Trends Biochem*. (2008); 33(2):80-90.

Bais MV, Nugent MA, Stephens DN, Sume SS, Kirsch KH, Sonenshein GE and Trackman PC. Recombinant lysyl oxidase propeptide protein inhibits growth and promotes apoptosis of pre-existing murine breast cancer xenografts. *PLoS One.* (2012); 7(2):e31188.

Bais MV, Ozdener GB, Sonenshein GE and Trackman PC. Effects of tumor-suppressor lysyl oxidase propeptide on prostate cancer xenograft growth and its direct interactions with DNA repair pathways. *Oncogene.* (2015); 34(15):1928-1937.

Baker AM, Cox TR, Bird D, Lang G, Murray GI, Sun XF, Southall SM, Wilson JR and Erler JT. The role of lysyl oxidase in SRC-dependent proliferation and metastasis of colorectal cancer. *J Natl Cancer Inst.* (2011); 103(5):407-424.

Baker AM, Bird D, Lang G, Cox TR and Erler JT. Lysyl oxidase enzymatic function increases stiffness to drive colorectal cancer progression through FAK. *Oncogene.* (2013); 32(14):1863-1868.

Barcellos-Hoff MH and Dix TA. Redox-mediated activation of latent transforming growth factor-beta 1. *Mol Endocrinol.* (1996); 10(9):1077-1083.

Barker HE, Cox TR and Erler JT. The rationale for targeting the LOX family in cancer. *Nat Rev Cancer.* (2012); 12(8):540-552.

Barry RE and Krek W. The von Hippel-Lindau tumour suppressor: a multi-faceted inhibitor of tumourigenesis. *Trends Mol Med.* (2004); 10(9):466-472.

Beaty BT, Sharma VP, Bravo-Cordero JJ, Simpson MA, Eddy RJ, Koleske AJ and Condeelis J. B1 integrin regulates Arg to promote invadopodial maturation and matrix degradation. *Mol Biol Cell.* (2013); 24(11):1661-1675.

Belldegrun AS, Klatte T, Shuch B, LaRochelle JC, Miller DC, Said JW, Riggs SB, Zomorodian N, Kabbinavar FF, Dekernion JB and Pantuck AJ. Cancer-specific survival

outcomes among patients treated during the cytokine era of kidney cancer (1989-2005): a benchmark for emerging targeted cancer therapies. *Cancer.* (2008); 113(9):2457-2463.

Bianchi C, Torsello B, Angeloni V, Bombelli S, Soldi M, Invernizzi L, Brambilla P and Perego RA. Eight full-length Abelson related gene (Arg) isoforms are constitutively expressed in Caki-1 cell line and cell distribution of two isoforms has been analyzed after transfection. *J Cell Biochem*. (2008); 105(5):1219-1227.

Bianchi C, Bombelli S, Raimondo F, Torsello B, Angeloni V, Ferrero S, Di Stefano V, Chinello C, Cifola I, Invernizzi L, Brambilla P, Magni F, Pitto M, Zanetti G, Mocarelli P and Perego RA. Primary cell cultures from human renal cortex and renal-cell carcinoma evidence a differential expression of two spliced isoforms of Annexin A3. *Am J Pathol.* (2010); 176(4):1660-1670.

Bianchi C, Torsello B, Di Stefano V, Zipeto MA, Facchetti R, Bombelli S and Perego RA. One isoform of Arg/Abl2 tyrosine kinase is nuclear and the other seven cytosolic isoforms differently modulate cell morphology, motility and the cytoskeleton. *Exp Cell Res*. (2013); 319(13):2091-2102.

Bianchi C, Meregalli C, Bombelli S, Di Stefano V, Salerno F, Torsello B, De Marco S, Bovo G, Cifola I, Mangano E, Battaglia C, Strada G, Lucarelli G, Weiss RH and Perego RA. The glucose and lipid metabolism reprogramming is grade-dependent in clear cell renal cell carcinoma primary cultures and is targetable to modulate cell viability and proliferation. *Oncotarget.* (2017); 8(69):113502-113515.

Bleu M, Gaulis S, Lopes R, Sprouffske K, Apfel V, Holwerda S, Pregnolato M, Yildiz U, Cordò V, Dost AFM, Knehr J, Carbone W, Lohmann F, Lin CY, Bradner JE, Kauffmann A, Tordella L, Roma G and Galli GG. PAX8 activates metabolic genes via enhacer elements in Renal Cell Carcinoma. *Nat*

Commun. (2019); 10(1):3739.

Boak AM, Roy R, Berk J, Taylor L, Polgar P, Goldestein RH and Kagan HM. Regulation of lysyl oxidase expression in lung fibroblasts by transforming growth factor-beta1 and prostaglandin E2. *Am J Respir Cell Mol Biol.* (1994); 11(6):751-755.

Boguslawska J, Kedzierska H, Poplawski P, Rybicka B, Tanski Z and Piekielko-Witkowska A. Expression of genes involved in cellular adhesion and extracellular matrix remodelling correlates with poor survival of patients with renal cancer. *J Urol.* (2016); 195(6):1892-1902.

Boström AK, Möller C, Nilsson E, Elfving P, Axelson H and Johansson ME. Sarcomatoid conversion of clear cell renal cell carcinoma in relation to epithelial-to-mesenchymal transition. *Hum Pathol.* (2012); 43(5):708-719.

Boström AK, Lindgren D, Johansson ME and Axelson H. Effects of TGF-β signaling in clear cell renal cell carcinoma cells. *Biochem Biophys Res Commun.* (2013); 435(1):126-133.

Bradley WD and Koleske AJ. Regulation of cell migration and morphogenesis by Abl-family kinases: emerging mechanisms and physiological contexts. *J Cell Sci*. (2009); 122(19):3441-3454.

Brylka LJ and Schinke T. Chemokine in physiological and pathological bone remodelling. *Front Immunol.* (2019); 10:2182.

Burton EA, Plattner P and Pendergast AM. Abl tyrosine kinases are required for infection by Shigella flexneri. *EMBO J*. (2003); 22(20):5471-5479.

Cai L, Xiong X, Kong X and Xie J. The role of the lysyl oxidases in tissue repair and remodeling: a concise review.

Tissue Eng Regen Med. (2017); 14(1):15-30.

Cao C, Ren X, Kharbanda S, Koleske AJ, Prasad KVS and Kufe D. The ARG tyrosine kinase interacts with Siva-1 in the apoptotic response to oxidative stress. *J Biol Chem*. (2001); 276(15):11465-11468.

Capitanio U, Bensalah K, Bex A, Boorjian SA, Bray F, Coleman J, Gore JL, Sun M, Wood C and Russo P. Epidemiology of renal cell carcinoma. *Eur Urol.* (2019); 75(1):74-84.

Cheville JC, Lohse CM, Zincke H, Weaver AL and Blute ML. Comparisons of outcome and prognostic features among histologic subtypes of renal cell carcinoma. *Am J Surg Pathol.* (2003); 27(5):612-624.

Cifola I, Bianchi C, Mangano E, Bombelli S, Frascati F, Fasoli E, Ferrero S, Di Stefano V, Zipeto MA, Magni F, Signorini S, Battaglia C and Perego RA. Renal cell carcinoma primary cultures maintain genomic and phenotypic profile of parental tumor tissues. *BMC Cancer.* (2011); 11:244.

Cohen HT and McGovern FJ. Renal-cell carcinoma. *N Engl J Med.* (2005); 353(23):2477-2490.

Condeelis J and Pollard JW. Macrophages: obligate partners for tumor cell migration, invasion and metastasis. *Cell.* (2006); 124(2):263-266.

Copland JA, Luxon BA, Ajani L, Maity T, Campagnaro E, Guo H, LeGrand SN, Tamboli P and Wood CG. Genomic profiling identifies alterations in TGFbeta signaling through loss of TGFbeta receptor expression in human renal cell carcinogenesis and progression. *Oncogene.* (2003); 22(39):8053-8062.

Cox TR, Rumney RM, Schoof EM, Perryman L, Hoye AM, Agrawal A, Bird D, Latif NA, Forrest H, Evans HR, Huggins

ID, Lang G, Linding R, Gartland A and Erler JT. The hypoxic cancer secretome induces pre-metastatic bone lesions through lysyl oxidase. *Nature.* (2015); 522(7554):106-110.

Cox TR, Gartland A and Erler JT. Lysyl oxidase, a targetable secreted molecule involved in cancer metastasis. *Cancer Res.* (2016); 76(2):188-192.

Dagher J, Delahunt B, Rioux-Leclercq N, Egevad L, Srigley JR, Coughlin G, Dunglinson N, Gianduzzo T, Kua B, Malone G, Martin B, Preston J, Pokorny M, Wood S, Yaxley J and Samaratunga H. Clear cell renal cell carcinoma: validation of World Health Organization/International Society of Urological Pathology grading. *Histopatology.* (2017); 71(6):918-925.

de Jong JS, van Diest PJ, van der Valk P and Baak JP. Expression of growth factors, growth-inhibiting factors, and their receptors in invasive breast cancer. II: Correlations with proliferation and angiogenesis. *J Pathol.* (1998); 184(1):53-7.

Di Stefano V, Torsello B, Bianchi C, Cifola I, Mangano E, Bovo G, Cassina V, De Marco S, Corti R, Meregalli C, Bombelli S, Viganò P, Battaglia C, Strada G and Perego RA. Major action of endogenous lysyl oxidase in clear cell renal cell carcinoma progression and collagen stiffness revealed by primary cell cultures. *Am J Pathol.* (2016); 186(9):2473-2485.

Dondeti VR, Wubbenhorst B, Lal P, Gordan JD, D'Andrea K, Attiyeh EF, Simon MC and Nathanson K. Integrative genomic analyses of sporadic clear cell renal cell carcinoma define disease subtypes and potential new therapeutic targets. *Cancer Res.* (2012); 72(1):112-121.

Erler JT, Bennewith KL, Nicolau M, Dornhöfer N, Kong C, Le QT, Chi JT, Jeffrey SS and Giaccia AJ. Lysyl oxidase is essential for hypoxia-induced metastasis. *Nature.* (2006); 440(7088):1222-1226.

Erler JT, Bennewith KL, Cox TR, Lang G, Bird D, Koong A, Le QT and Giaccia AJ. Hypoxia-induced lysyl oxidase is a critical mediator of bone marrow cell recruitment to form the premetastatic niche. *Cancer Cell.* (2009); 15(1):35-44.

Escudier B, Porta C, Schmidinger M, Rioux-Leclercq N, Bex A, Khoo V, Grünwald V, Gillessen S, Horwich A; EMSO Guidelines Committee. Renal cell carcinoma: ESMO Clinical Practice Guidelines for diagnosis, treatment and follow-up. *Ann Oncol.* (2019); 30(5):706-720.

Fidler IJ. The pathogenesis of cancer metastasis: the “seed and soil” hypothesis revisited. *Nat Rev Cancer*. (2003); 3:453-458.

Fiore LS, Ganguly SS, Sledziona J, Cibull ML, Wang C, Richards DL, Neltner JM, Beach C, McCorkle JR, Kaetzel DM and Plattner R. c-Abl and Arg induce cathepsin-mediated lysosomal degradation of the NM23-H1 metastasis suppressor in invasive cancer. *Oncogene*. (2014); 33(36):4508-4520.

Frank I, Blute ML, Cheville JC, Lohse CM, Weaver AL and Zincke H. An outcome prediction model for patients with clear cell renal cell carcinoma treated with radical nephrectomy based on tumor stage, size, grade, and necrosis: the SSIGN score. *J Urol.* (2002); 168(6):2395-2400.

Friesenhengst A, Pribitzer-Winner T and Schreiber M. Association of the G473A polymorphism and expression of lysyl oxidase with breast cancer risk and survival in European women: a hospital-based casecontrol study. *PLoS One.* (2014); 9(8):e105579.

Furstoss O, Dorey K, Simon V, Barila D, Superti-Furga G and Roche S. c-Abl is an effector of Src for growth factor-induced c-mycexpression and DNA synthesis. *EMBO J*. (2002); 21(4):514-524.

Ganguly SS, Fiore LS, Sims JT, Friend JW, Srinivasan D, Thacker MA, Cibull ML, Wang C, Novak M, Kaetzel DM and Plattner R. c-Abl and Arg are activated in human primary melanomas, promote melanoma cell invasion via distinct pathways, and drive metastatic progression. *Oncogene*. (2012); 31(14):1804-1816.

Gatto F, Nookaew I and Nielsen J. Chromosome 3p loss of heterozygosity is associated with a unique metabolic network in clear cell renal carcinoma. *Proc Natl Acad Sci USA.* (2014); 111(9):E866-875.

Ge G and Greenspan DS. BMP1 controls TGFbeta1 activation via cleavage of latent TGFbeta-binding protein. *J Cell Biol.* (2006); 175(1):111-120.

Gil-Henn H, Patsialou A, Wang Y, Warren MS, Condeelis JS and Koleske AJ. Arg/Abl2 promotes invasion and attenuates proliferation of breast cancer in vivo. *Oncogene*. (2013); 32(21):2622-2630.

Goto Y, Uchio-Yamada K, Anan S, Yamamoto Y, Ogura A and Manabe N. Transforming growth factor-beta1 mediated up-regulation of lysyl oxidase in the kidneys of hereditary nephrotic mouse with chronic renal fibrosis. *Virchows Arch.* (2005); 447(5):859-868.

Greuber EK, Smith-Pearson P, Wang J and Pendergast AM. Role of ABL Family Kinases in Cancer: from Leukemia to Solid Tumors. *Nat Rev Cancer*. (2013); 13(8):559-571.

Gu L, Gao Q, Ni L, Wang M and Shen F. Fasudil inhibits epithelial-myofibroblast transdifferentiation of human renal tubular epithelial HK-2 cells induced by high glucose. *Chem Pharm Bull.* (2013); 61(7):688-694.

Gupta GP and Massagué J. Cancer metastasis: building a framework. *Cell.* (2006); 127(4):679-695.

Hakimi AA, Reznik E, Lee CH, Creighton CJ, Brannon AR, Luna A, Aksoy BA, Liu EM, Shen R, Lee W, Chen Y, Stirdivant SM, Russo P, Chen YB, Tickoo SK, Reuter VE, Cheng EH, Sander C and Hsieh JJ. An integrated metabolic atlas of clear cell renal cell carcinoma. *Cancer Cell.* (2016); 29(1):104-116.

Hanahan D and Weinberg RA. The hallmarks of cancer. *Cell.* (2000); 100(1):57-70.

Hantschel O and Superti-Furga G. Regulation of the c-Abl and Bcr-Abl tyrosine kinases. *Nat Rev Mol Cell Biol*. (2004); 5(1):33-44.

Hasegawa Y, Takanashi S, Kanehira Y, Tsushima T, Imai T and Okumura K. Transforming growth factor-beta1 level correlates with angiogenesis, tumor progression, and prognosis in patients with nonsmall cell lung carcinoma. *Cancer.* (2001); 91(5):964-971.

Hegele A, Varga Z, von Knobloch R, Heidenreich A, Kropf J and Hofmann R. TGFbeta1 in patients with renal cell carcinoma. *Urol. Res.* (2002); 30(2):126-129.

Hernandez SE, Krishnaswami M, Miller AL and Koleske AJ. How do Abl family kinases regulate cell shape and movement? *Trends Cell Biol*. (2004a); 14(1):36-44.

Hernandez SE, Settleman J and Koleske AJ. Adhesion-dependent regulation of p190RhoGAP in the developing brain by the Abl-related gene tyrosine kinase. *Curr Biol*. (2004b); 14(8):691-696.

Higgins JP, Shinghal R, Gill H, Reese JH, Terris M, Cohen RJ, Fero M, Pollack JR, van de Rijn M and Brooks JD. Gene expression patterns in renal cell carcinoma assessed by complementary DNA microarray. *Am J Pathol.* (2003); 162(3):925-932.

Horiguchi K, Shirakihara T, Nakano A, Imamura T, Miyazono K and Saitoh M. Role of Ras signaling in the induction of snail by transforming growth factor-beta. *J Biol Chem.* (2009); 284(1):245-253.

Hsieh JJ, Purdue MP, Signoretti S, Swanton C, Albiges L, Schmidinger M, Heng DY, Larkin J and Ficarra V. Renal cell carcinoma. *Nat Rev Dis Primers.* (2017); 3:17009.

Huang Y, Comiskey EO, Dupree RS, Li S, Koleske AJ and Burkhardt JK. The c-Abl tyrosine kinase regulates actin remodeling at the immune synapse. *Blood*. (2008); 112(1):111-119.

Hudes GR. mTOR as a target for therapy of renal carcer. *Clin Adv Hemotol Oncol.* (2007); 5(10):772-4.

Ikushima H and Miyazono K. TGFbeta signaling: a complex web in cancer progression. *Nat Rev Cancer.* (2010); 10(6):415-424.

Inman GJ, Nicolás FJ, Callahan JF, Harling JD, Gaster LM, Reith AD, Laping NJ and Hill CS. SB-431542 is a potent and specific inhibitor of transforming growth factor-beta superfamily type I activing receptor-like kinase (ALK) receptors ALK4, ALK5 and ALK7. *Mol Pharmocol.* (2002); 62(1):65-74.

Isogai Z, Ono RN, Ushiro S, Keene DR, Chen Y, Mazzieri R, Charbonneau NL, Reinhardt DP, Rifkin DB and Sakai LY. Latent transforming growth factor beta-binding protein 1 interacts with fibrillin and is a microfibril-associated protein. *J Biol Chem.* (2003); 278(4):2750-2757.

Janssens K, ten Dijke P, Janssens S and Van Hul W. Transforming growth factor-β1 to the bone. *Endocr Rev.* (2005); 26(6):743-774.

Joung JW, Oh HK, Lee SJ, Kim YA and Jung HJ. Significance

of intratumoral fibrosis in clear cell renal cell carcinoma. *J Pathol Transl Med.* (2018); 52(5):323-330.

Juárez P and Guise TA. TGF-β in cancer and bone: Implications for treatment of bone metastases. *Bone.* (2011); 48(1):23-29.

Kaelin WG Jr. Molecular basis of the VHL hereditary cancer syndrome. *Nat Rev Cancer.* (2002); 2(9):673-682.

Kaelin WG. Von Hippel-Lindau disease. *Annu Rev Pathol.* (2007); 2:145-173.

Kan C, Vargas G, Pape FL and Clézardin P. Cancer cell colonization in the bone microenvironment. *Int J Mol Sci.* (2016); 17(10):E1674.

Kajdaniuk D, Marek B, Borgiel-Marek H and Kos-Kudla B. Transforming growth factor β1 (TGFβ1) in physiology and pathology. *Endokrynol Pol.* (2013); 64(5):384-396.

Kharbanda S, Ren R, Pandey P, Shafman TD, Feller SM, Weichselbaum RR and Kufe DW. Activation of the c-Abl tyrosine kinase in the stress response to DNA-damaging agents. *Nature*. (1995); 376(6543):785-788.

Kim WY and Kaelin WG. Role of VHL gene mutation in human cancer. *J Clin Oncol.* (2004); 22(24):4991-5004.

Kominsky SL, Doucet M, Brady K and Weber KL. TGF-beta promotes the establishment of renal cell carcinoma bone metastasis. *J Bone Miner Res.* (2007); 22(1):37-44.

Kovacs G, Akhtar M, Beckwith BJ, Bugert P, Cooper CS, Delahunt B, Eble JN, Fleming S, Ljungberg B, Medeiros LJ, Moch H, Reuter VE, Ritz E, Roos G, Schmind D, Srigley JR, Störkel S, van den Berg E and Zbar B. The Heidelberg classification of renal cell tumours. *J Pathol.* (1997); 183(2):131-133.

Kruh GD, King CR, Kraus MH, Popescu NC, Amsbaugh SC, McBride WO and Aaronson SA. A novel human gene closely related to the abl proto-oncogene. *Science*. (1986); 234(4783):1545-1548

Kruh GD, Perego R, Miki T and Aaronson SA. The complete coding sequence of arg defines the Abelson subfamily of cytoplasmic tyrosine kinases. *Proc Natl Acad Sci*. (1990); 87(15):5802-5806.

Laczko R, Szauter KM, Jansen MK, Hollosi P, Muranyi M, Molnar J, Fong KS, Hinek A and Csiszar K. Active lysyl oxidase (LOX) correlates with focal adhesion kinase (FAK)/paxillin activation and migration in invasive astrocytes. *Neuropathol Appl Neurobiol.* (2007); 33(6):631-643.

Lam JS, Shvarts O, Leppert JT, Figlin RA and Belldegrun AS. Renal cell carcinoma 2005: new frontiers in staging, prognostication and targeted molecular therapy. *J Urol.* (2005); 173(6):1853-1862.

Leibovich BC, Blute ML, Cheville JC, Lohse CM, Frank I, Know ED, Weaver AL, Parker AS and Zincke H. Prediction of progression after radical nephrectomy for patients with clear cell renal cell carcinoma: a stratification tool for prospective clinical trials. *Cancer.* (2003); 97(7):1663-1671.

Lewis JM, Baskaran R, Taagepera S, Schwartz MA and Wang JY. Integrin regulation of c-Abl tyrosine kinase activity and cytoplasmic-nuclear transport. *Proc Natl Acad Sci*. (1996); 93(26):15174-15179.

Li R, Knight JF, Park M and Pendergast AM. Abl kinases regulate HGF/Met signaling required for epithelial cell scattering, tubulogenesis and motility. *Plos One*. (2015); 10(5):1-23.

Li T, Wu C, Gao L, Qin F, Wei Q and Yuan J. Lysyl oxidase family members in urological tumorigenesis and fibrosis. *Oncotarget.* (2018); 9(28):20156-20164.

Liep J, Kilic E, Meyer HA, Busch J, Jung K and Rabien A. Cooperative effect of miR-141-3p and miR-145-5p in the regulation of targets in clear cell renal cell carcinoma. *PLoS One.* (2016); 11(6):e0157801.

Liu Y and Cao X. Characteristics and significance of the pre-metastatic niche. *Cancer Cell.* (2016); 30(5):668-681.

Ljungberg B, Bensalah K, Canfield S, Dabestani S, Hofmann F, Hora M, Kuczyk MA, Lam T, Marconi L, Merseburger AS, Mulders P, Powles T, Staehler M, Volpe A and Bex A. EAU guidelines on renal cell carcinoma: 2014 update. *Eur Urol.* (2015); 67(5):913-924.

Mader CC, Oser M, Magalhaes MA, BravoCordero JJ, Condeelis J, Koleske AJ and Gil-Henn H. An EGFR-Src-Arg-cortactin pathway mediates functional maturation of invadopodia and breast cancer cell invasion. *Cancer Res.*(2011); 71(5):1730-1741.

Maita S, Yuasa T, Tsuchiya N, Mitobe Y, Narita S, Horikawa Y, Hatake K, Fukui I, Kimura S, Maekawa T and Habuchi T. Antitumor effect of sunitinib against skeletal metastatic renal cell carcinoma through inhibition of osteoclast function. *Int J Cancer.* (2012); 130(3):677-684.

Massagué J. The transforming growth factor-beta family. *Annu Rev Cell Biol.* (1990); 6:597-641.

Massagué J and Gomis RR. The logic of TGFbeta signaling. *FEBS Lett.* (2006); 580(12):2811-2820.

Maxwell PH, Pugh CW and Ratcliffe PJ. Activation of the HIF pathway in cancer. *Curr Opin Genet Dev.* (2001); 11(3):293-299.

McDermott DF, Regan MM, Clark JI, Flaherty LE, Weiss GR, Logan TF, Kirkwood JM, Gordon MS, Sosman JA, Ernstoff MS, Tretter CP, Urba WJ, Smith JW, Margolin KA, Mier JW, Gollob JA, Dutcher JP and Atkins MB. Randomized phase III trial of high-dose interleukin-2 versus subcutaneous interleukin-2 and interferon in patients with metastatic renal cell carcinoma. *J Clin Oncol.* (2005); 23(1):133-141. Erratum in: *J Clin Oncol.* 2005; 23(12):2877.

Mikami S, Oya M, Mizuno R, Kosaka T, Ishida M, Kuroda N, Nagashima Y, Katsube K and Okada Y. Recent advances in renal cell carcinoma from a phatological point of view. *Pathol Int.* (2016); 66(9):481-490.

Miller AL, Wang Y, Mooseker MS and Koleske AJ. The Abl-related gene (Arg) requires its F-actin-microtubule cross-linking activity to regulate lamellipodial dynamics during fibroblast adhesion. *J Cell Biol*. (2004); 165(3):407-419.

Mitropoulos D, Kiroudi A, Christelli E, Serafetinidis E, Zervas A, Anastasiou I and Dimopoulos C. Expression of transforming growth factor beta in renal cell carcinoma and matched non-involved renal tissue. *Urol. Res.* (2004); 32(5):317-322.

Miyajima A, Asano T, Seta K, Kakoi N and Hayakawa M. Loss of expression of transforming growth factor-beta receptor as a prognostic factor in patients with renal cell carcinoma. *Urology.* (2003); 61(5):1072-1077.

Moustakas A and Heldin CH. The regulation of TGFbeta signal transduction. *Development.* (2009); 136(22): 3699-3714.

Motzer RJ and Basch E. Targeted drugs for metaststic renal cell carcinoma. *Lancet.* (2007); 370(9605):2071-2073.

Motzer RJ, Escudier B, McDermott DF, George S, Hammers HJ, Srinivas S, Tykodi SS, Sosman JA, Procopio G, Plimack ER, Castellano D, Choueiri TK, Gurney H, Donskov F, Bono P, Wagstaff J, Gauler TC, Ueda T, Tomita Y, Schutz FA, Kollmannsberger C, Larkin J, Ravaud A, Simon JS, Xu LA, Waxman IM and Sharma P. Nivolumab versus Everolimus in Advanced Renal Cell Carcinoma. *N Engl J Med.* (2015); 373(19):1803-1813.

Motzer RJ, Escudier B, Gannon A and Figlin RA. Sunitinib: ten years of successful clinical use and study in advanced renal cell carcinoma. *Oncologist.* (2017); 22(1):41-52.

Mundy GR. Metastasis to bone: causes, consequences and therapeutic opportunities. *Nature Reviews Cancer.* (2002); 2(8):584-593.

Munger JS, Huang X, Kawakatsu H, Griffiths MJ, Dalton SL, Wu J, Pittet JF, Kaminski N, Garat C, Matthay MA, Rifkin DB and Sheppard D. The integrin alpha v beta 6 binds and activates latent TGF beta 1: a mechanism for regulating pulmonary inflammation and fibrosis. *Cell.* (1999); 96(3):319-328.

Nabi S, Kessler ER, Bernard B, Flaig TW and Lam ET. Renal cell carcinoma: a review of biology and pathophysiology. *F1000Res.* (2018); 7:307.

Newsome TP, Weisswange I, Frischknecht F and Way M. Abl collaborates with Src family kinases to stimulate actin-based motility of vaccinia virus. *Cell Microbiol*. (2006); 8(2):233-241.

Okuda K, Oda A, Sato Y, Nakayama A, Fujita H, Sonoda Y and Griffin JD. Signal transduction and cellular functions of the TEL/ARG oncoprotein. *Leukemia.* (2005); 19(4):603-610.

Padua D and Massagué J. Roles of TGFbeta in metastasis. *Cell Res.* (2009); 19(1):89-102.

Palamakumbura AH, Jeay S, Guo Y, Pischon N, Sommer P, Sonenshein GE and Trackman PC.The propeptide domain of lysyl oxidase induces phenotypic reversion of ras-transformed cells. *J Biol Chem.* (2004); 279(39):40593-40600.

Parker AS, Lohse CM, Wu K, Kreinest P, Copland JA, Hilton T, Wehle M, Cheville JC and Blute M. Lower expression levels of the transforming growth factor beta receptor type II protein are associated with a less aggressive tumor phenotype and improved survival among patients with clear cell renal cell carcinoma. *Hum Pathol.* (2007); 38(3):453-461.

Payne SL, Fogelgren B, Hess AR, Seftor EA, Wiley EL, Fong SF, Csiszar K, Hendrix MJ and Kirschmann DA. Lysyl oxidase regulates breast cancer cell migration and adhesion through a hydrogen peroxide-mediated mechanism. *Cancer Res.* (2005); 65(24):11429-11436.

Pendergast AM. The Abl family kinases: mechanism of regulation and signaling. *Adv Cancer Res*. (2002); 85:51-100.

Perego R, Ron D and Kruh GD. Arg encodes a widely expressed 145 kDa protein-tyrosine kinase. *Oncogene.* (1991); 6(10):1899-1902.

Perego RA, Corizzato M, Bianchi C, Eroini B and Bosari S. N-and C-terminal isoforms of Arg quantified by Real-Time PCR are specifically expressed in human normal and neoplastic cells, in neoplastic cell lines, and in HL-60 cell differentiation. *Mol Carcinog*. (2005); 42(4):229-239.

Perryman L and Erler JT. Lysyl oxidase in cancer research. *Future Oncol.* (2014); 10(9):1709-1717.

Petejova N and Martinek A. Renal cell carcinoma: Review of

etiology, pathophysiology and risk factors. *Biomed Pap Med Fac Univ Palacky Olomouc Czech Repub.* (2016); 160(2):183-194.

Pez F, Dayan F, Durivault J, Kaniewski B, Aimond G, Le Provost GS, Deux B, Clézardine P, Sommer P, Pouysségur J and Reynaud C. The HIF-1-inducible lysyl oxidase activates HIF-1 via the Akt pathway in a positive regulation loop and synergizes with HIF-1 in promoting tumor cell growth. *Cancer Res.* (2011); 71(5):1647-1657.

Plattner R, Kadlec L, DeMali KA, Kazlauskas A and Pendergast AM. c-Abl is activated by growth factors and Src family kinases and has a role in the cellular response to PDGF. *Genes Dev*. (1999); 13(18):2400-2411.

Plattner R, Irvin BJ, Guo S, Blackburn K, Kazlauskas A, Abraham RT, York JD and Pendergast AM. A new link between the c-Abl tyrosine kinase and phosphoinositide signaling through PLC-gamma1. *Nat Cell Biol*. (2003); 5(4):309-319.

Plattner R, Koleske AJ, Kazlauskas A and Pendergast AM. Bidirectional signaling links the Abelson kinases to the platelet-derived growth factor receptor. *Mol Cell Biol*. (2004); 24(6):2573-2583.

Poppe M, Feller SM, Romer G and Wessler S. Phosphorylation of Helicobacter pylori CagA by c-Abl leads to cell motility. *Oncogene*. (2007); 26(24):3462-3472.

Principe DR, Doll JA, Bauer J, Jung B, Munshi HG, Bartholin L, Pasche B, Lee C, Grippo PJ. TGF-β: duality of function between tumor prevention and carcinogenesis. *J Natl Cancer Inst.* (2014); 106(2):djt369.

Pugh CW and Ratcliffe PJ. Regulation of angiogenesis by hypoxia: role of the HIF system. *Nat Med.* (2003); 9(6):677-684.

Raimondi A, Randon G, Sepe P, Claps M, Verzoni E, de Braud F and Procopio G. The evaluation of response to immunology in metastatic renal cell carcinoma: open challenges in the clinical practice. *Int J Mol Sci.* (2019); 20(17):pii:E4263.

Ren R. Mechanisms of BCR-ABL in the pathogenesis of chronic myelogenous leukaemia. *Nat Rev Cancer*. (2005); 5(3):172-183.

Renshaw MW, Lewis JM and Schwartz MA. The c-Abl tyrosine kinase contributes to the transient activation of MAP kinase in cells plated on fibronectin. *Oncogene*. (2000); 19(28):3216-3219.

Reynaud C, Ferreras L, Di Mauro P, Kan C, Croset M, Bonnelye E, Pez P, Thomas C, Aimond G, Kamoub AE, Brevet M and Clézardin P. Lysyl oxidase is a strong determinant of tumor cell colonization in bone. *Cancer Res.* (2017); 77(2):268-278.

Rifkin DB. Latent transforming growth factor-beta (TGF-beta) binding proteins: orchestrators of TGF-beta availability. *J Biol Chem.* (2005); 280(9):7409-7412.

Rogers CG, Tan MH and Teh BT. Gene expression profiling of renal cell carcinoma and clinical implications. *Urology.* (2005); 65(2):231-237.

Roodman GD. Role of cytokines in the regulation of bone resorption. *Calcif Tissue Int.* (1993); 53(Suppl 1):S94-S98.

Roy R, Polgar P, Wang Y, Goldstein RH, Taylor L and Kagan HM. Regulation of lysyl oxidase and cyclooxygenase expression in human lung fibroblasts: interactions among TGF-beta, IL-1beta and prostaglandin E. *J Cell Biochem.* (1996); 62(3):411-417.

Rühle A, Andratschke N, Siva S and Guckenberger M. Is

there a role for stereotactic radiotherapy in the treatment of renal cell carcinoma? *Clin Transl Radiat Oncol.* (2019); 18:104-112.

Schultz-Cherry S and Murphy-Ullrich JE. Thrombospondin causes activation of latent transforming growth factor-beta secreted by endothelial cells by a novel mechanism. *J Cell Biol.* (1993); 122(4):923-932.

Sethi A, Mao W, Wordinger RJ and Clark AF. Transforming growth factor-beta induces extracellular matrix protein cross-linking lysyl oxidase (LOX) genes in human trabecular meshwork cells. *Invest Ophthalmol Vis Sci.* (2011); 52(8):5240-5250.

Sethi A, Wordinger RJ and Clark AF. Gremlin utilizes canonical and non-canonical TGFβ signaling to induce lysyl oxidase (LOX) genes in human trabecular meshwork cells. *Exp Eye Res.* (2013); 113:117-127.

Simpson MA, Bradley WD, Harburger D, Parsons M, Calderwood DA and Koleske AJ. Direct interactions with the integrin β1 cytoplasmic tail activate the Abl2/Arg kinase. *J Biol Chem*. (2015); 290(13):8360-8372.

Sitaram RT, Mallikarjuna P, Landström M and Ljungberg B. Transforming growth factor-β promotes aggressiveness and invasion of clear cell renal cell carcinoma. *Oncotarget.* (2016); 7(24):35917-35931.

Sjölund J, Boström AK, Lindgren D, Manna S, Moustakas A, Ljungberg B, Johansson M, Fredlund E and Axelson H. The notch and TGF-β signaling pathways contribute to the aggressiveness of clear cell renal cell carcinoma. *PLoS One.* (2011); 6(8):e23057.

Smith-Pearson PS, Greuber EK, Yogalingam G and Pendergast AM. Abl kinases are required for invadopodia formation and chemokine-induced invasion. *Journal of*

Biological Chemistry. (2010); 285:40201-40211.

Song W, He D, Chen Y, Yeh CR, Hsu I, Huang Q, Zhang X, Chang LS, Zuo L, Chen J, Doersch KM, Chang C, Li L and Yeh S. Targeting newly identified ERβ/TGF-β1/SMAD3 signals with the FDA-approved anti-estrogen Faslodex or on ERβ selective antagonist in renal cell carcinoma. *Mol Oncol.* (2018); 12(12):2055-2071.

Srinivasan D and Plattner R. Activation of Abl tyrosine kinases promotes invasion of aggressive breast cancer cells. *Cancer Res*. (2006); 66(11):5648–5655.

Srinivasan D, Sims JT and Plattner R. Aggressive breast cancer cells are dependent on activated Abl kinases for proliferation, anchorage-independent growth and survival. *Oncogene*. (2008); 27(8):1095-1105.

Srinivasan D, Kaetzel DM and Plattner R. Reciprocal regulation of Abl and Receptor Tyrosine Kinases. *Cell Signal*. (2009); 21(7):1143-1150.

Störkel S, Eble JN, Adlakha K, Amin M, Blute ML, Bostwick DG, Darson M, Delahunt B and Iczkowski K. Classification of renal cell carcinoma: Workgroup No.1. Union Internationale Contre le Cancer (UICC) and the American Joint Committee on Cancer (AJCC). *Cancer.* (1997); 80(5):987-989.

Suarez-Carmona M, Lesage J, Cataldo D and Gilles C. EMT and inflammation: inseparable actors of cancer progression. *Mol Oncol.* (2017); 11(7):805-823.

Sun X, Majumder P, Shioya H, Wu F, Kumar S, Weichselbaum R, Kharbanda S and Kufe D. Activation of the cytoplasmic c-Abl tyrosine kinase by reactive oxygen species. *J Biol Chem*. (2000); 275(23):17237-17240.

Taipale J, Miyazono K, Heldin CH and Keski-Oja J. Latent transforming growth factor-beta 1 associates to fibroblast

extracellular matrix via latent TGF-beta binding protein. *J Cell Biol.* (1994); 124(1-2):171-181.

Takahashi M, Rhodes DR, Furge KA, Kanayama H, Kagawa S, Haab BB and The BT. Gene expression profiling of clear cell renal cell carcinoma: gene identification and prognostic classification. *Proc Natl Acad Sci USA.* (2001); 98(17):9754-9759.

Tammer I, Brandt S, Harting R, Konig W and Backert S. Activation of Abl by Helicobacter pylori: a novel kinase for CagA and crucial mediator of host cell scattering. *Gastroenterology*. (2007); 132(4):1309-1319.

Teitelbaum SL and Ross FP. Genetic regulation of osteoclast development and function. *Nat Rev Genet.* (2003); 4(8):638-649.

Thomas DA and Massagué J. TGF-beta directly targets cytotoxic T cell functions during tumor evasion of immune surveillance. *Cancer Cell.* (2005); 8(5):369-380.

Torsello B, Bianchi C, Meregalli C, Di Stefano V, Invernizzi L, De Marco S, Bovo G, Brivio R, Strada G, Bombelli S and Perego RA. Arg tyrosine kinase modulates TGF-β1 production in human renal tubular cells under high-glucose conditions. *J Cell Sci.* (2016); 129(15):2925-2936.

Torsello B, De Marco S, Bombelli S, Chisci E, Cassina V, Corti R, Bernasconi D, Giovannoni R, Bianchi C and Perego RA. The 1ALCTL and 1BLCTL isoforms of Arg/Abl2 induce fibroblast activation and extra cellular matrix remodelling differently. *Biol Open.* (2019); 8(3):1-9.

Trackman PC, Bedell-Hogan D, Tang J and Kagan HM. Post-translational glycosylation and proteolytic processing of a lysyl oxidase precursor. *J Biol Chem.* (1992); 267(12):8666-8671.

Tretbar S, Krausberck P, Müller A, Friedrich M, Vaxevanis C, Bukur J, Jasinski-Bergner S and Selinger B. TGF-β inducible epithelial-to-mesenchymal transition in renal cell carcinoma. *Oncotarget.* (2019); 10(15):1507-1524.

Tuxhorn JA, McAlhany SJ, Yang F, Dang TD and Rowley DR. Inhibition of transforming growth factor-beta activity decreases angiogenesis in a human prostate cancer-reactive stroma xenograft model. *Cancer Res.* (2002); 62(21):6021-6025.

Umer M, Mohib Y, Atif M and Nazim M. Skeletal metastasis in renal cell carcinoma: a review. *Ann Med Surg (Lond).* (2018); 27:9-16.

Voloshenyuk TG, Landesman ES, Khoutorova E, Hart AD and Gardner JD. Induction of cardiac fibroblast lysyl oxidase by TGF-β1 requires PI3K/Akt, Smad3, and MAPK signaling. *Cytokine.* (2011); 55(1):90-97.

Vuong L, Kotecha RR, Voss MH and Hakimi AA. Tumor microenvironment dynamics in clear-cell renal cell carcinoma. *Cancer Discov.* (2019); 9(10):1349-1357.

Wang JY. Abl tyrosine kinase in signal trasduction and cell-cycle regulation. *Curr Opin Genet Dev*. (1993); 3(1):35-43.

Wang J and Pendergast AM. The Emerging Role of ABL Kinases in Solid Tumors. *Trends Cancer*. (2015); 1(2): 110-123.

Wang Y, Miller AL, Mooseker MS and Koleske AJ. The Abl-related gene (Arg) nonreceptor tyrosine kinase uses two F-actin-binding domains to bundle F-actin. *Proc Natl Acad Sci*. (2001); 98(26):14865-14870.

Weber K, Doucet M and Kominsky S. Renal cell carcinoma bone metastasis-elucidating the molecular targets. *Cancer*

Metastasis Rev. (2007); 26(3-4):691-704.

Wettersten HI, Hakimi AA, Morin D, Bianchi C, Johnstone ME, Donohoe DR, Trott JF, Aboud OA, Stirdivant S, Neri B, Wolfert R, Stewart B, Perego R, Hsieh JJ and Weiss RH. Grade-dependent metabolic reprogramming in kidney cancer revealed by combined proteomics and metabolomics analysis. *Cancer Res.* (2015); 75(12):2541-2552.

Wipff PJ and Hinz B. Integrins and the activation of latent transforming growth factor beta1-an intimate relationship. *Eur J Cell Biol.* (2008); 87(8-9):601-615.

Yan X, Xiong X and Chen YG. Feedback regulation of TGF-β signaling. *Acta Biochim Biophys Sin (Shanghai).* (2018); 50(1):37-50.

Yi SJ, Lee H, Lee J, Lee K, Kim J, Kim Y, Park JI and Kim K. Bone remodeling: histone modifications as fate determinants of bone cell differentiation. *Int J Mol Sci.* (2019); 20(13):pii:E3147.

Yoon CH, Kim MJ, Park MJ, Park IC, Hwang SG, An S, Choi YH, Yoon G and Lee SJ. Claudin-1 acts through c-Abl-protein kinase Cdelta (PKCdelta) signaling and has a causal role in the acquisition of invasive capacity in human liver cells. *J. Biol. Chem*. (2010); 285(1):226-233.

Yoshida M, Yao M, Ishikawa I, Kishida T, Nagashima Y, Kondo K, Nakaigawa N and Hosaka M. Somatic Von Hippel-Lindau disease gene mutation in clear-cell renal carcinomas associated with end-stage renal disease/acquired cystic disease of the kidney. *Genes Chromosomes Cancer.* (2002); 35(4): 359-364.

Zandy NL, Playford M and Pendergast AM. Abl tyrosine kinases regulate cell-cell adhesion through Rho GTPases. *Proc Natl Acad Sci*. (2007); 104(45):17686-17691.

Zhang L, Zhou F and ten Dijke P. Signaling interplay between transforming growth factor-β receptor and PI3K/AKT pathways in cancer. *Trends Biochem Sci.* (2013); 38(12):612-620.

Zhao Z, Lu J, Han L, Wang X, Man Q and Liu S. Prognostic significance of two lipid metabolism enzymes, HADHA and ACAT2, in clear cell renal cell carcinoma. *Tumour Biol.* (2016); 37(6):8121-8130.

Chapter 2

The glucose and lipid metabolism reprogramming is grade-dependent in clear cell renal cell carcinoma primary cultures and is targetable to modulate cell viability and proliferation

Cristina Bianchi[1], Chiara Meregalli[1], Silvia Bombelli[1], Vitalba Di Stefano[1], Francesco Salerno[1], Barbara Torsello[1], Sofia De Marco[1], Giorgio Bovo[2,8], Ingrid Cifola[3], Eleonora Mangano[3], Cristina Battaglia[4], Guido Strada[5], Giuseppe Lucarelli[6], Robert H. Weiss[7] and Roberto A. Perego[1]

[1]School of Medicine and Surgery, University of Milano-Bicocca, Monza, Italy
[2]Pathology Unit, ASST Monza, San Gerardo Hospital, Monza, Italy
[3]Institute for Biomedical Technologies, National Research Council, Segrate, Italy
[4]Department of Medical Biotechnology and Translational Medicine, University of Milano, Segrate, Italy
[5]Urology Unit, ASST North Milan, Bassini Hospital, Cinisello Balsamo, Italy
[6]Department of Emergency and Organ Transplantation-Urology, University of Bari, Bari, Italy

[7]Division of Nephrology, Department of Internal Medicine, School of Medicine, and Cancer Center, University of California, Davis, CA, USA
[8]Current address: Pathology Unit, ASST North Milan, Vimercate Hospital, Vimercate, Italy

Oncotarget, 2017, Vol. 8, (No. 69), pp: 113502-113515

Abstract

Clear cell renal cell carcinoma (ccRCC) has a poor prognosis despite novel biological targeted therapies. Tumor aggressiveness and poor survival may correlate with tumor grade at diagnosis and with complex metabolic alterations, also involving glucose and lipid metabolism. However, currently no grade-specific metabolic therapy addresses these alterations. Here we used primary cell cultures from ccRCC of low- and high-grade to investigate the effect on energy state and reduced pyridine nucleotide level, and on viability and proliferation, of specific inhibition of glycolysis with 2-deoxy-D-glucose (2DG), or fatty acid oxidation with Etomoxir. Our primary cultures retained the tissue grade-dependent modulation of lipid and glycogen storage and aerobic glycolysis (Warburg effect). 2DG affected lactate production, energy state and reduced pyridine nucleotide level in high-grade ccRCC cultures, but the energy state only in low-grade. Rather, Etomoxir affected energy state in high-grade and reduced pyridine nucleotide level in low-grade cultures. Energy state and reduced pyridine nucleotide level were evaluated by ATP and reduced 3-(4,5-dimethylthiazol-2-yl)-2,5-diphenyltetrazolium (MTT) dye quantification, respectively. 2DG treatment impaired cell proliferation and viability of low-grade ccRCC and normal cortex cultures, whereas Etomoxir showed a cytostatic and cytotoxic effect only in high-grade ccRCC cultures. Our data indicate that in

ccRCC the Warburg effect is a grade-dependent feature, and fatty acid oxidation can be activated for different grade-dependent metabolic needs. A possible grade-dependent metabolic therapeutic approach in ccRCC is also highlighted.

Introduction

Clear cell renal cell carcinoma (ccRCC) is the most common (70-80%) and lethal subtype of renal cell carcinomas and accounts for 90% of all kidney cancers [1]. Although biological and targeted therapies have shown promising results for advanced ccRCC [2-3] its prognosis remains poor, with a median overall survival of 21.4 months [4]. In ccRCC the tumor grade at diagnosis may affect survival with a 5-year cancer specific mortality rate ranging from about 7% for grade I to about 58% for grade IV cases [5].

The most striking morphological feature of ccRCC cells is their clear cytoplasm due to lipid and glycogen accumulation [6], suggesting possible involvement of their metabolism in ccRCC progression. Transcriptomic, proteomic and metabolomic profiling of ccRCC tissues support this involvement revealing metabolic reprogramming characterized by up-regulation of aerobic glycolysis (Warburg effect), the pentose phosphate pathway, fatty acid synthesis, glutamine and glutathione metabolism, and by down-regulation of the tricarboxylic acid (TCA) cycle, fatty acid β oxidation (FAO), and oxidative phosphorylation [7-10]. More recently, by using different omics approaches, several groups revealed that specific metabolic alterations, in particular the down-regulation of TCA cycle and the up-regulation of pentose phosphate pathway and fatty acid synthesis, may correlate with tumor aggressiveness and poor

survival in ccRCC patients [11, 7]. Hakimi *et al*. investigated the association between metabolic shifts and ccRCC clinical stages, revealing an increase of fatty acid biosynthesis and a decrease of oxidative phosphorylation in early-stage tumors, whereas these metabolic patterns reversed and glutathione metabolism increased in late-stage tumors [8]. A decrease of specific FAO enzyme expression has also been found to correlate with an increase of tumour stage, size and grade, with a concomitant decrease in survival [12]. Furthermore, using a proteomic approach [13], and more recently by combining proteomics and metabolomics analysis [9], it has been revealed that grade-dependent metabolic reprogramming occurs in ccRCC tissues, with the Warburg effect relatively more prominent in higher grade tumors at the expense of the TCA cycle and oxidative metabolism. Grade-dependent alterations were also shown in fatty acid, glutamine and glutathione metabolisms [9]. Even if different targeted therapeutics interfering with various aspects of RCC metabolism are currently in clinical development [14], at present there is no grade-specific therapy addressing this metabolic reprogramming. To further characterize such grade-dependent reprogramming, in anticipation of rationally developing novel grade-specific metabolic targeted approaches, an *in vitro* model more representative of the ccRCC tissue with respect to the immortalized cell lines, and that maintains grade-dependent tissue metabolic features,

would be useful. From ccRCC tissue samples we established primary cell cultures that at the early passages retain the phenotypic, genomic, transcriptomic and proteomic profile of the corresponding tissues, and therefore share many biological processes known to be important for ccRCC development and progression [15-18].

Here we aim to investigate how the specific inhibition of glycolysis or fatty acid oxidation affect the reduced pyridine nucleotide level and energy state and consequently the viability and proliferation of low- and high-grade ccRCC cells. The primary cell cultures from ccRCC of low- and high-grade, which retain the metabolic phenotype of the corresponding tissues, were essential for these purposes.

Results

The "clear cell" morphology of ccRCC tissues due to neutral lipid and glycogen storage is maintained in primary cell cultures

Hematoxylin/Eosin (HE) staining showed that ccRCC primary cell cultures maintained the typical vacuoles responsible for the "clear cell" morphology of corresponding ccRCC tissue. The "clear" vacuoles contained neutral lipids and glycogen, as proved by Oil Red O (ORO) and Periodic Acid-Schiff (PAS) staining respectively, in both ccRCC tissues and primary cell cultures (Figure 1).

Metabolic gene expression profile of ccRCC primary cultures

To highlight the metabolic signature of ccRCC primary cultures we revised our previously published gene expression microarray data, generated on a collection of ccRCC and normal cortex primary cultures, and corresponding Gene Ontology (GO) enrichment analysis [17] to focus on metabolic processes. In ccRCC primary cultures, we found a significant enrichment for 35 GO-biological process (BP) terms related to several classes of metabolic processes (Figure 2). The same GO enrichment analysis performed on publicly available ccRCC tissue transcriptomic data generated by RNAseq technology [19] evidenced that these 35 metabolic processes were also shared by tumor tissues (Figure 2). In particular, among them we found 12 GO-BP terms specifically related to carbohydrate and lipid metabolism. These metabolic processes were reported as characteristics of ccRCC biology even in other transcriptomic analyses performed on tissues [20].

These findings indicate that ccRCC primary cultures retained, on the whole, the metabolic gene profiling of tumor tissues, in particular the gene profiling of glucose and lipid metabolism, supporting the use of these cultures for accurate metabolic functional studies.

Lactate fermentation is upregulated in ccRCC primary cell cultures

To further improve the metabolic characterization of our cultures, we measured lactate dehydrogenase A (LDHA) expression and L-lactate production as probes for aerobic glycolysis/lactate fermentation. An increment of LDHA protein level, the enzyme involved in converting pyruvate to lactate, and both intracellular and secreted L-lactate was observed in our ccRCC cultures as compared with normal cortex cultures (Figure 3A and 3B). These data confirm that the aerobic glycolysis/lactate fermentation was upregulated in our ccRCC primary cell cultures, in agreement with the behavior of ccRCC tissues [9].

The storage of neutral lipids and glycogen and the production of lactate are grade-dependent in ccRCC primary cell cultures

Morphological evaluation of the lipid and glycogen storages in ccRCC primary cell cultures and corresponding tissues stratified on the basis of Fuhrman low-grade (G1-G2) and high-grade (G3-G4), showed a decrease of ORO-stained lipid droplets and PAS-stained glycogen content in higher grade ccRCC primary cultures and in the corresponding tissue samples (Figure 4A). These observations were quantitatively confirmed by the evaluation of intracellular glycogen content in tissue samples and primary cell cultures

(Figure 4B and 4D) and of ORO stained area in tissue slides (Figure 4C). The grade-dependent decrease of lipid storage was also quantitatively confirmed in primary cell cultures by analyzing the expression of PLIN2, the lipid droplet coat protein of non-adipose tissues described as a marker of intracellular neutral lipid storage [21]. PLIN2 transcript and protein expression was significantly lower in normal cortex with respect to ccRCC primary cell cultures (Figure 4E and 4F), and notably PLIN2 protein level was lower in high-grade compared to low-grade ccRCC cells.

Moreover, to evaluate whether in ccRCC cultures aerobic glycolysis/lactate fermentation was also grade-dependent, we assayed LDHA protein expression and lactate secretion of low-grade and high-grade ccRCC primary cultures. Western blot analysis showed that LDHA protein level was increased in all grade ccRCC cultures as compared with normal cortex cells (Figure 4G), but L-lactate was significantly more abundant in culture media of high-grade with respect to low-grade ccRCC cells (Figure 4H). This discrepancy between LDHA expression and lactate secretion may be due to the fact that the activity of an enzyme may change even without an alteration of its protein concentration, as also previously noted [9]. These data indicate that aerobic glycolysis/lactate fermentation was upregulated in our high-grade ccRCC primary cell cultures as described in high-grade ccRCC tissues [9].

2DG treatment decreases the lactate, ATP and reduced MTT dye level in ccRCC cultures of high-grade but the ATP level only in those of low-grade

To study whether glucose metabolism contributed to reduced pyridine nucleotide level and energy state of low-and high-grade ccRCC cells, we treated primary cultures with 5 mM 2-Deoxy-D-glucose (2DG). 2DG is known to be phosphorylated by hexokinase in the first step of glycolysis resulting in a non-hydrolysable substrate which accumulates in the cells and leads to inhibition of both glycolysis and pentose phosphate pathway [22]. After 24 hours of treatment the residual glucose level in the medium of normal cortex and ccRCC cultures was significantly higher than in corresponding control medium (Figure 5A) proving that 5 mM 2DG efficiently inhibited the first step of glycolytic pathway. As expected, the 2DG treatment did not induce a decrease of lactate secretion into the medium of normal cortex cultures (Figure 5B), supporting the notion that normal cells do not preferentially use lactate fermentation to metabolize glucose. Even in low-grade ccRCC cells 2DG did not decrease lactate production. Instead, 2DG treatment significantly decreased lactate secretion in high-grade cells (Figure 5B), confirming that the aerobic glycolysis/lactate fermentation is up-regulated in high-grade ccRCC primary cultures, as shown in Figure 4H. Moreover, treatment with 5 mM 2DG for 72 hours significantly affected the capability of normal cortex and high-grade but

not low-grade ccRCC cells to chemically reduce the 3-(4,5-dimethylthiazol-2-yl)- 2,5-diphenyltetrazolium (MTT) dye (Figure 5C). The bioreduction of MTT dye is a NAD(P)H-dependent process [23] and thus it can be used as probe for evaluating the changes in reduced pyridine nucleotide level (NADH and to a lesser extent NADPH) [24].

Twenty-four hours of 2DG treatment also significantly affected ATP level in normal cortex and both high- and low-grade ccRCC cells (Figure 5D). Thus, the treatment with 2DG induced a concomitant decrease of lactate, NAD(P)H and ATP level only in high-grade ccRCC cells, and these data highlight that glucose metabolism driven through aerobic glycolysis mainly contributed to reduced pyridine nucleotide level and energy state of these cells.

Etomoxir treatment decreases the ATP level in ccRCC cultures of high-grade and the reduced MTT dye level in those of low- grade

To evaluate whether lipid metabolism contributed to reduced pyridine nucleotide level and energy state of low-grade and high-grade ccRCC cells, we treated primary cultures with Etomoxir known to inhibit the mitochondrial fatty acid transporter Carnitine palmitoyl transferase 1 (CPT1), responsible for synthesis and import of fatty acylcarnitines across the outer mitochondrial membrane. The reaction catalysed by CPT1 is considered the rate-limiting step of fatty

acid β-oxidation [25]. It has been previously shown [9] that the treatment with 50 μM Etomoxir for 72 hours induced an increase of lipid storage in both normal cortex and ccRCC primary cultures, proving that this drug concentration efficiently inhibited CPT1 in our cells. Here we show that the treatment with 50 μM Etomoxir also significantly affected the capability of normal cortex and low-grade but not high-grade ccRCC cells to bioreduce MTT dye (Figure 6A), whereas 24 hours of Etomoxir treatment affected ATP level in normal cortex and high-grade but not in low-grade ccRCC cells (Figure 6B). These data highlight that the inhibition of fatty acid oxidation affected only the reduced pyridine nucleotide level in low-grade and only the energy state in high-grade ccRCC cells, suggesting a different grade-dependent metabolic function of β oxidation process in ccRCC.

Cell proliferation and viability is affected by 2DG in low-grade ccRCC cultures and by Etomoxir in those of high-grade

To evaluate whether the inhibition of glycolysis or fatty acid oxidation might have a cytostatic effect in our ccRCC cultures, we quantified the cells positive for the proliferation marker Ki67 after 72 hours of treatment with 2DG or Etomoxir. Both treatments significantly decreased cell proliferation in normal cortex and in low- and high-grade ccRCC cultures (Figures 7A and 7B).

Instead, the cell viability, evaluated by FACS after Annexin V/IP staining, was differently affected based on the metabolic treatment. 2DG induced a significant decrease of cell viability in normal cortex and low-grade ccRCC cultures (Figure 7C). In normal cortex cultures the viability dropped to 47% and the apoptotic cells raised from about 12% to 51%, in low-grade ccRCC cultures the viable cells decreased to 79% and the apoptotic cells raised from 15% to 19%. Etomoxir induced a significant decrease of viable cells in high-grade ccRCC cultures only, the viable cells decreased to 68% and the dead cells significantly raised from 19% to 23%. It is noteworthy that the inhibition of fatty acid oxidation did not affect the viability and just slightly the proliferation of normal cortex cells, whereas the inhibition of glycolysis severely affected both their viability and proliferation.

These data evidence that a cytostatic and cytotoxic effect can be obtained by inhibition of glycolysis in low-grade ccRCC cells and by inhibition of fatty acid oxidation in high-grade ccRCC cells. The extension of treatment until five days did not quantitatively increase the difference in viability between control and treated cells (data not shown).

Discussion

In this study we showed that ccRCC primary cell cultures maintained in early passages the cytological, transcriptomic and metabolic features of the original tumor tissues,

confirming the up-regulation of aerobic glycolysis/lactate fermentation. Our primary cultures also showed a grade-dependent modulation of lipid and glycogen storage and aerobic glycolysis/lactate fermentation, accordingly to the grade-dependent metabolic reprogramming described in ccRCC tissues [9], and highlighted their suitability as ccRCC *in vitro* model for metabolic studies. The metabolic treatments of these ccRCC primary cell cultures induced interesting modifications in their energy state, reduced pyridine nucleotide level, cell proliferation and viability.

The treatment with 2DG significantly affected the capability of high-grade ccRCC cells, but not low-grade, to chemically reduce the MTT dye. MTT assay was here used as probe for the evaluation of changes in cellular reduced pyridine nucleotide level, NADH and to a lesser extent NADPH [23-24], to which the mitochondrial TCA and β-oxidation pathways, but also glycolysis and the pentose phosphate pathway, contribute. In 2DG treated high-grade ccRCC cells the decrease of reduced MTT dye level, associated with the decrease of lactate secretion, suggests involvement of glucose metabolism driven through the aerobic glycolysis/lactate fermentation pathway in NAD(P)H production. In fact, in high-grade cells fatty acid oxidation did not appear relevant for NAD(P)H production because Etomoxir treatment did not significantly affect the cell capability to reduce MTT dye. Thus, in our high-grade ccRCC

cultures the glucose metabolic pathway had a peculiar role in NAD(P)H production, although not fuelled by the poor glycogen storage.

In low-grade ccRCC cells the poor production of lactate in spite of glucose consumption, and the unchanged lactate secretion after 2DG treatment, demonstrated that glucose underwent mitochondrial catabolism in these cells. Otherwise, in our low-grade ccRCC cells the use of mitochondrial metabolism was also evidenced by the significant decrease of reduced MTT dye after the treatment with Etomoxir that inhibits mitochondrial fatty acid metabolism. However, the fact that MTT data did not change after treatment of these cells with 2DG suggested that the mitochondrial metabolism of glucose contributed only marginally to the NAD(P)H production in low grade ccRCC cells.

2DG treatment in low-grade ccRCC cells significantly affected ATP production that instead was not affected by the inhibition of fatty acid oxidation with Etomoxir. This result together with the unchanged lactate secretion after 2DG treatment highlighted the importance of the mitochondrial metabolism of glucose for energy production that in these low-grade cells might be also fuelled by the large glycogen storage. In high-grade ccRCC cells ATP production was significantly affected by Etomoxir, other than 2DG, suggesting that these cells relied mainly on fatty acid

oxidation, other than on aerobic glycolysis/lactate fermentation, for ATP production. In fact, the decrease of ATP in high-grade cells, in presence of 2DG, evidenced that the poor glycogen storage was not enough for efficiently fuelling the aerobic glycolysis that resulted to be inadequate to sustain alone the energy balance in these cells. As expected, the treatment with 2-DG did not affect lactate production in normal cortex cultures but, like Etomoxir, induced a decrease of reduced MTT dye and ATP level. This result confirmed the well-known relevant role that both glucose and lipid metabolism have in normal cells for NAD(P)H production and ATP synthesis, through mitochondrial oxidative phosphorylation.

In our *in vitro* model the inhibition of glycolysis with 2DG affected the viability of normal cortex and low-grade ccRCC cells. Conversely, the inhibition of fatty acid oxidation by Etomoxir induced a significant decrease of viable cells in high-grade ccRCC cultures only, without affecting cortex cell viability. These cytotoxic effects might be due to the significant decrease of ATP production mainly obtained by fatty acid oxidation in high-grade ccRCC cells and by mitochondrial glucose metabolism in low-grade cells.

Even the decreased cell proliferation observed after 2DG or Etomoxir treatment might be due to the decrement of ATP. In particular, the cytostatic effect of Etomoxir agrees with data showing a cell cycle arrest in Caki-1 and 786-O ccRCC cell

lines treated with Peroxisome proliferator-activated receptor a (PPARa) antagonists [26] that, downregulating the PPARa target CPT1 [27], might in part reproduce the metabolic and functional effects of Etomoxir. In low-grade ccRCC cells the cytostatic effect of Etomoxir seems to correlate with the observed decrease of the NAD(P)H-dependent MTT dye reduction. In cancer cells it is well known that fatty acid oxidation is relevant, through metabolic pathways fuelled by cytosolic citrate, to the production of NADPH involved in the synthesis of membrane fatty acids during cell proliferation [28]. The decrease of reduced MTT dye level, observed in 2DG treated high-grade ccRCC cells, might in part justify, through the same mechanism, the cytostatic effect in these cells.

Therefore, our data evidenced that in high-grade ccRCC cells fatty acid oxidation mainly, but also aerobic glycolysis, are important for energy production, whereas glucose metabolism uniquely contributes to the reduced pyridine nucleotide level. Instead, in low-grade ccRCC cells the fatty acid oxidation appeared to control the reduced pyridine nucleotide level, while the mitochondrial glucose metabolism controlled the cell energy state.

It is of note that the prevalent aerobic glycolysis (Warburg effect) and the active β-oxidation of our high-grade ccRCC cells have a strict link with the nuclear morphological features of high-grade Fuhrman classification, which are

characteristic of cycling or immature cells [29] and correlate with the more aggressive behavior of high-grade ccRCC tumor that has the worst prognosis [5]. The Fuhrman grade and the cell proliferation/cycling characteristics correlate even in our primary cell cultures in which a larger percentage of Ki-67 positive cells was measured in high-grade with respect to low-grade ccRCC cultures (33% versus 18%). In addition, the metabolic characteristics of our high-grade ccRCC cells justify the described higher 18F-fluorodeoxyglucose uptake of high-grade ccRCC [30] with respect to the low-grade tumors that likely relay on a prevalent oxidative mitochondrial metabolism as the normal cortex cells.

Our findings indicate that the Warburg effect is not a common feature shared by all ccRCC, and the β-oxidation can be activated for different metabolic needs in ccRCC of different grade. Our data also support the current trend that underline the importance of the classification of malignancies even on the basis of metabolic pathway alterations [31]. This trend will promote the use of metabolism reprogramming to open novel opportunities for new diagnostic and therapeutic options [32]. The cytotoxic effect that we observed exclusively in high-grade ccRCC cells and not in normal cortex cells after the inhibition of fatty acid oxidation, can be a strong incentive to attempt a metabolic grade-dependent therapeutic approach, not investigated yet in ccRCC [14].

Materials and methods

Tissues

Tumor (*n*=56) and normal kidney (*n*=36) tissues were obtained from 56 patients following nephrectomy due to the presence of ccRCC. The tissues collected were those exceeding the diagnostic needs. The normal cortex was taken from a healthy region of the kidney, without any indication of cancer. All procedures were performed after written consent and were approved by the Local Ethical Committee.

The clinico-pathological characteristics of enrolled ccRCC patients, reported in Table 1, also included the pathological stage and Fuhrman grade, according to 2004 World Health Organization classification.

Primary cell cultures

Primary cell cultures were obtained from normal cortex and tumor tissues, the culture conditions and immunophenotypic characterization were performed as described [15]. The primary cell cultures were used at the first confluence.

Tissue and primary cell culture staining

HE and PAS staining were conducted on formalin fixed and paraffin-embedded tissue sections, following standard protocols [33], and on first-confluent primary cell cultures grown on glass coverslips and fixed in 10% formalin for 1 hour. ORO staining was performed on cryostat tissue

sections and on formalin fixed cultures, as described [9]. The stained samples were analyzed by Nikon Eclipse E800 microscope with 10×, 20× and 40× objectives (Nikon Instruments spa, Firenze, Italy). Three/ four pictures for each slide were randomly captured and analyzed by LuciaG Image analysis system (Nikon). Lipid storage quantification was obtained by analysis, with ImageJ software (NIH, Bethesda, MD), of ORO stained tissue pictures captured at 100× magnification.

Gene expression microarray profiling

ccRCC and normal cortex primary cultures were characterized for transcriptome profile by microarray technology on Affymetrix GeneChip Human Exon 1.0 ST Arrays (Affymetrix, Santa Clara, CA, USA), as we previously described [17]. CEL files are available at Array Express repository under accession number E-MTAB-4074 (http://www.ebi.ac.uk/arrayexpress/ experiments/E-MTAB-4074/). The differentially expressed genes (DEGs) between ccRCC and cortex cultures were calculated using Partek Genomic Suite software (Partek Inc., St. Louis, MO) by ANOVA method. Gene Ontology biological processes (GO-BP) significantly enriched in our ccRCC cultures were identified by ToppGene suite (https://toppgene.cchmc.org/). ToppCluster tool (https:// toppcluster.cchmc.org/) was used to compare the GO-BP enriched in our ccRCC cultures to

those enriched in ccRCC tissues obtained from the RNA-seq DEG list reported by Wozniak *et al*. [19].

RNA extraction and real-time PCR

Total RNA extraction and reverse transcription (RT) were carried out as previously described [34]. Real-time PCR was performed with TaqMan Gene Expression Assay kits for PLIN2 transcript (Hs 00605340_m1) and for GAPDH (Hs99998805_m1 kit) according to manufacturer's instructions (Applied Biosystems, Foster City, CA). The amplifications were carried out in 20 µl reactions containing 100 ng of cDNA, 1X Universal PCR Master Mix, and corresponding primers and probes, in duplicate for each sample on an ABI PRISM® 7900HT Fast Real-Time PCR System (Applied Byosystems). PLIN2 transcript levels were represented as relative expression ($2^{-\Delta\Delta CT}$) with respect to normal cortex samples.

Protein extraction and western blot analysis

Thirty µg of protein lysates obtained from first-confluent primary cell cultures, quantified with BCA microassay (Sigma Aldrich, St. Louis, MO) and separated on NuPage 4 to 12% Bis-Tris pre-cast gels (Thermo Fisher, Waltham, MA) [35], were submitted to western blotting [36] with mouse monoclonal antibody against PLIN2 (dilution 1:500; AP125, Progen, Heidelberg, Germany), or rabbit polyclonal antibody

against LDHA (dilution 1:1000; Cell Signaling, Boston, MA), or against β-actin (dilution 1:1000; Sigma-Aldrich). Densitometric analysis of specific bands was performed by ImageJ software, and the specific band intensities were normalized with corresponding β-actin for quantification.

Glycogen quantification

Intracellular glycogen content was quantified in tissue homogenates and first-confluent primary cell culture lysates using a Glycogen Assay kit (Biovision, Milpitas, CA) following the manufacturer's instructions. Data were expressed as µg per µg of total protein content.

Metabolic treatments

An equal number of normal cortex and ccRCC cells from first-confluent primary cultures were plated and grown for 24 hours in culture medium (complete DMEM medium containing 5 mM glucose). The cells were then washed with PBS and incubated for 24 or 72 hours in culture medium with 5 mM 2-Deoxy-D-glucose 2DG, or 50 µM Etomoxir (Sigma-Aldrich).

Lactate quantification

Untreated first-confluent cells were lysed in 50 µl H_2O and centrifuged to remove the insoluble debris. Twenty µl of the cellular soluble fraction lysate, and of conditioned culture

medium of untreated or 24 hour 2DG treated cells, were respectively diluted in 1 ml pre-filled reaction cup containing Glucose/Lactate hemolyzing solution (Biosen, EFK diagnostics, Cardiff, England) and assayed for L-lactate content by a lactate analyzer (BiosenC-Line, EKF diagnostics). Concentration values were normalized for viable cell count or, when indicated, for cell protein concentration.

Glucose quantification

Five hundred µl of conditioned medium of untreated or 24 hour 2DG treated cells were collected, spinned for 5 min to eliminate floating cells and debris, and assayed for glucose content using Roche COBAS 8000 analyzer (Roche diagnostics spa, Monza, Italy). Values were normalized for viable cell count and expressed as percentage with respect to 2DG treated cells.

MTT assay

Quantification of the NAD(P)H-dependent capability of cells to reduce MTT dye in presence or absence of metabolic treatment was measured by MTT assay (Sigma-Aldrich) [37]. Briefly, 1×10^4 cells were plated in 96-well plates, and after 72 hour of 2DG or Etomoxir treatment the cells were incubated in MTT solution. After 3 hours, the MTT solution was removed, and the blue crystalline precipitate in each well was

dissolved in DMSO. Absorbance of each well at 570 nm was quantified using the microplate reader Victor Wolla C1420 (Perkin Elmer, Woltham, MA) and expressed as percentage with respect to untreated cells.

ATP quantification

Quantification of cellular ATP content in presence or absence of metabolic treatment was measured using ATP Bioluminescence Assay Kit CLS II (Roche Diagnostics, Mannheim Germany). 1.5×10^5 cells were plated in 12-well plates and treated for 24 hours with 2DG or Etomoxir. ATP content was quantified using the microplate luminometer Victor Wolla C1420 (Perkin Elmer) according to manufacturer's instructions. Data normalized for cell protein concentration were expressed as percentage with respect to untreated cells.

Ki67 immunofluorescence staining

To assess the effect of metabolic treatments on cell proliferation of ccRCC and normal cortex primary cultures 1×10^5 cells seeded onto coverslips were treated with 2DG or Etomoxir for 72 hours. Immunofluorescence staining was performed using mouse monoclonal antibody against Ki67 (1:75 dilution; Clone MIB-1; DAKO, Glostrup, Denmark) and Alexa Fluor 488 goat anti-mouse polyclonal secondary antibody (1:100 dilution; Molecular Probes, Carlsberg, CA) as previously described [15]. Nuclei were counterstained with

DAPI. For each treatment, Ki67 positive nuclei were quantified in at least five immunofluorescence micrographs, obtained at 400x magnification using a Zeiss LSM710 confocal microscope and Zen2009 software (Zeiss, Oberkochen, Germany), and normalized by total nuclei. Normalized Ki67 positive cells in treated samples were expressed as percentage of corresponding untreated samples.

Cell viability assay

Cell viability of metabolically treated ccRCC and normal cortex primary cultures was assessed. 2.5×10^5 cells were seeded in 6-well plates and treated with 2DG or Etomoxir for 72 hours. Cell viability was evaluated with FITC Annexin V Apoptosis detection kit and Propidium Iodide (PI) (Biolegend, San Diego, CA) according to the manufacturer's instructions. Briefly, after two washes with cold PBS, the cells were resuspended in 100 µl of Annexin V Binding Buffer. The cell solution was then incubated with 5 µl of FITC Annexin V and 10 µl of PI for 15 minutes at room temperature in the dark. After the incubation, 200 µl of Annexin V Binding Buffer were added. FACS analysis was performed on 10000 events with MoFlo Astrios Cell Sorter and Kaluza software (Beckman Coulter srl, Milano, Italy). Viable (Annexin V and PI negative), dead (PI positive) and apoptotic (Annexin V positive) cells in

treated and untreated samples were expressed as percentage with respect to total number of analysed events.

Statistical analysis

Data were analysed using unpaired Student's *t*-test or, where indicated, by paired Student's *t*-test. The results were expressed as mean ± SEM. *P*-values < 0.05 were considered as statistically significant.

Acknowledgments

We thank Massimiliano Cadamuro (Milano- Bicocca University, Monza) for providing Ki67 antibody and Nikon microscope, Francesca Lanfranconi (Milano- Bicocca University, Monza) for assistance with lactate quantification, Rinaldo Brivio (San Gerardo Hospital, Monza) for assistance with glucose quantification and Tatz Ishimaru (University of California, Davis) for critical revision of the manuscript.

Figure Legends

Figure 1: ccRCC primary cell cultures maintain the lipid and glycogen storage of tissues. Representative images of normal cortex and ccRCC tissue sections and primary cell cultures after Haematoxylin/Eosin (HE), Oil Red O (ORO) and Periodic Acid-Schiff (PAS) staining captured at original magnification of 200× (scale bar: 100 μm) and 400× (scale bar: 50 μm).

Figure 2: Enrichment for GO biological processes related to metabolism in ccRCC primary cultures and tissues. The 35 significant metabolic GO-BP terms shared between cultures (black bars) and tissues (white bars) are represented. The -log *P* value (-log*P*) represents the significance level. The twelve GO-BP terms specifically related to carbohydrate and lipid metabolism are indicated in bold.

Figure 3: Lactate production is upregulated in ccRCC primary cell cultures. (A) Representative western blot of normal cortex (*n*=2) and ccRCC (*n*=3) primary cell culture, showing LDHA and β-actin proteins. In the graph, the normalized LDHA band intensities of normal cortex (*n*=7) and ccRCC (*n*=19) primary cell cultures are shown. **(B)** Lactate quantification performed in cell lysates (cells) and conditioned culture medium (media) of normal cortex (*n*=6) and ccRCC (*n*=7) primary cultures. Lactate concentration values were normalized to cell protein concentration. Data expressed as mean ± SEM; **p* < 0.05.

Figure 4: Neutral lipid and glycogen storage is decreased and lactate production increased in high-grade ccRCC primary cultures. (A) Representative images of low-grade and high-grade ccRCC tissue sections and matched primary cell cultures after Oil Red O (ORO) and Periodic Acid-Schiff

(PAS) staining captured at original magnification of 200× (scale bar: 100 μm). **(B)** Glycogen quantification performed in normal cortex (*n*=4), low-grade (*n*=7) and high-grade (*n*=8) ccRCC tissue samples. **(C)** Neutral lipid quantification in ORO stained slides of normal cortex (*n*=3), low-grade (*n*=7) and high-grade (*n*=8) ccRCC tissue samples. ORO area was quantified in three to six fields per slides and expressed as percentage of total area analyzed. **(D)** Glycogen quantification performed in normal cortex (*n*=3), low-grade (*n*=4) and high-grade (*n*=3) ccRCC primary cultures. **(E)** Real-time PCR analysis of PLIN2 expression performed in normal cortex (*n*=15), low-grade (*n*=11) and high-grade (*n*=9) ccRCC primary cultures. Box and whiskers plot corresponds to 1-99th percentiles (bars), 25-75th percentiles (box), and median (line in box). **(F)** Representative western blot of three different normal cortex, low-grade and high-grade ccRCC primary cell cultures showing the PLIN2 and β-actin proteins. The graph shows the normalized PLIN2 band intensities of normal cortex (*n*=8), low-grade (*n*=8) and high-grade (*n*=7) ccRCC primary cultures. To evidence the difference between normal cortex and all ccRCC cultures, in B-F panels the average of low and high-grade ccRCC data is also reported. **(G)** Representative western blot of three different normal cortex, low-grade and high-grade ccRCC primary cell cultures showing the LDHA and β-actin proteins. The graph shows the normalized LDHA band intensities of normal

cortex (*n*=7), low-grade (*n*=11) and high-grade (*n*=8) ccRCC primary cultures. **(H)** Lactate quantification performed in conditioned culture medium of normal cortex (*n*=5), low-grade (*n*=4) and high-grade (*n*=3) ccRCC primary cultures. Data expressed as mean ± SEM; **p* < 0.05.

Figure 5: Metabolic effect of 2DG treatment in low- and high-grade ccRCC and normal cortex primary cultures. **(A)** Glucose quantification performed in conditioned culture medium of normal cortex (*n*=3), low-grade (*n*=4) and high-grade (*n*=3) ccRCC primary cultures treated for 24 hours with 5 mM 2DG. **(B)** Lactate quantification performed in conditioned culture medium of normal cortex (*n*=4), low-grade (*n*=3) and high-grade (*n*=3) ccRCC primary cultures treated for 24 hours with 5 mM 2DG. **(C)** Quantification of reduced MTT dye performed by MTT assay in normal cortex (*n*=4), low-grade (*n*=9) and high-grade (*n*=5) ccRCC cultures treated for 72 hours with 5 mM 2DG. **(D)** Quantification of ATP content in normal cortex (*n*=3), low-grade (*n*=5) and high- grade (*n*=4) ccRCC cultures treated for 24 hours with 5mM 2DG. All data are represented as percentage with respect to corresponding control (untreated) cells considered equal to 100%, except for panel A in which the treated cells are considered equal to 100%. Data expressed as mean ± SEM; **p* < 0.05.

Figure 6: Metabolic effect of Etomoxir treatment in low- and high-grade ccRCC and normal cortex primary cultures. (A) Quantification of reduced MTT dye performed by MTT assay in normal cortex (*n*=10), low-grade (*n*=11) and high-grade (*n*=13) ccRCC cultures treated for 72 hours with 50 µM Etomoxir. **(B)** Quantification of ATP content in normal cortex (*n*=3), low-grade (*n*=4) and high-grade (*n*=4) ccRCC cultures treated for 24 hours with 50 µM Etomoxir. Data, expressed as mean ± SEM, are represented as percentage with respect to corresponding control (untreated) cells; **p* < 0.05.

Figure 7: Cell proliferation and viability of low- and high-grade ccRCC and normal cortex primary cultures treated with 2DG or Etomoxir. (A-B) Quantification of cellular proliferation evaluated as Ki67 positive cells after immunofluorescence staining in normal cortex (*n*=3), low-grade (*n*=4) and high-grade (*n*=5) ccRCC cultures treated for 72 hours with 5 µM 2DG (A) or 50 µM Etomoxir **(B)**. Data, obtained in at least five 400x micrographs per sample, were represented as percentage with respect to corresponding control (untreated) samples; **p* < 0.05. **(C-D)** Representative images of FACS analysis of cell viability evaluated with Annexin V/propidium iodide in normal cortex (*n*=4), low-grade (*n*=4) and high-grade (*n*=5) ccRCC cultures treated for 72 hours with 5mM 2DG **(C)** or 50 µM Etomoxir **(D)**. Percentages

of viable cells (bottom left quadrant of each plot) are indicated; *p < 0.05, paired Student's t-test. Data are expressed as mean ± SEM.

Figure 1

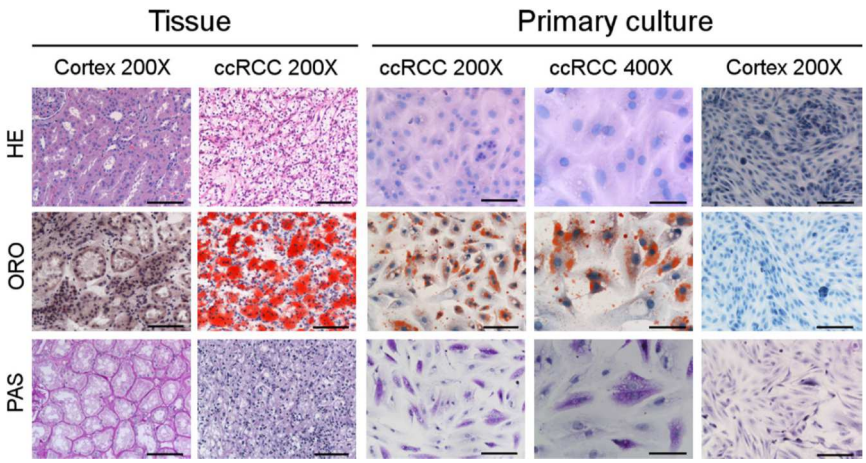
Tissue
Primary culture
Cortex 200X
ccRCC 200X
ccRCC 200X
ccRCC 400X
Cortex 200X
HE
ORO
PAS

Figure 2

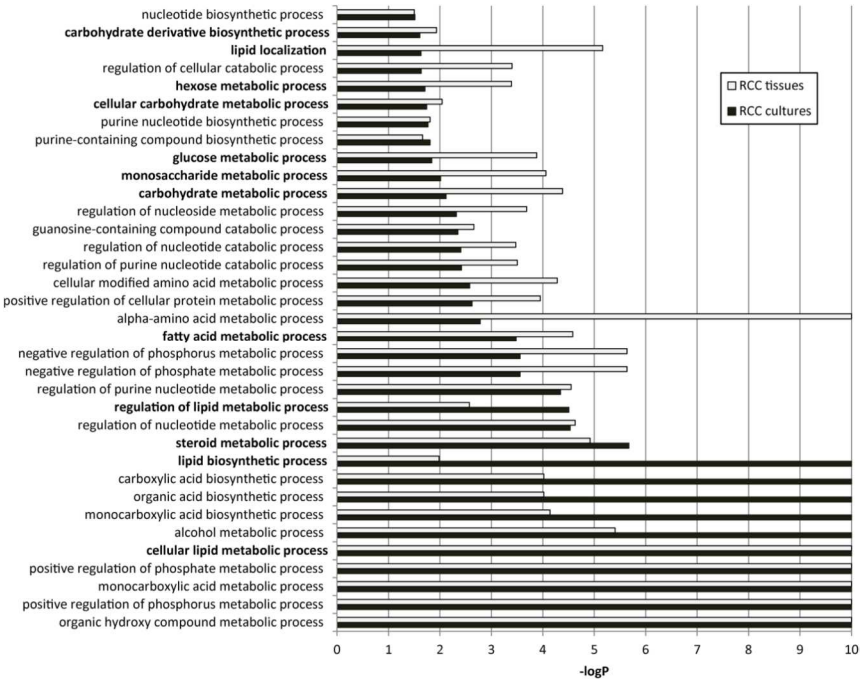
nucleotide biosynthetic process
carbohydrate derivative biosynthetic process
lipid localization
regulation of cellular catabolic process
hexose metabolic process
cellular carbohydrate metabolic process
purine nucleotide biosynthetic process
purine-containing compound biosynthetic process
glucose metabolic process
monosaccharide metabolic process
carbohydrate metabolic process
regulation of nucleoside metabolic process
guanosine-containing compound catabolic process
regulation of nucleotide catabolic process
regulation of purine nucleotide catabolic process
cellular modified amino acid metabolic process
positive regulation of cellular protein metabolic process
alpha-amino acid metabolic process
fatty acid metabolic process
negative regulation of phosphorus metabolic process
negative regulation of phosphate metabolic process
regulation of purine nucleotide metabolic process
regulation of lipid metabolic process
regulation of nucleotide metabolic process
steroid metabolic process
lipid biosynthetic process
carboxylic acid biosynthetic process
organic acid biosynthetic process
monocarboxylic acid biosynthetic process
alcohol metabolic process
cellular lipid metabolic process
positive regulation of phosphate metabolic process
monocarboxylic acid metabolic process
positive regulation of phosphorus metabolic process
organic hydroxy compound metabolic process
RCC tissues
RCC cultures
0
1
2
3
4
5
6
7
8
9
10
-logP

Figure 3

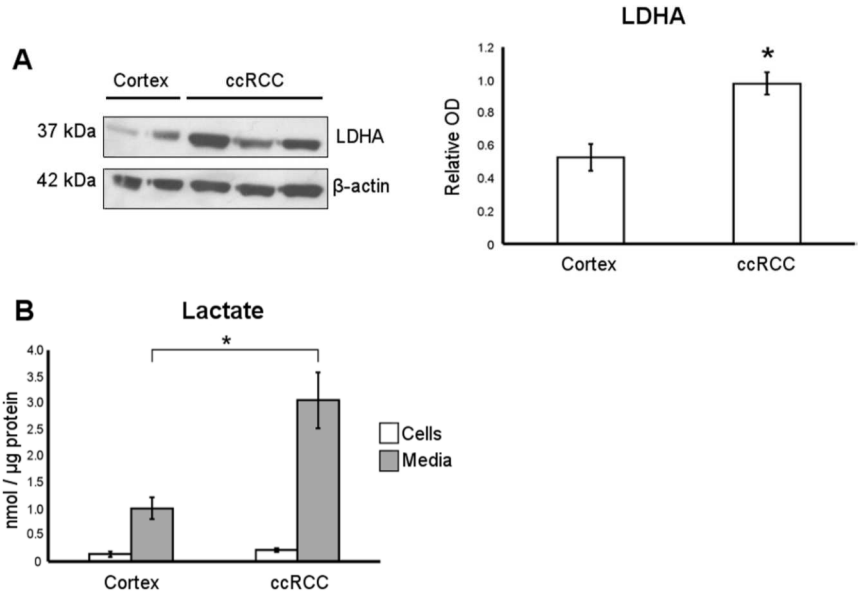
A
Cortex
ccRCC
37 kDa
LDHA
42 kDa
β-actin
LDHA
Relative OD
1.2
1.0
0.8
0.6
0.4
0.2
0
*
Cortex
ccRCC
B
Lactate
nmol / µg protein
4.0
3.5
3.0
2.5
2.0
1.5
1.0
0.5
0
*
Cells
Media
Cortex
ccRCC

Figure 4

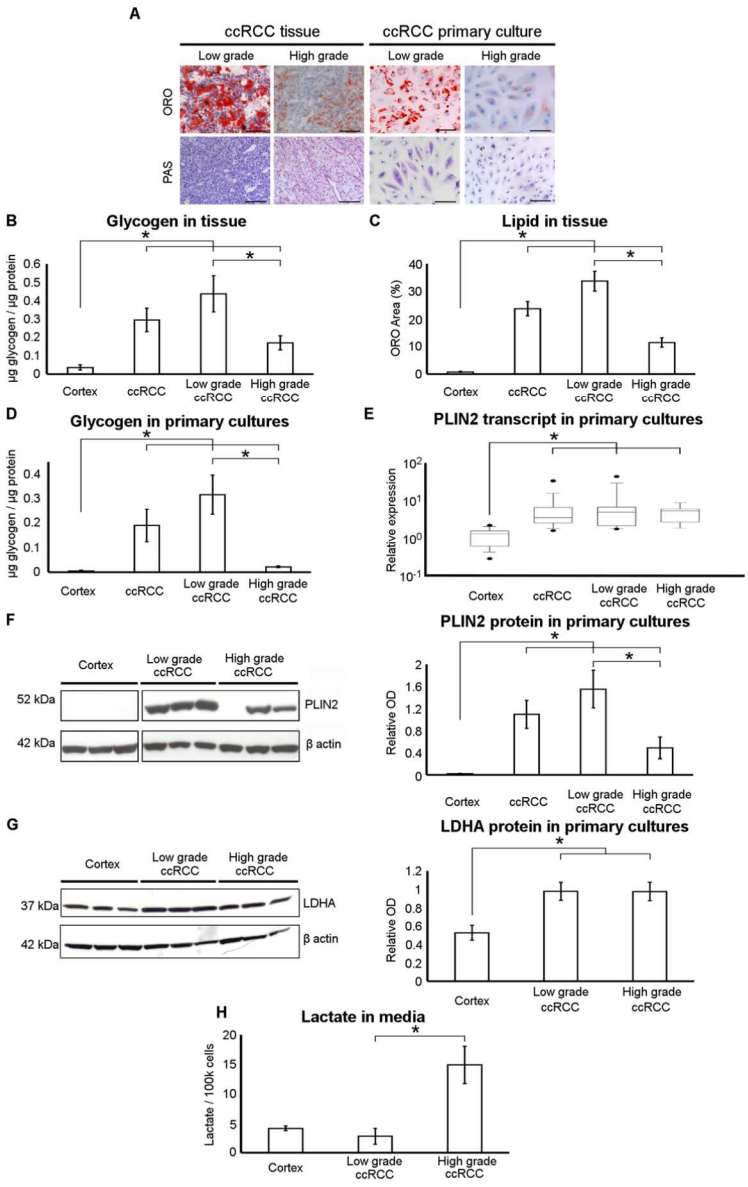
A
ccRCC tissue
ccRCC primary culture
Low grade
High grade
Low grade
High grade
ORO
PAS
B
Glycogen in tissue
µg glycogen / µg protein
Cortex
ccRCC
Low grade ccRCC
High grade ccRCC
C
Lipid in tissue
ORO Area (%)
D
Glycogen in primary cultures
E
PLIN2 transcript in primary cultures
Relative expression
F
PLIN2 protein in primary cultures
Relative OD
52 kDa
PLIN2
42 kDa
β actin
G
LDHA protein in primary cultures
37 kDa
LDHA
H
Lactate in media
Lactate / 100k cells

Figure 5

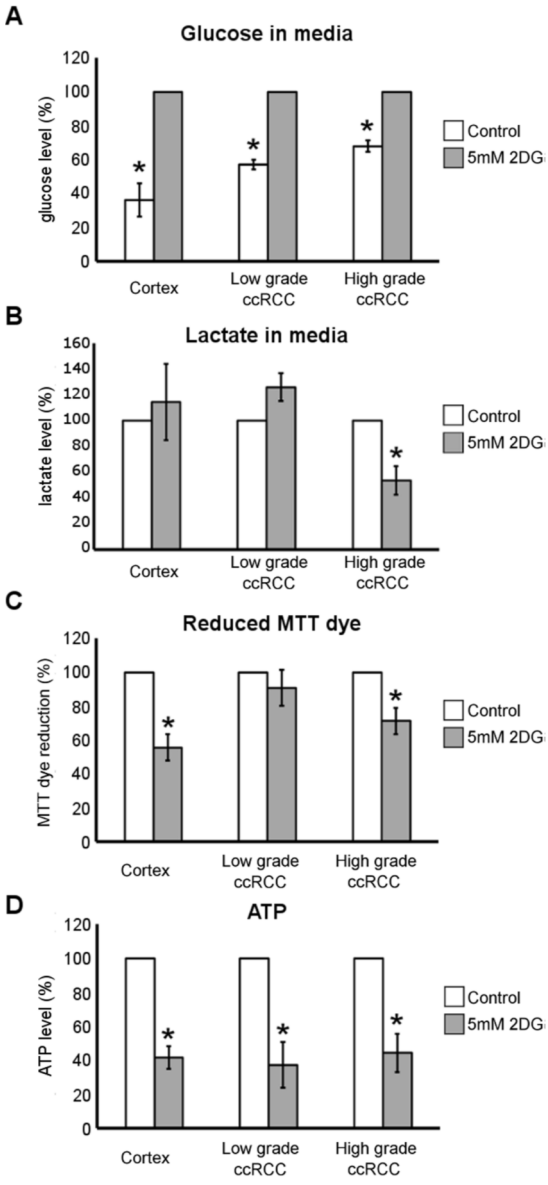
A
Glucose in media
glucose level (%)
120
100
80
60
40
20
0
*
*
*
Control
5mM 2DG
Cortex
Low grade ccRCC
High grade ccRCC
B
Lactate in media
lactate level (%)
160
140
120
100
80
60
40
20
0
*
Control
5mM 2DG
Cortex
Low grade ccRCC
High grade ccRCC
C
Reduced MTT dye
MTT dye reduction (%)
120
100
80
60
40
20
0
*
*
Control
5mM 2DG
Cortex
Low grade ccRCC
High grade ccRCC
D
ATP
ATP level (%)
120
100
80
60
40
20
0
*
*
*
Control
5mM 2DG
Cortex
Low grade ccRCC
High grade ccRCC

Figure 6

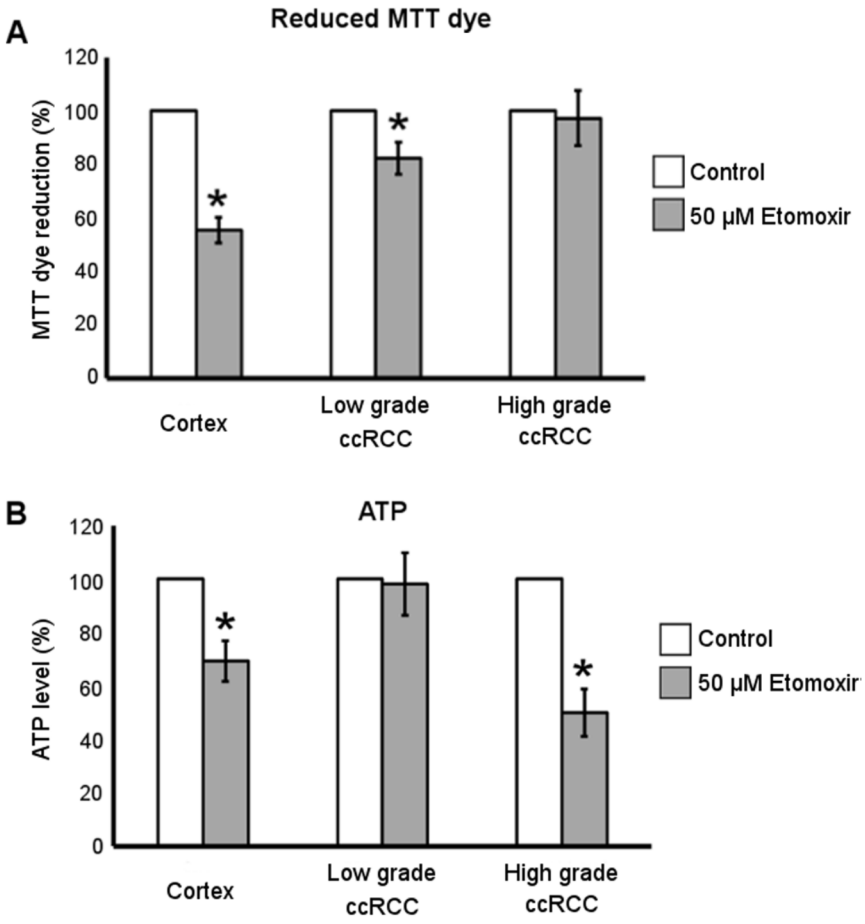
A
Reduced MTT dye
MTT dye reduction (%)
120
100
80
60
40
20
0
*
*
Control
50 µM Etomoxir
Cortex
Low grade ccRCC
High grade ccRCC
B
ATP
ATP level (%)
120
100
80
60
40
20
0
*
*
Control
50 µM Etomoxir
Cortex
Low grade ccRCC
High grade ccRCC

Figure 7

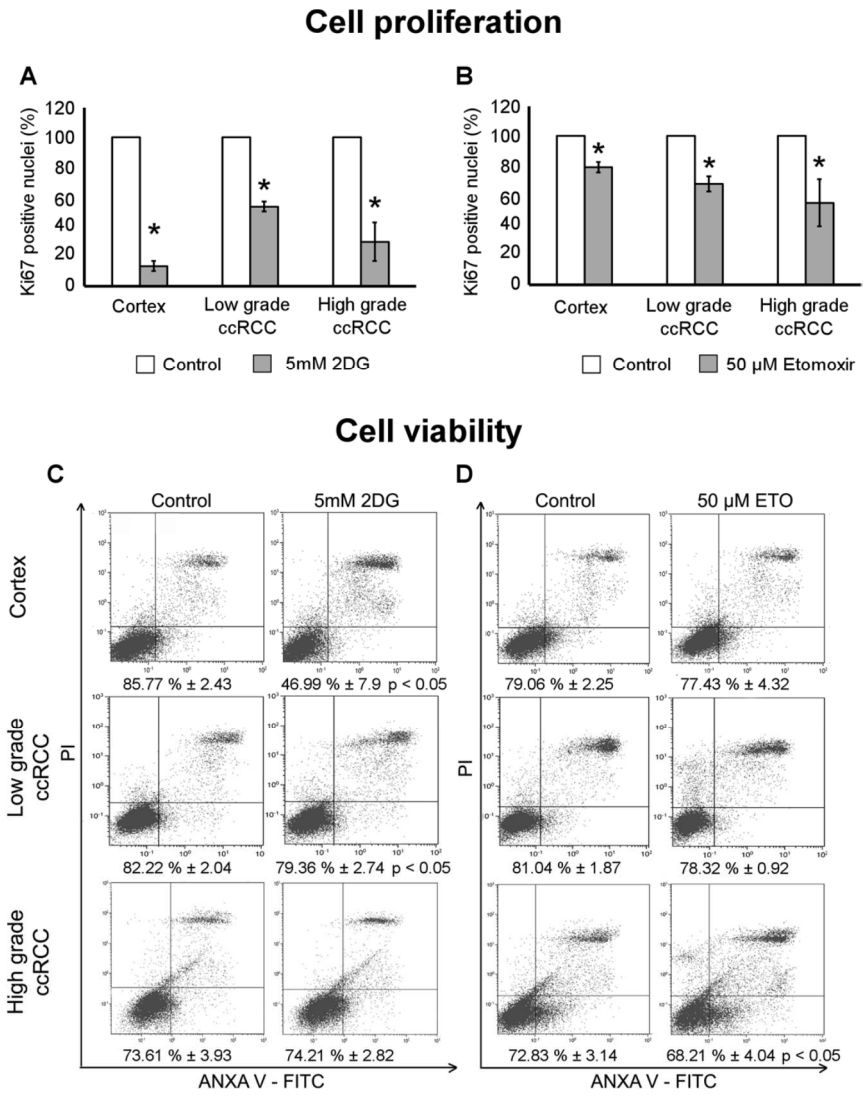
Cell proliferation
A
Ki67 positive nuclei (%)
120
100
80
60
40
20
0
Cortex
Low grade ccRCC
High grade ccRCC
Control
5mM 2DG
B
Ki67 positive nuclei (%)
Cortex
Low grade ccRCC
High grade ccRCC
Control
50 µM Etomoxir
Cell viability
C
Control
5mM 2DG
Cortex
Low grade ccRCC
High grade ccRCC
PI
85.77 % ± 2.43
46.99 % ± 7.9 p < 0.05
82.22 % ± 2.04
79.36 % ± 2.74 p < 0.05
73.61 % ± 3.93
74.21 % ± 2.82
ANXA V - FITC
D
Control
50 µM ETO
PI
79.06 % ± 2.25
77.43 % ± 4.32
81.04 % ± 1.87
78.32 % ± 0.92
72.83 % ± 3.14
68.21 % ± 4.04 p < 0.05
ANXA V - FITC

Table 1: Clinicopathological variables of 56 ccRCC cases analyzed in the study

Variable	n (%)
Age (years)	
median	71
range	41-86
Gender	
male	37 (66.1)
female	19 (33.9)
Tumor size (cm)	
median	4.5
range	2-10
Pathological stage	
pT1a	13 (23.2)
pT1b	12 (21.4)
pT2	10 (17.9)
pT3a	21 (37.5)
pN+	1 (1.8)
cM+	3 (5.4)
Fuhrman grade	
G1-2	32 (57.1)
G3-4	24 (42.9)

References

1. Hsieh JJ, Purdue MP, Signoretti S, Swanton C, Albiges L, Schmidinger M, Heng DY, Larkin J, Ficarra V. Renal cell carcinoma. Nature Rev Dis Primers. 2017; 3:17009.

2. Wei EY, Hsieh JJ. A river model to map convergent cancer evolution and guide therapy in RCC. Nature Rev Urol. 2015; 12:706-711.

3. Diekstra MHM, Swen JJ, Gelderblom H, Guchelaar HJ. A decade of pharmacogenomics research on tyrosine kinase inhibitors in metastatic renal stem cancer: a systematic review. Expert Rev Mol Diagn. 2016; 16:605-618.

4. Albiges L, Choueiri TK. Advances in treatment jostling for pole position. Nature Rev Clin Oncol. 2017; 14:82-84.

5. Sun M, Lughezzani G, Jeldres C, Isbarn H, Shariat SF, Arjane P, Widmer HD, Pharand DD, Latour M, Perrotte PD, Patard JJE, Karakiewicz PIA. A proposal for reclassification of the Fuhrman grading system in patients with clear cell Renal Cell Carcinoma. Eur Urol. 2009; 56:775-781.

6. Gebhard RL, Clayman RV, Prigge WF, Figenshau RT, Staley NA, Reesey C, Beart A. Abnormal cholesterol metabolism in renal clear cell carcinoma. J Lipid Res. 1987; 28:1177-1184.

7. The Cancer Genome Atlas Research Network. Comprehensive molecular characterization of clear cell renal cell carcinoma. Nature. 2013; 499:43-49.

8. Hakimi AA, Reznik E, Lee CH, Cheng EH, Sander C, Hsieh JJ. An integrated metabolic atlas of clear cell renal cell carcinoma. Cancer Cell. 2016; 29:104-116.

9. Wettersten H, Hakimi AA, Morin D, Bianchi C, Johnstone ME, Donohoe DR, Trott JF, Abu Aboud O, Stirdivant S, Neri B, Wolfert R, Stewart B, Perego R, et al. Grade-dependent metabolic reprogramming in kidney cancer revealed by combined proteomics and metabolomics analysis. Cancer Res. 2015; 75:2541-2552.

10. Neely BA, Wilkins CF, Marlow CA, Malyarenko D, Kim Y, Ignatchenko A, Sasinowska M, Sasinowski M, Nyalwidhe JO, Kislinger T, Copland JA, Drake RR. Proteotranscriptomic analysis reveals stage specific changes in the molecular landscape of Clear-Cell Renal Cell Carcinoma. PLOS One. 2016; 11:e0154074.

11. Gatto F, Nookaew I, Nielsen J. Chromosome 3p loss of heterozygosity is associated with a unique metabolic network in clear cell renal carcinoma. Proc Natl Acad Sci. 2014; 111:E866-E875.

12. Zhao Z, Lu J, Han L, Wang X, Man Q, Liu S. Prognostic significance of two lipid metabolism enzymes, HADHA and ACAT2, in clear cell renal cell carcinoma. Tumor Biol. 2016; 37:8121-8130.

13. Perroud B, Ishimaru T, Borowsky AD, Weiss RH. Grade-dependent proteomics characterization of kidney cancer. Mol Cell Proteomics. 2009; 8:971-985.

14. van der Mijn JC, Panka DJ, Geissler AK, Verheul HM, Mier JW. Novel drugs that target the metabolic reprogramming in renal cell cancer. Cancer & Metabolism. 2016; 4:14-18.

15. Bianchi C, Bombelli S, Raimondo F, Torsello B, Angeloni V, Ferrero S, Di Stefano V, Chinello C, Cifola I, Invernizzi L, Brambilla P, Magni F, Pitto M, et al. Primary cell cultures from human renal cortex and renal cell carcinoma evidence a differential expression of two spliced isoforms of Annexin A3. Am J Pathol. 2010; 176:1660-1670.

16. Cifola I, Bianchi C, Mangano E, Bombelli S, Frascati F, Fasoli E, Ferrero S, Di Stefano V, Zipeto MA, Magni F, Signorini S, Battaglia C, Perego RA. Renal cell carcinoma primary cultures maintain genomic and phenotypic profile of parental tumor tissues. BMC Cancer. 2011; 11:244.

17. Di Stefano V, Torsello B, Bianchi C, Cifola I, Mangano E, Bovo G, Cassina V, De Marco S, Corti R, Meregalli C, Bombelli S, Viganò P, Battaglia C, et al. Major action of endogenous lysyl oxidase in clear cell renal cell carcinoma progression and collagen stiffness revealed by primary cell cultures. Am J Pathol. 2016; 186:2473-2485.

18. Perego RA, Bianchi C, Corizzato M, Eroini B, Torsello B, Valsecchi C, Di Fonzo A, Cordani N, Favini P, Ferrero S, Pitto M, Sarto C, Magni F, et al. Primary cell cultures arising from normal kidney and renal cell carcinoma retain the proteomic profile of corresponding tissues. J Proteome Res. 2005; 4:1503-1510.

19. Wozniak MB, Le Calvez-Kelm F, Abedi-Ardekani B, Byrnes G, Durand G, Carreira C, Michelon J, Janout V, Holcatova I, Foretova L, Brisuda A, Lesueur F, McKay J, et al. Integrative Genome-Wide Gene Expression Profiling of Clear Cell Renal Cell Carcinoma in Czech Republic and in the United States. PLOS One. 2013; 8:e57886.

20. Tun HW, Marlow LA, von Roemeling CA, Cooper SJ, Kreinest P, Wu K, Luxon BA, Sinha M, Panos Z. Anastasiadis PZ, Copland JA. Pathway signature and cellular differentiation in clear cell renal cell carcinoma. PLOS One. 2010; 5:e10696.

21. Greenberg AS, Coleman RA, Kraemer FB, McManaman JL, Obin MS, Puri V, Yan QW, Miyoshi H, Mashek DG. The role of lipid droplets in metabolic disease in rodents and humans. J Clin Inv. 2011; 121:2102-2110.

22. Pelicano H, Martin DS, Xu RH, Huang P. Glycolysis inhibition for anticancer treatment. Oncogene. 2006; 25:4633-4646.

23. Berridge MV, Tan AS, McCoy KD, Wang R. The biochemical and cellular basis of cell proliferation assays that use tetrazolium salts. Biochemica. 1996; 4:14-19.

24. Marshall NJ, Goodwin CJ, Holt SJ. A critical assessment of the use of microculture tetrazolium assay to measure cell growth and function. Growth Regul. 1995; 5:69-74.

25. Schreurs M, Kuipers F, van der Leij FR. Regulatory enzymes of mitochondrial b-oxidation as targets for treatment of the metabolic syndrome. Obesity Rev. 2010; 11:380-388.

26. Abu Aboud O, Wettersten HI, Weiss RH. Inhibition of PPARa induces cell cycle arrest and apoptosis, and synergizes with glycolysis inhibition in kidney cancer cells. PLOS one. 2013; 8:e71115.

27. Zhang YF, Yuan ZQ, Song DG, Zhou XH, Wang YZ. Effects of cannabinoid receptor 1 (brain) on lipid accumulation by transcriptional control of CPT1A and CPT1B. Animal Genetics. 2013; 45:38-47.

28. Carracedo A, Cantley LC, Pandolfi PP. Cancer metabolism: fatty acid oxidation in the limelight. Nature Rev Cancer. 2013; 13:227-232.

29. Mukhopadhyay SG, Mukherjee K, Manna AK. Renal tumors in adults with correlation between Fuhrman grading and proliferative marker. Iran J Pathol. 2015; 10:281-289.

30. Nakajima R, Nozaki S, Kondo T, Nagashima Y, Abe K, Sakai S.

Evaluation of renal cell carcinoma histological subtype and Fuhrman grade using 18F-fluorodeoxyglucose-positron emission tomography/computed tomography. Eur Radiol. 2017; https://doi.org/10.1007/s00330-017-4875-z.

31. Wettersten HI, Abu Aboud O, Lara PN, Weiss RH. Metabolic reprogramming in clear cell renal cell carcinoma. Nature Rev Nephrol. 2017; https://doi.org/10.1038/nrneph.2017.59.

32. Abu Aboud O, Habib SL, Trott J, Stewart B, Liang S, Chaudhari AJ, Sutcliffe J, Weiss RH. Glutamine addiction in kidney cancer suppresses oxidative stress and can be exploited for real-time imaging. Cancer Res. 2017; https://doi.org/10.1158/0008-5472.CAN-17-0930.

33. Bombelli S, Zipeto MA, Torsello B, Bovo G, Di Stefano V, Bugarin C, Zordan P, Viganò P, Cattoretti G, Strada G, Bianchi C, Perego RA. PKHhigh cells within clonal human nephrospheres provide a purified adult renal stem cell population. Stem Cell Res. 2013; 11:1163-1177.

34. Bianchi C, Torsello B, Angeloni V, Bombelli S, Soldi M, Invernizzi L, Brambilla P, Perego RA. Eight full-length abelson related gene (Arg) isoforms are constitutively expressed in Caki-1 cell line and cell distribution of two isoforms has been analyzed after transfection. J Cell Biochem. 2008; 105:1219-1227.

35. Raimondo F, Morosi L, Chinello C, Perego R, Bianchi C, Albo G, Ferrero S, Rocco F, Magni F, Pitto M. Protein profiling of microdomains purified from renal cell carcinoma and normal kidney tissue samples. Mol Biosyst. 2012; 8:1007-1016.

36. Bianchi C, Torsello B, Di Stefano V, Zipeto MA, Facchetti R, Bombelli S, Perego RA. One isoform of Arg/ Abl2 tyrosine kinase is nuclear and the other seven cytosolic

isoforms differently modulate cell morphology, motility and the cytoskeleton. Exp Cell Res. 2013; 319:2091-2102.

37. Berridge MV, Tan AS.
Characterization of the cellular reduction of 3-(4,5-dimethylthiazol-2yl)-2,5-diphenyltetrazolium bromide (MTT): subcellular localization, substrate dependence, and involvement of mitochondrial electron transport in MTT reduction. Arch Biochem Biophys. 1993; 303:474-482.

Chapter 3

The 1ALCTL and 1BLCTL isoforms of Arg/abl2 induce fibroblast activation and extra cellular matrix remodeling differently

Barbara Torsello[1,*], Sofia De Marco[1], Silvia Bombelli[1], Elisa Chisci[1], Valeria Cassina[1], Roberta Corti[1,2], Davide Bernasconi[1], Roberto Giovannoni[1], Cristina Bianchi[1] and Roberto A. Perego[1,*].

[1]School of Medicine & Surgery, University of Milano-Bicocca, 20900 Monza, Italy.
[2]Department of Materials Science, University of Milano-Bicocca, 20125 Milan, Italy.
*Authors for correspondence (roberto.perego@unimib.it; barbara.torsello@unimib.it)

Biology Open (2019) 8, bio038554.
doi:10.1242/bio.038554

Abstract

The fibrotic tissue and the stroma adjacent to cancer cells are characterised by the presence of activated fibroblasts (myofibroblasts) which play a role in creating a supportive tissue characterised by abundant extracellular matrix (ECM) secretion. The myofibroblasts remodel this tissue through secreted molecules and modulation of their cytoskeleton and specialized contractile structures. The non-receptor protein tyrosine kinase Arg (also called Abl2) has the unique ability to bind directly to the actin cytoskeleton, transducing diverse extracellular signals into cytoskeletal rearrangements. In this study we analysed the 1ALCTL and 1BLCTL Arg isoforms in $Arg^{-/-}$ murine embryonal fibroblasts (MEF) cell line, focusing on their capacity to activate fibroblasts and to remodel ECM. The results obtained showed that Arg isoform 1BLCTL has a major role in proliferation, migration/invasion of MEF and in inducing amilieu able tomodulate tumour cellmorphology, while 1ALCTL isoform has a role in MEF adhesion maintaining active focal adhesions. On the whole, the presence of Arg in MEF supports the proliferation, activation, adhesion, ECM contraction and stiffness, while the absence of Arg affected these myofibroblast features.

Introduction

The fibrotic process, after a chronic injury, results in an excessive scar tissue deposition and development of fibrosis, and has in the activated fibroblasts (myofibroblasts) themain players (Yazdani et al., 2017). In fact, myofibroblasts secrete extra cellular matrix (ECM) proteins and also awide range of cytokines promoting cell proliferation, migration, angiogenesis and recruitment of inflammatory cells (Mueller and Fusenig, 2004; Orimo et al., 2005). Fibroblast activation not only occurs as a result of chronic injury, but also during tumour growth that leads to tumour stroma formation. The stroma adjacent to cancer cells is a permissive and supportive environment (Mueller and Fusenig, 2004) in which there is a variable presence of myofibroblasts, also called cancer associated fibroblasts (CAF). Increasing attention has been focused on CAF because of their important role on tumour progression by the secretion of ECM and several cytokines.

Myofibroblasts are also capable of remodelling ECM and acquiring specialised contractile features, which result in the reorganisation and contraction of ECM both in fibrotic and in tumour stroma. In particular, CAF promote matrix remodelling by soluble factors (Kalluri and Zeisberg, 2006) and by the generation of tracks that enable the collective invasion of the tumour cells. RhoGTPase activity in myofibroblasts is necessary for track generation (Gaggioli et al., 2007).

Remodelling of the ECM and promotion of cancer cell invasion also requires myofibroblast cytoskeletal rearrangement through contraction of the actomyosin cytoskeleton assembled in stress fibres (Barron and Rowley, 2012; Calvo et al., 2013).

The non-receptor tyrosine kinase Arg (also called Abl2) (Kruh et al., 1990; Perego et al., 1991) shares with Abl1 the unique ability, among the tyrosine kinases, to bind directly to the cytoskeleton, transducing diverse extracellular signals into cytoskeletal rearrangements (Bradley and Koleske, 2009). In particular Arg, due to the presence in its sequence of two actin-binding domains, can bind and stabilise F-actin filaments preventing their cut by cofilin. Arg is able to fasciculate F-actin and both domains are necessary for actin bundling and cytoplasmic distribution of stress fibres (Miller et al., 2004). ARG gene, through alternative splicing events, codes eight different isoforms, based on the reciprocal presence or absence of exons IA, IB and II in 5′-ends and a ΔCT sequence, including part of one of the F-actin-binding domain, in 3′-ends of the specific Arg transcript (Bianchi et al., 2008). The eight different Arg isoforms are expressed in normal and neoplastic cells with different ratios (Perego et al., 2005). Overexpression of the different Arg isoforms in COS cells induces different effects on cell morphology and cytoskeleton organisation. In particular, 1ALCTL and 1BLCTL Arg isoforms, differing only in the 1A and 1B exons,

determine a different behaviour of transfected COS cells. The 1BLCTL isoform induces a higher reduction of cell surface area and stress fibre density with respect to 1ALCTL isoform and enhances the formation of filopodia structures instead of lamellipodia and retraction tails (Bianchi et al., 2013).

The aim of this study was to analyse more deeply the difference of two 1ALCTL and 1BLCTL Arg isoforms transfected in $Arg^{-/-}$ murine embryonal fibroblasts (MEF) cell line, in particular focusing on their capacity to activate fibroblasts, to modulate their functionality and to remodel ECM.

Results

Stable expression and tyrosine kinase activity of 1ALCTL and 1BLCTL Arg isoforms transfected in $Arg^{-/-}$ MEF

To study the role of 1ALCTL and 1BLCTL Arg isoforms in fibroblast activation, we cloned into the stable expression vector pCX-C1-EGFP plasmid (Cinti et al., 2015) the corresponding Arg cDNA sequences. The vectors containing the inserts 1ALCTL or 1BLCTL have been transfected in $Arg^{-/-}$ MEF (indicated as 1ALCTL MEF and 1BLCTL MEF, respectively) and the EGFP empty vector has been transfected in wt and $Arg^{-/-}$ MEF (indicated as wt MEF and $Arg^{-/-}$ MEF, respectively). After 2-4 steps of purification by cell sorting, the percentage of EGFP positive cells was from

90 to 95% for all types of transfection (Fig. S1A). Western blot confirmed that 1ALCTL MEF and 1BLCTL MEF expressed the Flag-Arg proteins at the expected molecular weight and at the same level of wt MEF (1BLCTL/wt Arg was 1.06, 1ALCTL/wt Arg was 1.08) (Fig. 1A). The tyrosine kinase activity of the two isoforms has been evaluated with anti-phosphotyrosine antibody on the isoforms immunoprecipitated with anti-Flag antibody (Fig. 1B; Fig. S1C). We performed an in vitro kinase assay on Hek cells transfected with the two Arg isoforms and we showed that both immunoprecipitated isoforms were able to phosphorylate the enolase protein (Fig. 1C; Fig. S1B). In addition, the transfected Hek cells treated with Imatinib, an inhibitor of Arg tyrosine kinase activity, evidenced that the two isoforms were sensitive to the drug, in particular to Imatinib concentration of 10 μM (Fig. 1D).

The 1ALCTL and 1BLCTL Arg isoforms are differently able to activate Arg$^{-/-}$ MEF

A characteristic of activated fibroblasts is the high proliferation rate (Barron and Rowley, 2012; Li et al., 2016), therefore, we evaluated the effect of Arg isoforms on MEF proliferation counting the viable cells at different time points. At 96 h the wt MEF were significantly more proliferating than Arg$^{-/-}$ MEF. The 1ALCTL isoform maintained the MEF proliferation at the level of Arg$^{-/-}$ MEF, while 1BLCTL induced

a significantly higher proliferation activity than $Arg^{-/-}$ and only slightly lower, in a non-significative manner, with respect to wt MEF (Fig. 2A). These data have been confirmed, evaluating by immunofluorescence the nuclear positivity of the proliferation markers PCNA (Fig. 2B). These findings highlighted the role of Arg, particularly of 1BLCTL, in fibroblast proliferation.

An index of fibroblast activation, both in non-tumour myofibroblasts and in CAF, is the expression of α-sma (O'Connell et al., 2011). As shown, α-smawas expressed in wt MEF, while in $Arg^{-/-}$ MEF it was almost undetectable. In 1BLCTL MEF α-sma was overexpressed with respect to $Arg^{-/-}$ MEF, while in presence of 1ALCTL the expression mean value was level with wt MEF (Fig. 2C). Even the localisation of α-sma incorporated in stress fibres is a marker of activated fibroblasts (Goffin et al., 2006). The immunofluorescence evaluation showed that in $Arg^{-/-}$ MEF and 1ALCTL MEF α-sma is diffusely localised in cytoplasm, while in wt MEF and 1BLCTL MEF the majority of α-sma colocalised with stress fibres (Fig. S2A).

It is of note that the different MEF studied have a different capacity to produce TGFß1. In particular, the absence of Arg determined the increase of TGFß1 expression (Fig. 2D). The migratory ability of all MEF were analysed by wound healing and the wound recovery in $Arg^{-/-}$ MEF significantly increased as compared to wt (Fig. 3A), confirming the already described

inhibitory role of Arg on fibroblast migration (Peacock et al., 2007). Interestingly, in $Arg^{-/-}$ MEF the migration ability increased further with respect to wt MEF after the transfection of 1BLCTL isoform, whose expression was at the same level of endogenous Arg in wt MEF (Fig. 3A). To test if Arg and its isoforms had a role in MEF invasiveness, we performed a collagenbased cell invasion assay. The invasiveness capacity determined by 1BLCTL is higher with respect to all the other cell types, which shared a similar invasive capacity (Fig. 3B). These data suggest that the Arg exon 1B and 1A differently modulate the migration and invasion of MEF.

1ALCTL and 1BLCTL Arg isoforms differently regulate cellular contractile structures

The cellular focal adhesions and stress fibres that are contractile structures essential for the force transmission between cells and matrix, which is a further characteristic of myofibroblast (Calvo et al., 2013), were evaluated. After plating MEF on collagencoated glass for 4 h, we analysed by immunofluorescence the focal adhesion and stress fibre distribution in the cells. The wt MEF, grown on surface of collagen I gel as a 2D culture, showed a preferential peripheral distribution of the paxillin-positive focal adhesions and prominent phalloidin-positive stress fibres crossing the cytoplasm, in addition, wt MEF also had the highest cell spreading (Fig. S2B). $Arg^{-/-}$ MEF were characterised by less

evident focal adhesions and by thinner stress fibres that had a prevalent cortical distribution. 1ALCTL MEF had stress fibres crossing the cytoplasm and focal adhesions more evident in the retraction tail and in the opposite side of retraction tail (lamellipodia). 1BLCTL MEF maintained a cortical F-actin and a delocalisation of focal adhesions to filopodial structures (Fig. 4A).

Given the morphology and the cell surface area of our MEF, we evaluated whether these features correlated to a specific adhesion ability. The cellular adhesion assay on collagen-coated wells showed that in $Arg^{-/-}$ MEF the adhesion ability decreased significantly in respect to wt MEF. Only 1ALCTL isoform was able to restore it in $Arg^{-/-}$ MEF at higher level than in wt MEF, although not significant (Fig. 4B). The adhesion ability of larger wt MEF is in accordance with literature data that correlate cell spreading with adhesion (Nardone et al., 2017). However, to explain why 1ALCTL MEF displayed an increased adhesion, despite a smaller spreading respect to wt MEF (Fig. S2B), we analysed phospho-Y118 paxillin. As shown in Fig. 4C, 1ALCTL MEF had a decreased phosphorylation of paxillin-Y118 with respect to all the other cellular types analysed and this result may justify the increased cellular adhesion of 1ALCTL MEF (Fig. 4B). In fact, it is known that phosphorylation of paxillin-Y118 leads to a focal adhesion disassembly and activity reduction (Coló et al., 2012). We also evaluated our cells'

migration for 4 h inside the collagen gel representing a 3D environment (Fig. 4D), as documented by the confocal microscope orthogonal views (Fig. S2D). In Fig. 4D the migrated wt MEF maintained phalloidin staining across the cytoplasm. $Arg^{-/-}$ MEF had a more spheroid shape without a typical F-actin organisation. 1ALCTL and wt MEF inside the collagen were associated in groups of cells, 1BLCTL MEF had filopodia structures. 1ALCTL and 1BLCTL showed diffuse paxillin staining, but at 4 h of migration they did not show the focal adhesion organisation. Finally, the different MEF types were analysed for their ability to shrink the collagen plug in which they had been embedded for 72 h. The $Arg^{-/-}$ MEF lost the ability to contract the collagen matrix. Both 1ALCTL and 1BLCTL restored the contraction to wt values (Fig. 4E). These data proved that Arg is essential for collagen-ECM contraction by fibroblasts.

Wt and $Arg^{-/-}$ transfected MEF generate ECM, which are architecturally and functionally different

To test whether Arg and its isoforms had the ability to influence the production of stroma with different characteristics, we allowed the different MEF cells to produce and remodel their matrix for 10 days.

Immunofluorescence staining was performed after the complete removal of MEF cells. The wt and 1BLCTL MEF produced bundles of fibronectin morphologically denser and

more uniform than those produced by $Arg^{-/-}$ and 1ALCTL MEF, in which the fibronectin frameworks appeared with larger mesh size. The staining of collagen I evidenced that $Arg^{-/-}$ MEF had an undetectable deposition of the protein as compared to wt MEF, while the two transfected Arg isoforms enabled MEF to deposit collagen I (Fig. 5A). As fibronectin and collagen I deposition is relevant in determining matrix stiffness, a peculiar characteristic of fibrosis and tumour stroma (Bordeleau et al., 2015; Calvo et al., 2013), we assessed the relation between the newly produced ECM and their respective stiffness after removing MEF cells. Fig. 5B showed a decreased stiffness of ECM produced by $Arg^{-/-}$ MEF with respect to wt MEF. The 1ALCTL Arg isoform was unable to elicit the production of matrix with stiffness at the level of wt MEF, while 1BLCTL transfection elicited the production of ECM with the highest stiffness. Finally, we investigated whether these differently Arg-modulated matrices were able to influence the cell morphology of invading tumour cells. As spindle-shape cells are associated to a more invasive phenotype (Tanaka et al., 2016), we evaluated the elliptical factor (EF) of 786-O RCC cells plated on ECM produced by our different MEF. The highest EF was observed in 786-O cells grown in the stiffest matrices produced by wt and 1BLCTL MEF, while in those produced by $Arg^{-/-}$ and 1ALCTL MEF the tumour cells maintained a cobblestone shape (Fig. 5C). These results showed that the

lack of Arg altered the ECM structure in terms of fibronectin, collagen I deposition and stiffness, and that the MEF expressing the 1BLCTL Arg isoform was able to produce ECM that enhance the elongation of the tumour cells.

Discussion

During the fibrosis process myofibroblasts, the activated form of fibroblasts continue to produce ECM resulting in abnormal scar tissue deposition. Myofibroblasts also occur in the context of growing tumour, and in some solid tumours they can generate a very abundant fibrotic stroma. The increase of the proliferation rate, the expression of several markers, the ECM production and remodelling are features of myofibroblasts (Yazdani et al., 2017) The knowledge of molecular players involved in fibroblast activation is important for the development of novel therapeutic strategies against fibrosis and growing tumours. Our data evidence the role of Arg in fibroblast activation. We previously showed that the 1ALCTL and 1BLCTL Arg isoforms determine some morphological and molecular changes in COS-7 cells (Bianchi et al., 2013).

Now, we have shown that Arg is necessary for fibroblast proliferation. Considering our two transfected isoforms, which maintained their tyrosine kinase activity (Fig. 1), the 1BLCTL isoform alone is sufficient to restore the proliferation rate of wt MEF (Fig. 2A,B). However, literature data show that Arg

knockdown in MDA-MB-231, a breast tumour cell line, improves the proliferation of tumour epithelial cells (Gil-Henn et al., 2013), highlighting that the role of Arg in cellular proliferation could be cell specific.

Numerous papers report the expression and localisation of α-sma as common markers of activated fibroblasts (O'Connell et al., 2011; Shi et al., 2016; Goffin et al., 2006). Our data showed that 1BLCTL isoform is able to restore both the α-sma expression and colocalization with stress fibres, negligible in $Arg^{-/-}$ MEF (Fig. 2C; Fig. S2A). This finding suggests that Arg is necessary for fibroblast activation and that the fibrotic or the primary tumour stroma could be characterised by 1BLCTL Arg upregulation. Also an intriguing finding, in $Arg^{-/-}$ MEF, showed us that TGFß1 expression was inversely related to Arg expression (Fig. 2D). We also described this interesting inverse relation between Arg and TGFß1 in renal tubular cells after Arg silencing (Torsello et al., 2016). It seems that the absence of Arg make the fibroblasts less responsive to the proliferative and activating effects of TGFß1 signals, suggesting that the TGFβ1 signalling is less efficient in absence of Arg, therefore, TGFβ1 production is upregulated. The TGFß1-mediated effects, carried out in wt MEF, were restored by 1BLCTL but not completely by 1ALCTL isoforms (Fig. 2A-C). A defined Arg isoform expression pattern may also be relevant for the movement ability of myofibroblasts in both tumour and fibrotic

milieu. In accordance with this hypothesis, the wound recovery and the invasion of collagen matrices revealed that 1BLCTL isoform sustains this ability at the highest level in comparison with all the other MEF analysed. In particular, it seems that the Arg 1BLCTL protein level into the cell can modulate the migration. In fact, 1BLCTL, overexpressed either in Arg-endogenous-expressing or in $Arg^{-/-}$ fibroblasts, determines a decrement of migration ability (Peacock et al., 2007; Bianchi et al., 2013). However, when in $Arg^{-/-}$ cells the expression of recombinant Arg is only twofold over the endogenous Arg level the cells recover the migration abilty of wt cells (Peacock et al., 2007). In our transfected 1BLCTL MEF, in which the recombinant Arg is at the same level of wt MEF, their migration is higher than wt MEF. Instead, the 1ALCTL MEF were not able to reach the migration and invasion capacity shown by 1BLCTL MEF and an inhibitory activity of 1ALCTL cannot be excluded (Fig. 3A,B). The 4-h cultures evaluated in 2D or 3D environment of the different MEF could help to explain their behaviour. In fact, the highest spreading of wt MEF in 2D (Fig. S2B) may justify their adhesion capacity (Fig. 4B) (Nardone et al., 2017), despite the increased phosphorylation of Y118-paxillin. Instead, in 1ALCTL MEF the inhibition of paxillin phosphorylation, seems to account for the increment of cell adhesion. In 2D culture the decreased adhesion ability of 1BLCTL MEF (Fig. 4B) could contribute to a faster migration as it happens in

Arg$^{-/-}$ MEF (Fig. 3A). In the 3D environment of collagen matrix, 1BLCTL MEF are present as single cells (Fig. 4D) and this 3D-organisation associated with the decreased adhesion ability (Fig. 4B) can justify their high invasion capacity. 1ALCTL and wt MEF in addition to higher adhesion were also grouped together and this conformation could have delayed their invasion ability (Wong et al., 2014). In 3D culture the different spatial organization of cells can be due even to different modulation of adherent junctions. However, preliminary data in our different MEF (not shown) did not evidence significant differences in N-Cadherin expression, a marker of cell–cell adhesion in fibroblasts (Labernadie et al., 2017) and other cell–cell adhesion molecules need to be evaluated.

The ECM-contraction ability, another feature of myofibroblasts (Calvo et al., 2013), demonstrated that Arg is essential for collagen I contraction and that both 1ALCTL and 1BLCTL Arg isoforms are able, after 72 h, to restore the wt MEF contraction ability (Fig. 4E).

An efficient ECM-contraction is due to working stress fibres and focal adhesions as well as to α-sma expression and incorporation in intracellular stress fibres (Calvo et al., 2013; Shinde et al., 2017; Shuttleworth et al., 2018). Our 1ALCTL and 1BLCTL MEF grown for 4 h inside collagen showed no focal adhesions (Fig. 4D).

Otherwise, no difference in plug contractions was observed after 24 h (not shown). However, after leaving the 3D culture for 72 h the focal adhesions could have taken place, giving rise to plug contraction. It has to be noted that the dynamics of focal adhesions seems to be different in a 2D culture compared to a 3D culture (Chiu et al., 2014). Moreover, the α-sma expression (Fig. 2C) with its incorporation in stress fibres (Fig. S2A) may counteract the lack of functional focal adhesion preserving cell contractility.

The MEF analysed in this study were able to secrete and organise fibronectin and collagen I differently (Fig. 5). It is of note that $Arg^{-/-}$ MEF failed to deposit the collagen I, which is currently deposited by myofibroblasts during fibrosis and tumour progression (Karsdal et al., 2017). This finding underlines the unique role of Arg in the production of collagen matrix. Otherwise, 1BLCTL MEF produced networks of collagen I and fibronectin that are similar to those produced by wt MEF and this condition correlated with the highest stiffness of ECM, measured after removal of MEF. The ECM stiffness is due to the amount of collagen and fibronectin fibres, their cross-link and ECM morphology (Di Stefano et al., 2016; Mierke et al., 2017). The specific role of Arg in producing fibronectin and collagen matrix turned out to be also significant in producing a specific matrix framework able to modulate the tumour cell morphology. In fact, the highest elliptical factor was induced in 786-O RCC cells when they

grew in the high-stiffness-ECM produced by wt and 1BLCTL MEF (Fig. 5B,C). This finding is particularly relevant since it has been described that a fabricated matrix when forces the cells to assume an elongated morphology becomes able to select the cells with a more aggressive behaviour (Mazzini et al., 2015). In fact, the elongated morphology of tumour cells reveals a more invasive phenotype (Tanaka et al., 2016).

In conclusion, Arg isoform 1BLCTL has a major role in proliferation, migration/invasion of fibroblasts and in inducing a milieu able to modulate tumour cell morphology, while 1ALCTL isoform has a role in MEF adhesion maintaining active focal adhesions. On the whole, the presence of Arg in MEF supports the proliferation, activation, adhesion, ECM contraction and stiffness, while the absence of Arg affected these myofibroblast features.

Material and methods

Molecular cloning of human Arg isoforms 1BLCTL and 1ALCTL

Full-length human Arg 1BLCTL and 1ASCTL cDNA maintaining the inframe FLAG sequence, were excised from pFLAG-CMV2 vectors (Bianchi et al., 2008) and cloned into a pCX-C1-EGFP plasmid (Cinti et al., 2015).

After cloning, the 1ALCTL cDNA has been obtained by inserting the Arg exon II in 1ASCTL using a QuickChange site-directed mutagenesis assay (Stratagene) as described

in Bianchi et al. (2013). Restriction and sequencing analyses were performed on all the intermediate and also in the final constructs. Empty pCX-C1-EGFP plasmid was used as negative control vector for mock transfections.

Cell culture and transfection

Wild-type (wt) or $Arg^{-/-}$ MEF (Koleske et al., 1998) were grown in Dulbecco's minimum essential medium (DMEM) supplemented with 10% FBS, 1% of Pen/Strep, Fungizone and Glutamine (Euroclone), at 37°C and 5% CO_2. These cells were split and plated to reach a 70–80% confluence on the day of transfection. pCX-1ALCTL-EGFP, pCX-1BLCTL-EGFP and empty vector plasmids were alternatively transfected into $Arg^{-/-}$ MEF and the empty vector also into wt MEF by electroporation using Neon Transfection System (Life Technologies) according to the manufacturer's instructions. Transfected cells, resuspended in growth medium without antibiotics were plated and after 24 h transferred in growth medium containing 1 mg/ml of G418 (Sigma-Aldrich) for a 10 day selection.

Transfected cells were stained by Propidium Iodide solution (Biolegend) to exclude dead cells and sorted on the basis of EGFP expression using MOFLO Astrios Cell Sorter and analysed by Kaluza software (Beckman Coulter). All the transfected cells were sorted to reach a EGFP purification level from 90 to 95%.

The human embryonic kidney Hek cell line, and the 786-O renal cell carcinoma cell line (ATCC) have been cultured in DMEM supplemented with 10% FBS (Euroclone), at 37°C and 5% CO2. These cell types (75×10^4cells) have been transfected using the vectors pCX-1ALCTL-EGFP, pCX-1BLCTL-EGFP in the Hek cells, pCX-C1-EGFP in 786-O cells using Lipofectamine 3000 Reagent (Invitrogen) following the manufacturer's instructions. The transfected Hek cells, when requested, were cultured for 3 h in presence of 1 μM or 10 μM Imatinib mesylate as Arg tyrosine kinase inhibitor (Cayman Chemicals).

Western blot

Cell lysates were prepared, separated by SDS Nupage 4-12% and blotted on nitrocellulose membrane (all Life Technologies) as described (Cifola et al., 2011). The protein standard Dual Color Marker loaded on the gel were from Bio-Rad. The blotted membranes were probed with antibodies against: Flag (1:1000, Sigma-Aldrich), GFP (1:1000, Invitrogen), Arg (1:400, Millipore), PhoshoY (4G10, 1:1000, Millipore), α-sma (1:1000, Dako), PhosphoY118-Paxillin (1:1000, Cell Signaling Boston), paxillin (1:1000, Cell Signaling).

ECL (Pierce, Thermo Fisher Scientific) detected the antigen-antibody complexes. Densitometry of the bands was analysed by ImageJ software (NIH).

Tyrosine kinase activity

The tyrosine kinase activity of 1ALCTL and 1BLCTL isoforms has been assessed as described (Spirli et al., 2012) on the immunoprecipitated protein using antibody against Flag (10 µg/ml) as described (Torsello et al., 2016) and evaluating the autophosphorylation of Arg isoforms transfected in $Arg^{-/-}$ MEF. The ability to tyrosine phosphorylate the enolase substrate (Sigma-Aldrich) has been evaluated by an in vitro kinase assay on the immunoprecipitated Arg isoforms transfected in Hek cells (0.5 mg of cell lysates). The reaction has been performed in 20 µl of the following solution: 16 µl of 50 mM MgCl2, 2 µl of 1 mM ATP (Sigma-Aldrich) and 2 µg of enolase. After 30 min of incubation at 30°C, the reaction was stopped by adding SDS sample buffer. The reaction product was blotted and probed with antibodies against anti-PhosphoY and anti-enolase (Santa Cruz Biotechnology Heidelberg) and visualised by the ECL system.

Immunofluorescence

MEF cells (1×10^5) were seeded for 4 h on glass coverslips coated with collagen I Rat tail (Gibco, Life Technologies), fixed and incubated with antibody against paxillin (1:50, Becton Dickinson) to evidence focal adhesion or against α-sma (1:50, Abcam). Stress fibres have been labelled by Alexa 594-phalloidin (1:100, Molecular Probes Invitrogen)

and nuclei were counterstained with Mounting DAPI (Molecular Probes Invitrogen).

The cell surface area was evaluated as described (Bianchi et al., 2013) in EGFP positive cells plated as above. MEF cells proliferating for 24 h on glass coverslips were stained with PCNA (1:50, Clone PC10, Santa Cruz Biotechnology). Immunofluorescence pictures were obtained with confocal microscope Zeiss LSM710, using 63× or 40× objectives, equipped with Zen2009 software (Zeiss).

Real-time quantitative PCR

Total RNA extraction and reverse transcription were performed as described (Bianchi et al., 2008). Real-time quantitative PCR was carried out with a TaqMan Gene Expression Assay (Applied Biosystems) according to manufacturer's instructions, using commercial kits (TGFß1 Hs00998133_m1 Human; GAPDH Hs99998805_m1 Human, both Applied Biosystem). The relative levels of the different transcripts were calculated as $2^{-\Delta\Delta Ct}$ that represented the fold change with respect to the calibrator sample considered equal to 1.

Cell proliferation

Cell proliferation was monitored by Trypan Blue exclusion counting living cells. MEF were seeded at 50×10^4/60 mm dish and trypsinized after 24, 72 and 96 h of culture. The

proliferating cells were also monitored at 24 h evaluating the percentage on nuclear positivity of PCNA marker on 100 DAPI positive cells analysed for each MEF type in randomly chosen fields of several independent experiments.

Cell migration and invasion

Wound healing has been performed as described (Di Stefano et al., 2016). Monolayers of MEF cultures on six-well plates, were scratched with a pipette tip and photographed with a digital camera mounted on an inverted microscope Olympus (100× magnification). The cultures were photographed again after 6 h. Initial and final wound width was measured using *segmented lines* ImageJ software tool to track two segmented lines corresponding to the wound edges. *Save XY coordinates* tool was used to obtain the straight line equation by which the distance between the two straight lines corresponding to the edges of the wound was calculated.

Wound recovery was calculated as a mean difference between initial and final wound width obtained in three different fields for each well of the same experiment. Invasion has been evaluated using QCM™ 24-Well Collagen-Based Cell Invasion Assay, the membrane of Boyden chamber was coated by manufacturer (Millipore) with a solution of 0.3% collagen, composed by type I (85%) and type III (15%) collagen from chicken. The manufacturer's instructions were followed and 60×10^3 fibroblasts were plated on the upper

chamber. After 3 h at 37°C, we stained and microphotographed the porous membrane. The migrated cells were counted by two blinded operators at 400× in 10 different fields randomly chosen for each sample in all independent experiments with ImageJ software.

Cell adhesion and ECM contraction

Adhesion assay has been performed as described (Di Stefano et al., 2016).

ECM contraction has been performed using 75×10^3 fibroblasts embedded in 100 µl of collagen I rat tail. The mixture of collagen and cells was seeded on a 35-mm glass-bottom MetTek dish. Once the gels were set, photographs have been taken (t0) and gels containing fibroblasts were maintained in culture medium for 72 h (t72) when other photographs have been taken. To obtain the gel contraction value, the specific areas of the gel at t0 and t72 were measured using ImageJ software. The percentage of gel contraction of different independent experiments was calculated using the formula 100×[(gel area t0-gel area t72)/gel area t0].

Cell-derived matrices and stiffness

Cell-derived matrices were obtained on coverslips prepared as described (Kaukonen et al., 2016). 1.5×10^5 MEF of each type were respectively plated on coverslip. When the cells

were confluent, ascorbic acid (50 µg/ml, Sigma-Aldrich) was added and the medium changed every 2 days for 10 days. Cells were then removed by extraction buffer (0.2% sodium deoxycholate in 10 mM Tris-HCl, pH 8.0, supplemented with protease inhibitors).

Solubilized cellular material was then gently washed two to three times for 5 min each on ice with a washing buffer composed of 2 mM Tris-HCl, pH 8.0, supplemented with protease inhibitors. A subsequent treatment at 37°C with DNAse I (Sigma-Aldrich) for 20 min was performed to assure removal of DNA associated with nuclear debris (Hedman et al., 1979). These MEFderived matrices (MEF-DM) have been stained with antibodies against Fibronectin (1:1000, Dako) or collagen I (1:500, Abcam). The stiffness of these matrices has been measured by Atomic Force Microscopy as described (Di Stefano et al., 2016). 15×10^4 786-O cells, transfected with the pCX-C1-EGFP vector, have been plated on each of these MEF-DM for 48 h. The EF of 786-O cells has been calculated as the cell length/breadth ratio by ImageJ software (NIH). Cell pictures have been taken with an Eclipse E800 microscope (Nikon) and LuciaG 5.0 software (Nikon) supported by a digital camera (Nikon, DS-U1). In three different independent experiments 20 to 40 cells have been analysed for each conditions.

Statistical analysis

All molecular and functional effects of different cellular typeswere evaluated and/or quantified by two different operators blinded to experimental treatment. Differences between multiple groups were analysed using oneway ANOVA followed by post-hoc Tukey's test using OriginPro 2016 64BIT software. Values of $P<0.05$ were considered statistically significant. In the box/dot graphs showed, representing at least three independent experiments, the individual dot represents the single independent experiment, the boxes indicate the 25°-75° percentile, the continuous horizontal line into the box represents the median (—), while the dotted horizontal line represent the mean (- - -). Max and min (⊤ and ⊥) are indicated.

Acknowledgments

We would like to thank Pier Andrea Nicolosi for support with matrix decellularization experiment, Mario Bossi for helping in confocal microscopy, Carlo Spirli for input in kinase assay, Massimiliano Cadamuro for support with antibodies, Romina Fiorotto for useful discussion and Karen Boullier for English revision.

Figure Legends

Fig. 1. Stable transfected Arg isoforms and their kinase activity.

(A) Western blots of lysates of wt MEF, $Arg^{-/-}$ MEF transfected with empty vector (EGFP) and $Arg^{-/-}$ MEF transfected with1ALCTL or 1BLCTL isoforms. Blots were hybridised with antibodies against Arg and β-actin; endogenous (square bracket) and recombinant (dash). Arg bands are indicated. (B) Western blot of $Arg^{-/-}$ MEF transfected with the indicated Arg isoforms, immunoprecipitated (IP) with antibody against Flag, blotted and hybridized (IB) with antibodies against phosphotyrosine (PY) and Flag.

(C) Tyrosine kinase assay *in vitro* of the indicated Arg isoforms transfected in Hek cell line. (D) Tyrosine kinase assay *in vitro* of the indicated Arg isoforms transfected in Hek cell line cultured for 3 h in presence of Imatinib 1 μM or 10 μM. In C and D, the cellular lysates were IP with antibody against Flag. Kinase reaction of IP proteins was performed in presence of ATP and enolase. IB with antibodies against PY and enolase.

Fig. 2. Proliferation and activation of the different type of MEF.

(A) Growth curves of MEF, number of growing cells at 72 and 96 h with respect to 24 h of culture (n=5). (B) Images by

confocal microscope of the indicated MEF stained with anti-PCNA antibody (red) and with DAPI (blue) after 24 h of culture.

In the graph, the percentage of nuclear PCNA positive cells obtained counting 100 DAPI positive cells in fields randomly chosen. Dots represent the mean percentage of independent experiments (n=5). (C) Western blot of the indicated MEF hybridized with antibodies against α-sma and β-Actin. The box plot of normalized bands are shown (n=3). (D) TGFß1 transcript evaluated by real-time PCR in the indicated MEF. The values, calculated as $2^{-\Delta\Delta Ct}$, represented the fold change with respect to wt MEF chosen as calibrator sample (n=3).*P<0.05. Scale bars: 10 μm.

Fig. 3. Migration and invasion of transfected MEF.

(A) Wound healing assay at the scratch (0 h) and after 6 h of wound recovering, the graph represents the recovery expressed as μm in independent experiments (n=3). (B) Invading cells in Boyden chamber coated by collagen, the graph reports the mean number of invading cells counted in 10 randomly chosen fields for each sample in independent experiments (n=3). *P<0.05.

Fig. 4. Cytoskeletal components of transfected MEF and their interaction with collagen I.

(A) Distribution of paxillin (green) that represents focal adhesion and phalloidin (red) that represents stress fibres in the indicated MEF analysed on surface of collagen I gel after 4 h from plating.

Nuclei were stained with DAPI (blue) and images were captured by confocal microscopy (63×).

Asterisk, lamellipodia; arrow, retraction tail; double arrow, filopodia. (B) Graph of the adhesion ability of indicated MEF. The adhesion assay has been performed on 96-well collagen-coated plates and the values of absorbance measured at 590 nm represent independent experiments (n=5). (C) Western blot of indicated MEF hybridised with antibodies against phosphoY118-paxillin and paxillin. (D) Indicated MEF migrated for 4 h inside the collagen I gel, representing a 3D environment, and staining of paxillin (green) and phalloidin (red). Pictures have been captured by confocal microscopy (63×) in the z-stack range of 5-20 μm from the gel surface. (E) Collagen contraction by MEF embedded into collagen I gels. Areas of collagen I plugs with indicated embedded fibroblasts at zero (0 h) and 72 h of incubation. The graph shows the percentage of contraction induced by the MEF analysed in independent experiments (n=4). *P<0.05. Scale bars: 10 μm.

Fig. 5. Architecture and functionality of ECM produced by different MEF.

(A) Fibronectin and collagen I staining of MEF-derived matrices (MEF-DM) after the removal of MEF. (B) Evaluation of stiffness of the MEF-DM. Dot plot shows the stiffness expressed as Young modulus (Pa) of the different matrices, each dot represents a measure performed in different positions of MEF-DM during independent experiments (n=3). (C) 786-O cells transfected with pCX-C1- EGFP vector and grown on the indicated MEF-DM for 48 h, the graph shows the elliptical factor (ratio of the cell length/cell breadth) of 786-O cells evaluated in independent experiments (n=3). *P<0.05. Scale bars: 10 μm.

Supplemental figure legends

Figure S1. A: Percentage of recovering of EGFP positive cells of the indicated transfected MEF. B: Western blot of 2 μg of Enolase hybridized with antibodies against PhosphoTyrosine (PY) and Eno-lase. C: western blot of $Arg^{-/-}$ MEF transfected with the indicated vectors, immunoprecipitated (IP) with antibodies against Flag, blotted and hybridised (IB) with antibodies against Phosphotyrosine and Flag.

Figure S2. A: distribution of α-sma and stress fibers, respectively stained with antibody against α-sma (green) and

phalloidin (red), in the indicated MEF. B: Dot blot of cell spreading of indicated MEF. The Cell Area expressed in μm has been measured by Image as described (Bianchi et al., 2013). Each dot represents ameasure of single cell area in independent experiments (n=3). *P<0.05.

C: Dot plot of PY 118-Paxillin bands normalised for Paxillin (n=3). D: Representative image of transfected Arg-/- MEF migrated inside the collagen gel. Immunofluorescence staining of Phalloidin captured by Zeiss confocal microscopy. YZ and XZ sections have been obtained with ImageJ software (*Orthogonal Views Plugin*), after acquiring Z-Stack sections. 50 pictures along the Z-plane, 0.50 μm each, have been taken.

Fig. 1

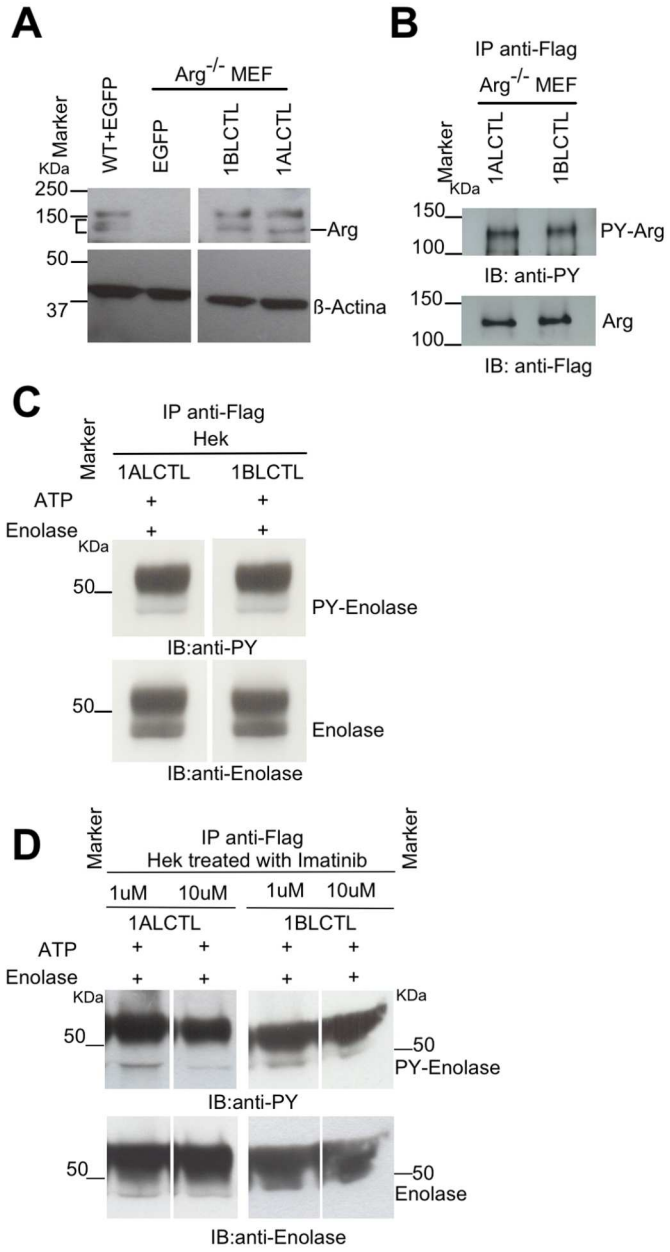
A
Marker
KDa
250
150
50
37
WT+EGFP
Arg-/- MEF
EGFP
1BLCTL
1ALCTL
Arg
ß-Actina
B
IP anti-Flag
Arg-/- MEF
Marker
KDa
1ALCTL
1BLCTL
150
100
PY-Arg
IB: anti-PY
150
100
Arg
IB: anti-Flag
C
IP anti-Flag
Hek
Marker
1ALCTL
1BLCTL
ATP
+
+
Enolase
+
+
KDa
50
PY-Enolase
IB:anti-PY
50
Enolase
IB:anti-Enolase
D
Marker
IP anti-Flag
Hek treated with Imatinib
Marker
1uM
10uM
1uM
10uM
1ALCTL
1BLCTL
ATP
+
+
+
+
Enolase
+
+
+
+
KDa
50
50
PY-Enolase
IB:anti-PY
50
50
Enolase
IB:anti-Enolase

Fig. 2

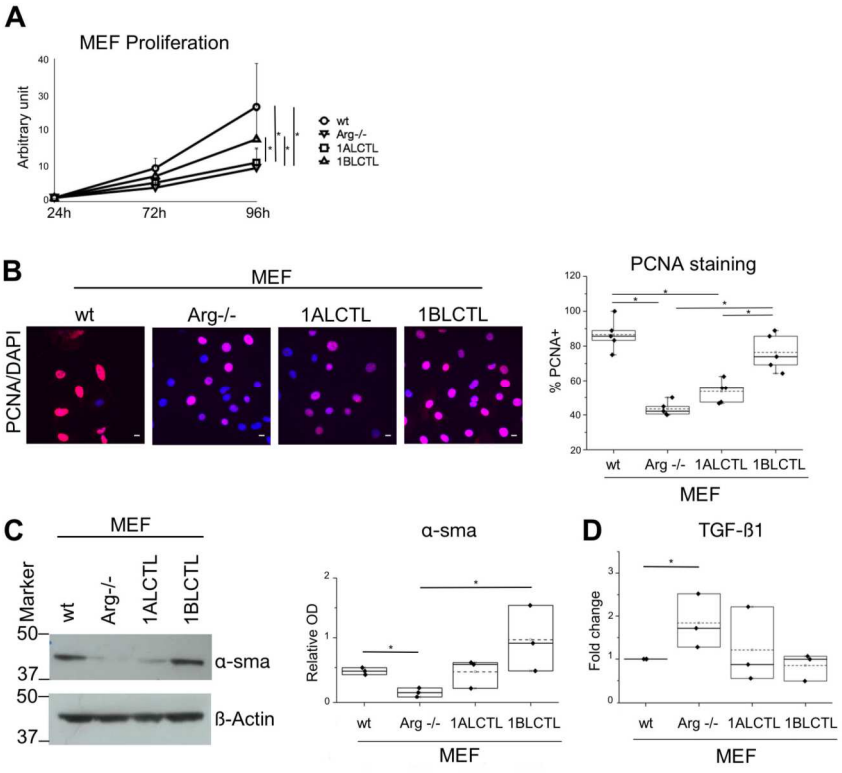
A
MEF Proliferation
Arbitrary unit
40
30
10
10
0
24h
72h
96h
wt
Arg-/-
1ALCTL
1BLCTL
B
MEF
wt
Arg-/-
1ALCTL
1BLCTL
PCNA/DAPI
PCNA staining
% PCNA+
120
100
80
60
40
20
wt
Arg -/-
1ALCTL
1BLCTL
MEF
C
MEF
Marker
wt
Arg-/-
1ALCTL
1BLCTL
50
37
50
37
α-sma
β-Actin
α-sma
Relative OD
2
1
0
wt
Arg -/-
1ALCTL
1BLCTL
MEF
D
TGF-ß1
Fold change
3
2
1
0
wt
Arg -/-
1ALCTL
1BLCTL
MEF

Fig. 3

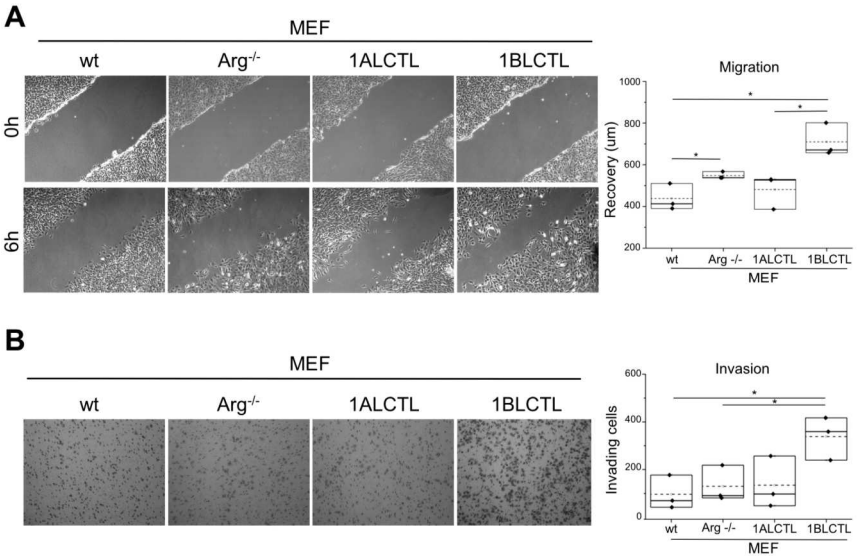
A
MEF
wt
Arg-/-
1ALCTL
1BLCTL
0h
6h
Migration
Recovery (um)
1000
800
600
400
200
wt
Arg -/-
1ALCTL
1BLCTL
MEF
B
MEF
wt
Arg-/-
1ALCTL
1BLCTL
Invasion
Invading cells
600
400
200
0
wt
Arg -/-
1ALCTL
1BLCTL
MEF

Fig. 4

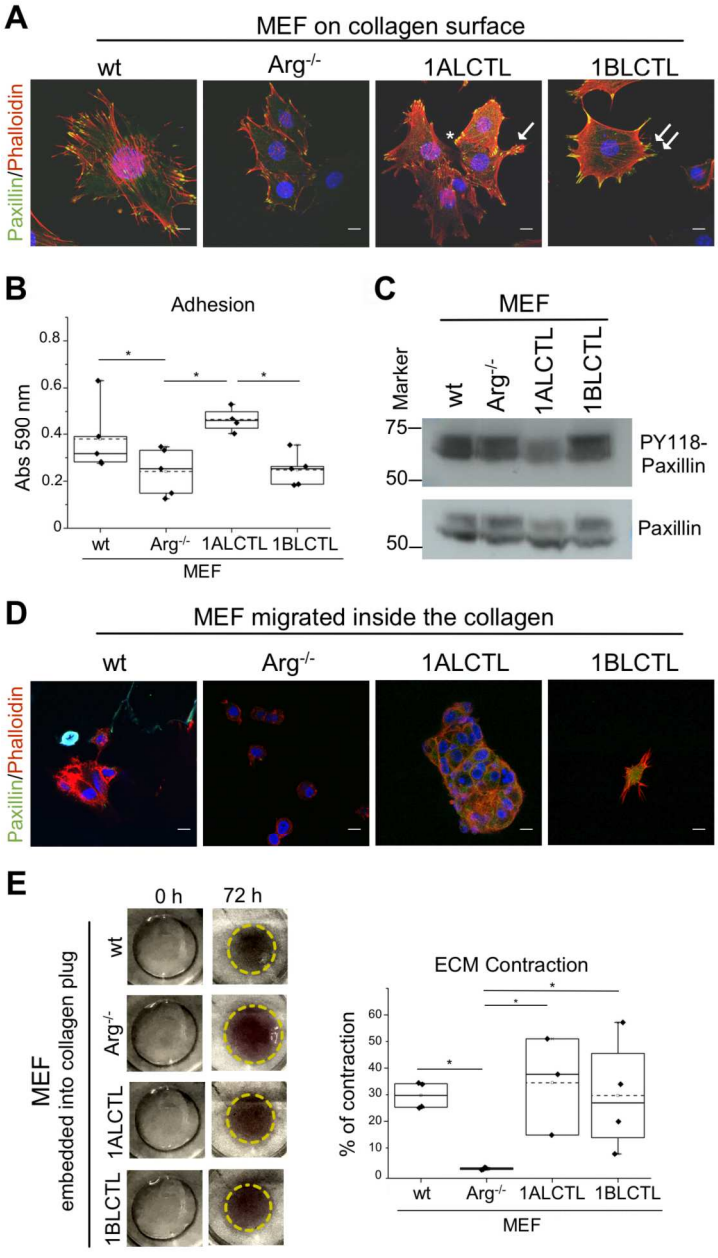
A
MEF on collagen surface
wt
Arg-/-
1ALCTL
1BLCTL
Paxillin/Phalloidin
B
Adhesion
Abs 590 nm
0.8
0.6
0.4
0.2
0
wt
Arg-/-
1ALCTL
1BLCTL
MEF
C
MEF
Marker
wt
Arg-/-
1ALCTL
1BLCTL
75
50
PY118-Paxillin
50
Paxillin
D
MEF migrated inside the collagen
wt
Arg-/-
1ALCTL
1BLCTL
Paxillin/Phalloidin
E
0 h
72 h
MEF embedded into collagen plug
wt
Arg-/-
1ALCTL
1BLCTL
ECM Contraction
% of contraction
60
50
40
30
20
10
0
wt
Arg-/-
1ALCTL
1BLCTL
MEF

Fig. 5

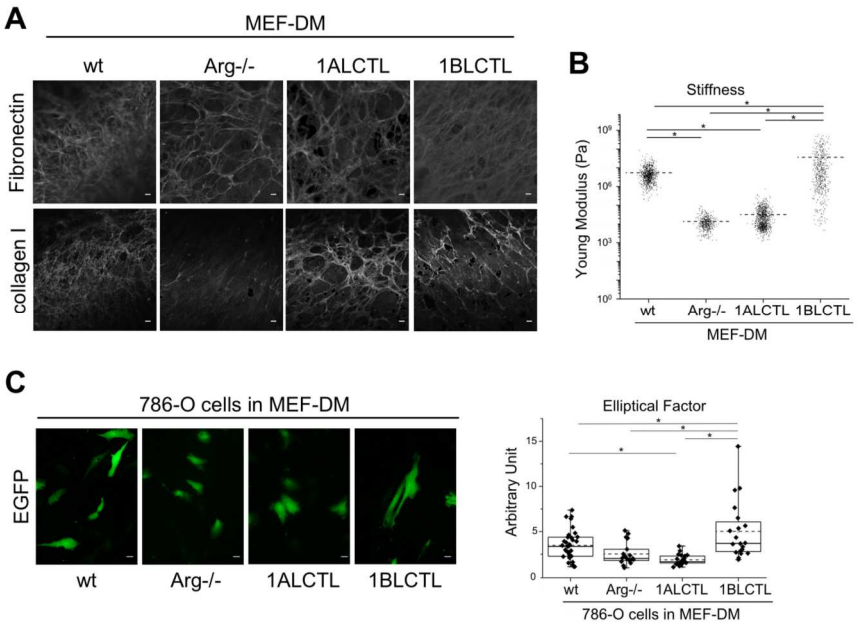
A
MEF-DM
wt
Arg-/-
1ALCTL
1BLCTL
Fibronectin
collagen I
B
Stiffness
Young Modulus (Pa)
wt
Arg-/-
1ALCTL
1BLCTL
MEF-DM
C
786-O cells in MEF-DM
EGFP
wt
Arg-/-
1ALCTL
1BLCTL
Elliptical Factor
Arbitrary Unit
786-O cells in MEF-DM

Supplemental figure S1

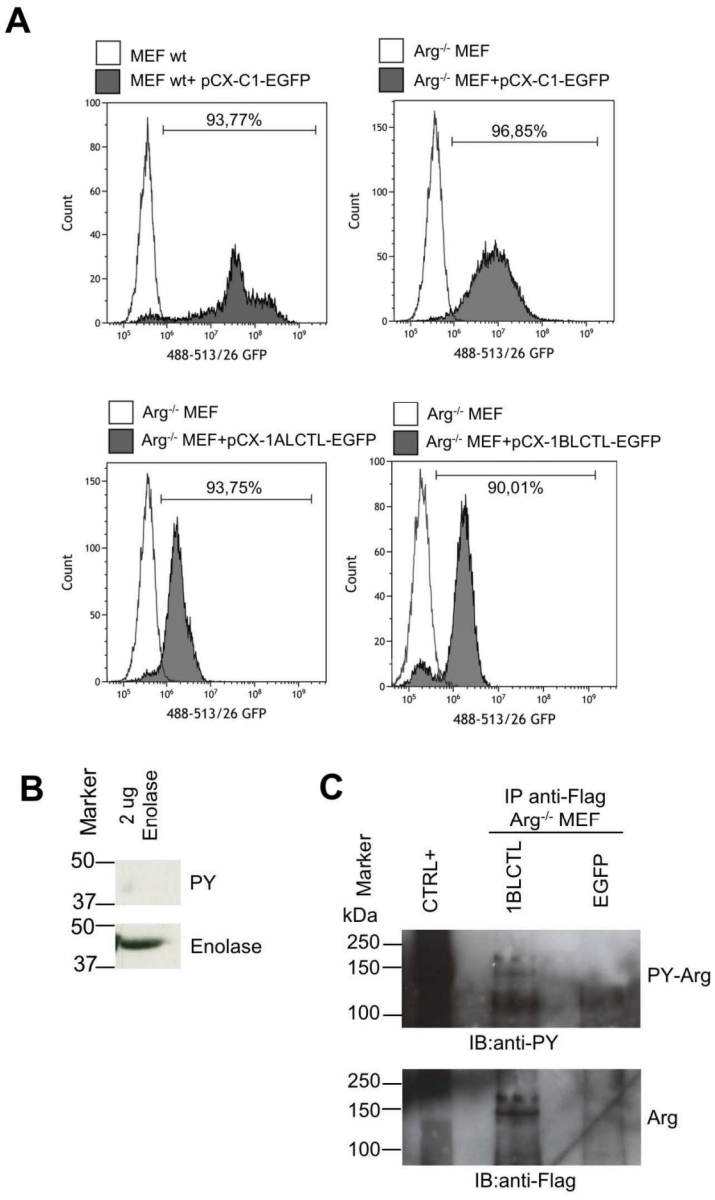

Supplemental figure S2

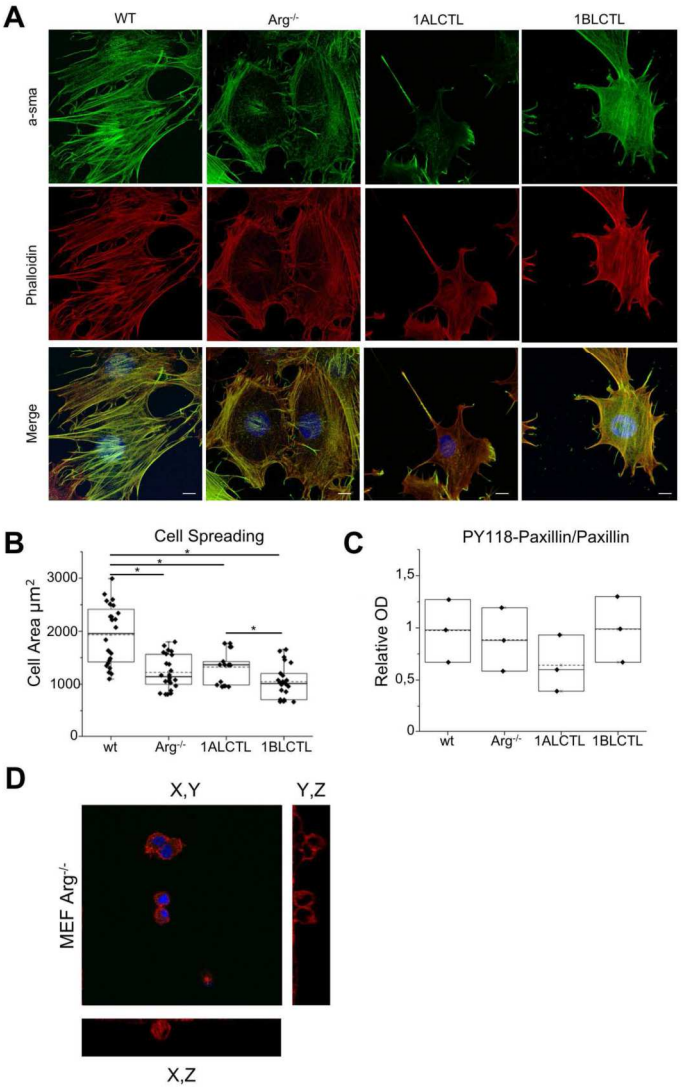

References

Barron, D. A. and Rowley, D. R. (2012). The reactive stroma microenvironment and prostate cancer progression. *Endocr. Relat. Cancer* **19,** R187-R204.

Bianchi, C., Torsello, B., Angeloni, V., Bombelli, S., Soldi, M., Invernizzi, L., Brambilla, P. and Perego, R. A. (2008). Eight full-length Abelson related gene (Arg) isoforms are constitutively expressed in Caki-1 cell line and cell distribution of two isoforms has been analyzed after transfection. *J. Cell. Biochem*. **105**, 1219-1227.

Bianchi, C., Torsello, B., Di Stefano, V., Zipeto, M. A., Facchetti, R., Bombelli, S. and Perego, R. A. (2013). One isoform of Arg/Abl2 tyrosine kinase is nuclear and the other seven cytosolic isoforms differently modulate cell morphology, motility and the cytoskeleton. *Exp. Cell Res*. **319**, 2091-2102.

Bordeleau, F., Califano, J. P., Negrón Abril, Y. L., Mason, B. N., LaValley, D. J., Shin, S. J., Weiss, R. S. and Reinhart-King, C. A. (2015). Tissue stiffness regulates serine/arginine-rich protein-mediated splicing of the extra domain Bfibronectin isoform in tumors. *Proc. Natl. Acad. Sci. USA* **112**, 8314-8319.

Bradley, W. D. and Koleske, A. J. (2009). Regulation of cell migration and morphogenesis by Abl-family kinases: emerging mechanisms and physiological contexts. *J. Cell Sci.* **122**, 3441-3454.

Calvo, F., Ege, N., Grande-Garcia, A., Hooper, S., Jenkins, R. P., Chaudhry, S. I., Harrington, K., Williamson, P., Moeendarbary, E., Charras, G. et al. (2013). Mechanotransduction and YAP-dependent matrix remodelling is required for the generation and maintenance of cancer-associated fibroblasts. *Nat. Cell Biol.* **15**, 637-646.

Chiu, C.-L., Aguilar, J. S., Tsai, C. Y., Wu, G. K., Gratton, E. and Digman, M. A. (2014). Nanoimaging of focal adhesion dynamics in 3D. *PLoS ONE* **9**, e99896.

Cifola, I., Bianchi, C., Mangano, E., Bombelli, S., Frascati, F., Fasoli, E., Ferrero, S., Di Stefano, V., Zipeto, M. A., Magni, F. et al. (2011). Renal cell carcinoma primary cultures maintain genomic and phenotypic profile of parental tumor tissues. *BMC Cancer* **11**, 244.

Cinti, A., De Giorgi, M., Chisci, E., Arena, C., Galimberti, G., Farina, L., Bugarin, C., Rivolta, I., Gaipa, G., Smolenski, R. T. et al. (2015). Simultaneous overexpression of functional human HO-1, E5NT and ENTPD1 protects murine fibroblasts against TNF-α-induced injury in vitro. *PLoS ONE* **10**, e0141933.

Coló, G. P., Hernández-Varas, P., Lock, J., Bartolomé, R. A., Arellano-Sánchez, N., Strö mblad, S. and Teixidó, J. (2012). Focal adhesion disassembly is regulated by a RIAM to MEK-1 pathway. *J. Cell Sci.* **125**, 5338-5352.

Di Stefano, V., Torsello, B., Bianchi, C., Cifola, I., Mangano, E., Bovo, G., Cassina, V., De Marco, S., Corti, R., Meregalli, C. et al. (2016). Major action of endogenous lysyl oxidase in clear cell renal cell carcinoma progression and collagen stiffness revealed by primary cell cultures. *Am. J. Pathol.* **186**, 2473-2485.

Gaggioli, C., Hooper, S., Hidalgo-Carcedo, C., Grosse, R., Marshall, J. F., Harrington, K. and Sahai, E. (2007). Fibroblast-led collective invasion of carcinoma cells with differing roles for RhoGTPases in leading and following cells. *Nat. Cell Biol.* **9**, 1392-1400.

Gil-Henn, H., Patsialou, A., Wang, Y., Warren, M. S., Condeelis, J. S. and Koleske, A. J. (2013). Arg/Abl2 promotes invasion and attenuates proliferation of breast cancer in vivo. *Oncogene* **32**, 2622-2630.

Goffin, J. M., Pittet, P., Csucs, G., Lussi, J.W., Meister, J.-J. and Hinz, B. (2006). Focal adhesion size controls tension-dependent recruitment of α-smooth muscle actin to stress fibers. *J.Cell Sci.* **172**, 259-268.

Hedman, K., Kurkinen, M., Alitalo, K., Vaheri, A., Johansson, S. and Höö k, M. (1979). Isolation of the pericellular matrix of human fibroblast cultures. *J. Cell Biol.* **81**, 83-91.

Kalluri, R. and Zeisberg, M. (2006). Fibroblasts in cancer. *Nat. Rev. Cancer* **6**, 392-401.

Karsdal, M. A., Nielsen, S. H., Leeming, D. J., Langholm, L. L., Nielsen, M. J., Manon-Jensen, T., Siebuhr, A., Gudmann, N. S., Rønnow, S., Sand, J. M. et al. (2017). The good and the bad collagens of fibrosis – their role in signaling and organ function. *Adv. Drug Deliv. Rev.* **121**, 43-56.

Kaukonen, R., Mai, A., Georgiadou, M., Saari, M., De Franceschi, N., Betz, T., Sihto, H., Ventelä, S., Elo, L., Jokitalo, E. et al. (2016). Normal stroma suppresses cancer cell proliferation via mechanosensitive regulation of JMJD1amediated transcription. *Nat. Commun.* **7**, 12237.

Koleske, A. J., Gifford, A. M., Scott, M. L., Nee, M., Bronson, R. T., Miczek, K. A. and Baltimore, D. (1998). Essential roles for the Abl and Arg tyrosine kinases in neurulation. *Neuron* **21**, 1259-1272.

Kruh, G. D., Perego, R., Miki, T. and Aaronson, S. A. (1990). The complete coding sequence of arg defines the Abelson subfamily of cytoplasmic tyrosine kinases. *Proc. Natl. Acad. Sci. USA* **87**, 5802-5806.

Labernadie, A., Kato, T., Brugués, A., Serra-Picamal, X., Derzsi, S., Arwert, E., Weston, A., González-Tarragó, V., Elosegui-Artola, A., Albertazzi, L. et al. (2017). A

mechanically active heterotypic E-cadherin/N-cadherin adhesion enables fibroblasts to drive cancer cell invasion. *Nat. Cell Biol.* **19**, 224-237.

Li, J., Jia, Z., Kong, J., Zhang, F., Fang, S., Li, X., Li,W., Yang, X., Luo, Y., Lin, B. et al. (2016). Carcinoma-associated fibroblasts lead the invasion of salivary gland adenoid cystic carcinoma cells by creating an invasive track. *PLoS ONE* **11**, e0150247.

Mazzini, G., Carpignano, F., Surdo, S., Aredia, F., Panini, N., Torchio, M., Erba, E., Danova, M., Scovassi, A. I., Barillaro, G. et al. (2015). 3D silicon microstructures: a new tool for evaluating biological aggressiveness of tumor cells. *IEEE Trans. Nanobioscience* **14**, 797-805.

Mierke, C. T., Sauer, F., Grosser, S., Puder, S., Fischer, T. and Kä s, J. A. (2017). The two faces of enhanced stroma: stroma acts as a tumor promoter and a steric obstacle. *NMR Biomed.* **31**, e3831.

Miller, A. L.,Wang, Y., Mooseker, M. S. and Koleske, A. J. (2004). The Abl-related gene (Arg) requires its F-actin-microtubule cross-linking activity to regulate lamellipodial dynamics during fibroblast adhesion. *J. Cell Biol.* **165**, 407-419.

Mueller, M. M. and Fusenig, N. E. (2004). Friends or foes - Bipolar effects of the tumour stroma in cancer. *Nat. Rev. Cancer* **4**, 839-849.

Nardone, G., Oliver-De La Cruz, J., Vrbsky, J., Martini, C., Pribyl, J., Skládal, P., Peš l, M., Caluori, G., Pagliari, S., Martino, F. et al. (2017). YAP regulates cell mechanics by controlling focal adhesion assembly. *Nat. Commun.* **8**, 1-13.

O'Connell, J. T., Sugimoto, H., Cooke, V. G., Macdonald, B. A., Mehta, A. I., LeBleu, V. S., Dewar, R., Rocha, R. M., Brentani, R. R., Resnick, M. B. et al. (2011). VEGF-A and

Tenascin-C produced by S100A4+ stromal cells are important for metastatic colonization. *Proc. Natl. Acad. Sci. USA* **108**, 16002-16007.

Orimo, A., Gupta, P. B., Sgroi, D. C., Arenzana-Seisdedos, F., Delaunay, T., Naeem, R., Carey, V. J., Richardson, A. L. andWeinberg, R. A. (2005). Stromal fibroblasts present in invasive human breast carcinomas promote tumor growth and angiogenesis through elevated SDF-1/CXCL12 secretion. *Cell* **121**, 335-348.

Peacock, J. G., Miller, A. L., Bradley, W. D., Rodriguez, O. C., Webb, D. J. and Koleske, A. J. (2007). The Abl-related gene tyrosine kinase acts through p190RhoGAP to inhibit actomyosin contractility and regulate focal adhesion dynamics upon adhesion to fibronectin. *Mol. Biol. Cell* **19**, 308-317.

Perego, R., Ron, D. and Kruh, G. D. (1991). Arg encodes a widely expressed 145 kDa protein-tyrosine kinase. *Oncogene* **6**, 1899-1902.

Perego, R. A., Bianchi, C., Corizzato, M., Eroini, B., Torsello, B., Valsecchi, C., Di Fonzo, A., Cordani, N., Favini, P., Ferrero, S. et al. (2005). Primary cell cultures arising from normal kidney and renal cell carcinoma retain the proteomic profile of corresponding tissues. *J. Proteome Res.* **4**, 1503-1510.

Shi, Y., Du, L., Lin, L. and Wang, Y. (2016). Tumour-associated mesenchymal stem/stromal cells: emerging therapeutic targets. *Nat. Rev. Drug Discov.* **16**, 35-52.

Shinde, A. V., Humeres, C. and Frangogiannis, N. G. (2017). The role of α-smooth muscle actin in fibroblast-mediated matrix contraction and remodeling. *Biochim. Biophys. Acta* **1863**, 298-309.

Shuttleworth, V. G., Gaughan, L., Nawafa, L., Mooney, C. A., Cobb, S. L., Sheerin, N. S. and Logan, I. R. (2018). The methyltransferase SET9 regulates TGFB1 activation of renal fibroblasts via interaction with SMAD3. *J. Cell Sci.* **131**, jcs207761.

Spirli, C., Morell, C. M., Locatelli, L., Okolicsanyi, S. Ferrero, C., Kim, A. K., Fabris, L., Fiorotto, R. and Strazzabosco, M. (2012). Cyclic AMP/PKAdependent paradoxical activation of Raf/MEK/ERK signaling in polycystin-2 defective mice treated with Sorafenib. *Hepatology* **56**, 2363-2374.

Tanaka, S., Kobayashi, W., Haraguchi, M., Ishihata, K., Nakamura, N. and Ozawa, M. (2016). Snail1 expression in human colon cancer DLD-1 cells confers invasive properties without N-cadherin expression. *Biochem. Biophys. Rep.* **8**, 120-126.

Torsello, B., Bianchi, C., Meregalli, C., Di Stefano, V., Invernizzi, L., De Marco, S., Bovo, G., Brivio, R., Strada, G., Bombelli, S. et al. (2016). Arg tyrosine kinase modulates TGF-β1 production in human renal tubular cells under highglucose conditions. *J. Cell Sci.* **129**, 2925-2936.

Wong, I. Y., Javaid, S., Wong, E. A., Perk, S., Haber, D. A., Toner, M. and Irimia, D. (2014). Collective and individual migration following the epithelialmesenchymal transition. *Nat. Mater.* **13**, 1063-1071.

Yazdani, S., Bansal, R. and Prakash, J. (2017). Drug targeting to myofibroblasts: implications for fibrosis and cancer. *Adv. Drug Deliv. Rev.* **121**, 101-116.

Chapter 4

Study of the interactions among Arg/Abl2, TGF-β1 and Lox in clear cell Renal Cell Carcinoma progression

Sofia De Marco[1] et al.

[1]School of Medicine and Surgery, Milano-Bicocca University, Via Cadore 48, 20900 Monza, Italy

Manuscript in preparation

Abstract

About 25-30% of clear cell Renal Cell Carcinoma (ccRCC) patients show an advanced stage of disease at the time of diagnosis, and about 30% of these patients have matastasis affecting bones. An involvement of TGF-β1 in promoting ccRCC aggressiveness, invasion and bone metastasis has been described. We previously showed that the extracellular matrix modifying enzyme lysyl oxidase (Lox), which promotes cell migration and invasion through cytoskeleton rearrangement, was overexpressed in ccRCC. Lox has a key role in the formation of premetastatic bone lesions in breast and colon cancer through osteoclast activation and osteoblast inhibition. Previous data evidenced that TGF-β1 production is modulated by Arg tyrosine kinase in human renal tubular cells. Arg modulates invasion and metastasis of breast and prostate cancer through cytoskeleton rearrangement. Based on these data and using *in vitro* models of primary cell cultures and cell lines, we evaluated the molecular interactions among TGF-β1, Lox and Arg in ccRCC cells and the functional effects of these interactions on tumor invasion and osteoclast and osteoblast behavior responsible for premetastatic bone lesion formation.

The expression and secretion of TGF-β1 and Lox, and Arg protein were increased in ccRCC versus normal cortex primary cultures. In ccRCC cultures, TGF-β1 and Lox secretion were positively correlated. TGF-β1 treatment of

ccRCC 786-O cell line upregulated Lox expression and secretion, and downregulated Arg protein level. The TGFβ-receptor inhibitor SB431542 reversed these effects. Inhibition of Smad-dependent TGF-β pathway by SIS3 and proteasome activity by MG132 rescued Arg protein level. Arg silencing by siRNA in 786-O cells induced an increment of TGF-β1 and Lox secretion, reversed by SB431542 treatment. Moreover, Arg silencing in 786-O cells decreased cell invasion analyzed by 3D invasion assay in collagen, with TGF-β1 treatment as well. TGF-β1 signalling inhibition with SB431542 reduced cell invasion in Arg silenced cells as well. Treatment with 786-O conditioned media inhibited MC3T3-E1 osteoblast proliferation and increased osteoclastic differentiation of RAW264.7 cells, as evaluated by TRAP staining. Lox inhibitor βAPN partially reverted these effects. Preliminary results obtained using conditioned media of ccRCC primary cultures confirmed these observations.

Overall, these data suggest that in ccRCC cells Arg modulates Lox production by secretion of TGF-β1 that, in turn, modulates Arg protein stability through a Smad-dependent pathway.

The characterization of the complex interactions among TGF-β1, Lox and Arg, which modulate ccRCC cell invasion and osteoblast and osteoclast behavior involved in premetastatic bone lesion formation, can shed light on the molecular mechanisms of ccRCC progression.

Introduction

Renal cell carcinoma (RCC) represents approximately 3% of all human adult malignancies and is resistant to chemotherapy and radiotherapy (Petejova N, 2016). Partial and radical nephrectomy may be curative but only in the early stages of disease (Petejova N, 2016). It is estimated that approximately 25-30% of RCC patients have metastasis at the time of diagnosis (Song W, 2018; Motzer RJ, 2017), and another 30% of patients ultimately develop metastasis after initial nephrectomy. The prognosis of metastatic RCC is generally considered poor, with a predicted 5 year survival rate, inferior to 20% (Raimondi A, 2019). Clear-cell RCC (ccRCC) is the most common (70-80%) and aggressive RCC subtype (Voung L, 2019). About 30% of metastasis in ccRCC patients affect bones, mainly leading to osteolytic lesions that compromise bone integrity and negatively impact patients prognosis (Umer M, 2018).

During tumor progression, neoplastic cells are capable of invasion and metastasis and frequently in the site of the future metastasis a premetastatic niche develops to create an environment which allows for the subsequent invasion and growth by tumor cells (Condeelis J, 2006). Tumor-secreted factors capable of modulating the behavior of resident host cells that remodel the local environment in secondary organs in absence of tumor cells are essential for premetastatic niche formation (Cox TR, 2016).

The extracellular matrix enzyme lysyl oxidase (Lox) secreted by tumor cells has a key role in the formation of premetastatic bone niche in breast and colon cancer through osteoclast activation and osteoblast inhibition (Cox TR, 2015; Reynaud C, 2017). The 32 kDa active Lox enzyme comes from extracellular proteolysis of 50 kDa pro-Lox precursor through bone morphogenetic protein 1 (BMP1) and catalyzes the covalent crosslinking of collagen and elastin in the ECM increasing tensile strength and structural stability and integrity of tissues (Barker HE, 2012; Cox TR, 2016; Di Stefano V, 2016). Moreover, Lox inside the cells promotes cellular adhesion and migration through cytoskeleton rearrangement favoring tumor progression, invasion and metastasis (Payne SL, 2005; Laczko R, 2007; Baker AM, 2013; Cox TR, 2015). We previously demonstrated that Lox is overexpressed in human ccRCC primary cell cultures and has a key role in promoting tumor cell migration and adhesion as well as matrix stiffness, all aspects involved in tumor progression and metastasis (Di Stefano V, 2016). Consistent with these data, in advanced stages of human malignancies, TGF-β contributes to create a microenvironment stimulating cancer growth and metastasis (Kajdaniuk D, 2013; Boguslawska J, 2016). Notably, an involvement in promoting ccRCC aggressiveness, invasion and bone metastasis has been previously described for TGF-β1 (Kominsky SL, 2007; Sitaram RT, 2016). Elevated expression of TGF-β1 is

correlated to poor prognosis in ccRCC patients (Hegele A, 2002; Mitropoulos D, 2004; Ananth S, 1999; Sjölund J, 2011). Interestingly, Lox expression is induced by the TGF-β pathway activation in cellular models of cardiac fibroblasts (Voloshenyuk TG, 2011) and trabecular meshwork cells (Sethi A, 2011; Sethi A, 2013). Our recent data show that TGF-β1 production is modulated by Arg/Abl2 tyrosine kinase in human renal tubular cells exposed to high level of glucose (Torsello B, 2016). In particular, a decrease in Arg kinase, induced by Arg silencing as well as an Arg kinase inhibitor, is specifically involved in the increase of TGF-β1 expression and secretion (Torsello B, 2016). The non-receptor tyrosine kinase Arg/Abl2 (Kruh GD, 1990; Perego RA, 1991) through F-actin and microtubule binding domains is able to transduce different extracellular signals into cytoskeletal rearrangements (Bradley WD, 2009). Moreover, the cytoskeleton rearrangements induced by Arg in fibroblasts modulate extracellular matrix contraction and stiffness (Torsello B, 2019) and in breast and prostate cancer cells promote tumor cell invasion and metastasis (Beaty BT, 2013; Gil-Henn H, 2013). All these data suggest the putative existence in ccRCC of molecular interactions among TGF-β1, Lox and Arg functionally involved in modulation of invasion and premetastatic bone lesion formation. Here we studied these molecular and functional aspects using an i*n vitro* model of ccRCC primary cell cultures and cell lines.

Materials and methods

Primary Cell Cultures and cell lines

Primary cell cultures were obtained from normal cortex (n=42) and tumor (n=50) tissue specimens obtained from 50 ccRCC patients (34 men and 16 women; median age, 67 years; range, 41 to 86 years) following nephrectomy. The tissues collected were those exceeding the diagnostic needs. Normal cortexes were taken from a healthy region of the kidney without any indication of cancer. All procedures were performed after written informed consent and approved by the local Ethical Committee. Histologic types, grade, and tumor stage were defined according to the World Health Organization classification. Tumors were classified as 23 pT1, 7 pT2, 18 pT3 and 2 pT4. Fuhrman grade were 4 G1, 29 G2, 12 G3 and 5 G4. The culture conditions and immune phenotypic characterization of primary cell cultures were performed as described (Bianchi C, 2010; Bianchi C, 2017). All the experiments were performed on cultures at first or second confluence.

The human ccRCC cell line 786-O and the murine macrophagic cell line RAW264.7, obtained from ATCC, were cultured in high-glucose Dulbecco's minimum essential medium (DMEM-HG) supplemented with 10% FBS, 1% of Pen/Strep, Fungizone and Glutamine (Euroclone, Milan, Italy), at 37°C and 5% CO_2. The murine preosteoblastic cell line MC3T3-E1, obtained from ATCC, was cultured in alpha

minimum essential medium (αMEM) with ribonucleosides, deoxyribonucleoside and L-glutamine (GIBCO, Thermofisher, Waltham, MA) supplemented with 10% FBS, 1% of Pen/Strep and Fungizone, at 37°C and 5% CO_2. All the experiments were performed using cell lines within 15 passages.

Treatments and Arg/Abl2 siRNA transfection in 786-O cells

After 24 hours of serum starvation, $1x10^5$ 786-O cells were treated with 5ng/ml Recombinant Human TGF-β1 (PeproTech, Rocky Hill, NJ USA) for 24 hours with and without 10μM proteasome inhibitor MG132 (Sigma-Aldrich, St Louis, MO), 10μM TGF-β receptor inhibitor SB431542 (Selleckchem, Houston, TX), 2μM PI3K inhibitor Wortmannin (Sigma-Aldrich) and 10μM Smad3 phosphorylation inhibitor SIS3 (Sigma-Aldrich) in complete medium. The inhibitors were added 1 hour prior to TGF-β1 stimulation. Control cells were only incubated in the presence of a vehicle.

Subconfluent 786-O cells were transfected with ON-TARGETplus SMART pool Human Abl2 siRNA (L-003101-000005) or ON-TARGETplus Control Pool siRNA (D-001810-10-05) (Thermo Scientific Dharmacon, Lafayette, CO), using Interferin siRNA transfection reagent (Polyplus transfection; Thermo Scientific, Waltham, MA) according to the manufacturer's instructions. Transfected cells were analyzed

after 48 hours even in the presence of SB431542.

RNA extraction and real-time quantitative PCR

Total RNA extraction and reverse transcription were performed as described (Bianchi C, 2008). Real-time quantitative PCR was carried out with a TaqMan Gene Expression Assay (Applied Biosystems, Foster City, CA) according to the manufacturer's instructions, using commercial kits (LOX Hs00942480_m1 Human; BMP1 Hs00986796_m1 Human and GAPDH Hs99998805_m1 Human; Applied Biosystems) and specific primers and probe for total ARG amplification (Perego RA, 2005). The amplifications were carried out in 20µl reactions containing 100ng of cDNA, 1X Universal PCR Master Mix, and corresponding primers and probes, in an ABI PRISM® 7900HT Fast Real-Time PCR System (Applied Biosystems) in duplicate for each sample. The relative levels of the different transcripts were expressed as $2^{-\Delta Ct}$ or as $2^{-\Delta\Delta Ct}$ and represented as fold change when referred to a calibrator considered equal to 1.

Protein extraction and western blotting

Primary cell cultures and 786-O cell line were lysed in a buffer containing 50mmol/L Tris pH 7.4, Nonidet P40, 0.25% deoxycholate, 150mmol/L NaCl, 1mmol/L EDTA, protease and phosphatase inhibitor cocktails (Sigma-Aldrich).

30µg of protein lysates quantified with a BCA microassay (Sigma-Aldrich) were separated on NuPage 4% to 12% Bis-Tris precast gels (Invitrogen, Carlsbad, CA) and transferred to nitrocellulose membranes. The blotted membranes were probed with antibodies against: Arg/Abl2 (1:250, Abcam, Cambridge, UK), β-actin (1:1000, Sigma-Aldrich), Smad2/3 (1:1000, Cell Signaling, Danvers, MA), Ser 423/425 Phospho-Smad3 (1:1000, Cell Signaling), Akt (1:2000, Cell Signaling) and Ser 473 Phospho-Akt (1:2000, Cell Signaling). Secondary antibodies coupled with horseradish peroxidase and SuperSignal West Detection System (Pierce, Rockford, IL) were used to detect protein bands.

Densitometric analysis of specific bands was performed by Image Scan Scanner with ImageJ software (NIH).

Secreted TGF-β1 and Lox quantification by ELISA

Quantification of TGF-β1 and Lox secreted in the different cell culture media was performed with a Human TGF-β1 Platinum ELISA kit (BMS249/4, eBioscience) and a Human Lox ELISA kit (EH3299 FineTest, Wuhan, China) respectively, according to the manufacturer's instructions. Absorbance at 450nm was measured using an automated microplate reader (Victor Wolla C1420, Perkin Elmer, Waltham, MA). Concentration values (pg/ml for TGF-β1 and ng/ml for Lox) were normalized to the cell count and expressed as ng/10^5 cells or fold change with respect to a calibrator considered equal to 1.

3D invasion assay

3D invasion assay was performed as described (Naber HP, 2011). To induce cellular spheroid formation $2x10^4$ Arg silenced or control 786-O cells were resuspended in 20% methocel solution (Sigma-Aldrich) and 100µl of this cell suspension were added to each well of a 96-well round bottom plate. After 24 hours the single spheroids assembled inside the methocel suspension (six for each experimental condition) were sucked up, added to 100µl of 1:1 collagen/methocel solution and plated into a 96-well plate previously coated with 50µl of neutralized collagen I solution (1,5mg/ml collagen I Rat tail, GIBCO, Life Thechology, Waltham, MA). After 30 minutes at 37°C, 50µl of low serum (1,6%) culture media containing TGF-β1 (5ng/ml) with and without SB431542 (10µM) or veichle were added to each well. Pictures of the spheroids were captured by microscopy (Leica, 10X objective) after 48 hours and the invasion area was measured using ImageJ software showing the difference between the spheroid area measured after 48 hours and the initial spheroid area.

Osteoblast growth curve

$1x10^4$ MC3T3-E1 cells were plated in duplicate in 12-well plates and grown for 72 hours in 6:1 mixture of αMEM complete media and conditioned media obtained from

ccRCC primary cultures and untreated or TGF-β-treated 786-O cells, in the presence of or absence of SB431542 (10μM) and βAPN (350μM) (Sigma-Aldrich). MC3T3-E1 cells were treated even with recombinant-Lox (rLox) (150ng/ml) (OriGene Thechnologies, Rockville, MD) added to complete fresh medium. Cell count was performed using Trypan Blue (Sigma-Aldrich) in a Thoma chamber.

Osteoclastogenesis assay

$1x10^4$ RAW264.7 cells were plated in 12-well plates and grown for 8 days in 1:1 mixture of DMEM-HG complete media and conditioned media obtained from untreated or TGF-β-treated 786-O cells, in the presence of recombinant murine sRANK-ligand (30ng/ml, PeproTech) and with and without βAPN (350μM). RAW264.7 cells were also treated with 150ng/ml rLox added to complete fresh medium. Culture media were restored every 2-3 days. On the day of harvest, cells were fixed on the culture plates with a citrate-acetone solution and stained for TRAP expression (Sigma-Aldrich). Osteoclasts were identified and enumerated as $TRAP^+$ multinucleated (≥3 nuclei) cells by microscopy (Leica; 20X objective).

Statistical analysis

Data were analyzed using unpaired or paired Student's *t*-tests. The results were expressed as mean ± SEM.

Correlation analysis was performed by computing the Pearson correlation coefficient (r) using Origin software (Originlab, Northampton, MA). P-values < 0.05 were considered as statistically significant.

Results

Lox expression is upregulated by TGF-β1 treatment in ccRCC cells

To evaluate the molecular interactions among TGF-β1, Lox and Arg in ccRCC cells we started to study the interaction between TGF-β1 and Lox in the 786-O cell line, representative of ccRCC cells with VHL biallelic inactivation. In particular, we treated 786-O cells with 5ng/ml TGF-β1 in presence or absence of the TGF-β1 receptor inhibitor SB431542. TGF-β1 treatment induced an increase of transcript expression of Lox and of Lox-activating enzyme BMP1 after 24 hours (Fig.1A). An increment of Lox active enzyme secretion was also detected in corresponding culture media (Fig.1B). The presence of SB431542 reverted these effects suggesting that TGF-β1 and its signaling are involved in the modulation of Lox production in 786-O ccRCC cells. The molecular link between TGF-β1 and Lox has been evidenced analyzing the expression of these two targets in primary cell cultures established from ccRCC and normal cortex specimens. Both TGF-β1 and Lox transcripts were upregulated in ccRCC compared to normal cortex cultures

(Fig.1C) and corresponding active proteins secreted in culture media were more abundant in ccRCC samples (Fig.1D). Notably, a significant positive correlation was also found between Lox and TGF-β1 concentration (Pearson coefficient r=0,864; p=0,012) in ccRCC primary culture media. The corresponding linear regression analysis is showed in Fig.1E.

Arg protein is downregulated by TGF-β1 treatment in ccRCC cells

We used an *in vitro* model of ccRCC to study the molecular interaction between TGF-β1 and the tyrosine kinase Arg, whose expression was upregulated at both transcript and protein level in ccRCC compared to normal cortex primary cell cultures (Fig.2 A-B).

The treatment of 786-O cells with TGF-β1 did not affect Arg transcript expression (Fig.2C), but induced a downregulation of Arg protein after 24 hours (Fig.2D). Both SB431542 and the proteasome inhibitor MG132 reversed the downregulation of Arg protein induced by TGF-β1 treatment (Fig.2D). These data suggested that TGF-β1 signaling was involved in modulation of Arg protein stability in ccRCC cells. Overall, these data suggest that in ccRCC cells the activation of TGF-β1 signaling at the same time upregulates Lox and downregulates Arg production.

Analysis of TGF-β pathways involved in Lox and Arg expression modulation in ccRCC cells

To investigate which TGF-β pathways were involved in Lox upregulation and Arg downregulation induced by TGF-β1 treatment in 786-O cells, we treated the cells with TGF-β1 in the presence of SIS3, a specific inhibitor of the canonical Smad-dependent TGF-β pathway, and of Wortmannin, a specific inhibitor of PI3K/Akt signaling, one of the non-canonical TGF-β pathways. Firstly, we proved that TGF-β1 treatment activated Akt, the downstream mediator of PI3K signaling, as indicated by the increment of its phosphorylation, and that treatment with Wortmannin was able to inhibit PI3K preventing the downstream phosphorylation of Akt in TGF-β1 treated cells (Fig.3A). Likewise, TGF-β1 treatment induced an increase of Smad3 phosphorylation, which was attenuated by SIS3 treatment (Fig.3A). However, the two inhibitors were not able to prevent the TGF-β1-dependent upregulation of Lox and BMP1 transcripts (Fig.3B), suggesting that other TGF-β pathways in ccRCC cells are likely to be involved in the observed Lox expression modulation. Conversely, treatment with SIS3, but not with Wortmannin, prevented the downregulation of Arg protein induced by TGF-β1 treatment, suggesting an involvement of the Smad-dependent TGF-β pathway in the modulation of the Arg protein level in ccRCC cells (Fig.3C).

Arg silencing in ccRCC cells increases TGF-β1 and Lox secretion

After proving that TGF-β1 signaling modulated Lox and Arg expression in ccRCC cells, we evaluated if, conversely, the modulation of Arg expression in these cells affected TGF-β1 and Lox secretion in culture media. For this purpose, Arg silencing by siRNA was performed in 786-O ccRCC cells (Fig.4A). A significant increase of both TGF-β1 and Lox secretion was detected in culture media of Arg silenced cells (Fig.4B). The presence of TGF-β-receptor inhibitor SB431542 in silenced cells prevented the increment of Lox secretion induced by TGF-β1 (Fig.4B). These data suggested that Arg modulates TGF-β1 and Lox production in ccRCC cells and that the Arg-dependent modulation of Lox expression (data not shown) and secretion (Fig.4B) is mediated by TGF-β signaling activation.

To investigate the TGF-β signaling involved in this Arg-dependent modulation, we analyzed in Arg silenced 786-O cells the phosphorylation level of Smad3 and Akt. However, in Arg silenced cells neither Smad3 nor Akt phosphorylation increased and SB431542 treatment did not significantly affect the phosphorylation level of these targets (Fig.4C). These preliminary data proved that neither PI3K/Akt- nor Smad-dependent TGF-β pathway was modulated by Arg silencing and suggested that it was likely, that other TGF-β pathways were involved in TGF-β-dependent Lox upregulation induced

by Arg silencing.

Arg and TGF-β1 modulate ccRCC cell invasion

To evaluate the functional role of the interactions among TGF-β1, Lox and Arg in ccRCC invasion, a key aspect of tumor progression, we performed a 3D invasion assay in collagen using Arg silenced 786-O ccRCC cells treated with and without TGF-β1 in the presence of or absence of SB431542. We observed that in Arg silenced cells (Fig.5A) the invasion ability was reduced compared to control cells in all the experimental conditions. The treatment with TGF-β1 slightly increased the invasion ability of both control and Arg silenced 786-O cells and the treatment with SB431542 decreased invasion ability of corresponding TGF-β1-treated cells (Fig.5B). These data suggested a key role of Arg in ccRCC cell invasion and in modulation of invasion induced by TGF-β1 stimulation.

Conditioned media of ccRCC cells inhibit osteoblast proliferation and induce osteoclast differentiation

We also started to investigate the effect of the molecular interactions among TGF-β1, Lox and Arg observed in ccRCC cells on the activity of osteoblasts and osteoclasts, which are involved in the formation of premetastatic osteolytic lesions. In particular, we analyzed the effect of conditioned media (CM) from 786-O cells treated with or without TGF-β1 on

proliferation of MC3T3-E1 osteoblasts and on osteoclastic differentiation of RAW264.7 macrophages. The treatment with 786-O cell CM for 72 hours induced inhibition of osteoblast proliferation compared to fresh medium (Fig.6A). The CM of 786-O cells treated with TGF-β1 further inhibited osteoblast proliferation (Fig.6A). Lox inhibitor βAPN efficiently reverted the inhibition of osteoblast proliferation induced by rLox added to fresh medium (Fig.6B). Instead, βAPN addition to untreated and TGF-β1 treated 786-O cell CM counteracted only partially the inhibition of osteoblast proliferation induced by corresponding CM (Fig.6A). Conversely, the addition of TGF-β-receptor inhibitor SB431542 to CM of both TGF-β treated and untreated 786-O cells further decreased osteoblast proliferation (Fig.6A). Notably, we obtained the same results using CM of ccRCC primary cell cultures (Fig.6C).

RAW264.7 cells were treated for 8 days with CM of untreated or TGF-β1 treated 786-O cells in the presence of RANK-ligand, necessary to induce osteoclastogenesis (Janssens K, 2005), and $TRAP^+$ multinucleated osteoclasts (Fig.6D) were enumerated (Fig.6F). The addition of CM from untreated 786-O cells slightly increased the osteoclastogenesis respect to fresh medium (M) containing RANK-ligand (Fig.6F). Treatment of this CM with βAPN, which efficiently reversed the increment of osteoclastogenesis induced by rLox addition to RANK-ligand containg fresh medium (Fig.6E), reversed

the increase of osteoclastogenesis induced by 786-O CM as well (Fig.6F), suggesting a key role of Lox secreted by ccRCC cells in this process. Conversely, CM of TGF-β1 treated 786-O cells did not increase the level of osteoclastogenesis induced by RANK-ligand containing fresh medium. Overall, these data suggest that, in our *in vitro* model ccRCC conditioned media inhibits osteoblast proliferation and slightly activates osteoclast differentiation. The increment of Lox secretion induced by TGF-β1 in ccRCC cells is responsible, only partially, for the further inhibition of osteoblast proliferation and does not induce an increase of osteoclastogenesis.

Discussion

In this study we investigated the molecular interactions among TGF-β1, Lox and Arg in ccRCC cells and their involvement in ccRCC progression, in particular in modulation of tumor cell invasion and osteoblast and osteoclast behavior responsible for premetastatic bone lesion formation. These aspects are particularly important in ccRCC because little is currently known about the molecular mechanisms involved in its progression and bone metastasis formation. The use of 786-O ccRCC cell line and human primary cell cultures, established from renal cortex and ccRCC tissue samples, has been instrumental for this study. 786-O cells are one of the most commonly used RCC cell

lines that harbor mutated VHL with altered HIF protein stability like most of sporadic form of ccRCC. This cell line has been chosen for our experimental purposes because it is known to give rise to clear cell tumors in nude mice and it is currently used to model bone metastasis in RCC (Brodaczewska KK, 2016). Our primary cell cultures represent a reproducible and well-characterized cellular model of ccRCC suitable for functional studies because they maintain the phenotypic, molecular and metabolic characteristics of the corresponding tissue during the first passages (Perego RA, 2005; Bianchi C, 2010; Cifola I, 2011; Bianchi C, 2017).

Firstly, using 786-O cells we demonstrated an involvement of TGF-β1 and its signaling in the modulation of Lox expression and secretion (Fig.1A-B). The molecular link between TGF-β1 and Lox has also been evidenced when analyzing the level of these two targets. They were both upregulated in ccRCC compared to normal cortex primary cell cultures and we observed that TGF-β1 secretion is positively and significantly correlated with Lox in ccRCC conditioned media (Fig.1C-E). Other authors observed that TGF-β stimulation induced the upregulation of Lox transcript and secreted active form in other cellular models (Boak AM, 1994; Roy R, 1996; Goto Y, 2005), but never in neoplastic cells. We also observed in 786-O cells that TGF-β1 induced an overexpression of BMP1 required for proteolytic extracellular

processing of pro-Lox to form the active Lox enzyme. This result suggests that the TGF-β-dependent increment of Lox level may be due not only to an upregulation of its transcript but to an improvement in its extracellular processing. A TGF-β-dependent upregulation of BMP1 expression was also found in dermal and cardiac fibroblasts and in other fibrogenic cells (Lee S, 1997; Parsons M, 1999; Voloshenyuk TG, 2011). In *in vitro* and *in vivo* models of fibrosis (Cai L, 2017) it has been shown that BMP1 can cleave extracellularly the latent form of TGF-β1 leading to its activation (Trackman PC, 2005; Liu X, 2006). Thus, the TGF-β1-mediated increase in BMP1 expression, if confirmed at protein level, in our cellular model could activate TGF-β1 present in tumor microenvironment (Pickup M, 2013) providing a positive feedback to generate more Lox. Since our previous results (Di Stefano V, 2016) showed that Lox promoted different aspects of ccRCC progression such as cell migration, invasion and matrix stiffness, this putative BMP1-mediated positive feedback between TGF-β1 and Lox may have a role in ccRCC progression.

In our *in vitro* model of ccRCC we analyzed the effect of TGF-β1 treatment on the expression of the non-receptor tyrosine kinase Arg, upregulated in ccRCC cultures compared to normal cortex (Fig.2A-B) as expected on the basis of its documented role in the promotion of key steps in tumor progression like migration, invasion and metastatization

(Beaty BT, 2013; Gil-Henn H, 2013). TGF-β1 stimulation of 786-O cells induced a significant decrease of Arg protein (Fig.2D), but did not affect its transcript (Fig.2C). As expected, specific proteasome inhibition by MG132 significantly reverted the downregulation of Arg protein induced by TGF-β1 (Fig.2D). The ongoing analysis of the ubiquitination level of Arg after TGF-β1 treatment in the presence of or absence of SB431542 may confirm the involvement of TGF-β1 signaling in the modulation of Arg protein stability.

To investigate which TGF-β1 pathways may be involved in the modulation of Lox, BMP1 and Arg expression, we started to analyse two out of three pathways described which are involved in TGF-β1-dependent upregulation of Lox and BMP1 in cardiac fibroblasts (Voloshenyuk TG, 2011) and trabecular meshwork endothelial cells (Sethi A, 2011; Sethi A, 2013), namely the canonical Smad-dependent and non-canonical PI3K/Akt-dependent pathways. However, neither the Smad3 nor the PI3K inhibitor was able to prevent the TGF-β-dependent upregulation of Lox and BMP1 (Fig.3A-B), suggesting that in ccRCC cells other non-canonical TGF-β1 pathways not analysed here, such as the MAPK-dependent pathway, may be responsible for this modulation. Otherwise, the downregulation of Arg protein was prevented after treatment with the Smad3 inhibitor SIS3, suggesting the involvement of the Smad-dependent TGF-β1 pathway in the

modulation of Arg protein level (Fig.3C). The production of reactive oxygen species (ROS) might be involved in TGF-β-mediated downregulation of Arg protein. It has been described that TGF-β1 stimulates ROS production by increasing the expression of the NOX4 enzyme and decreasing the level of some antioxidant enzymes (Islam KN, 1997; Sturrock A, 2006). In vascular smooth muscle cells TGF-β-dependent ROS production induced senescence (You W, 2019). In MCF-7 breast cancer and embryonal renal 293 cells ROS promoted Arg degradation by ubiquitination (Cao C, 2005). The detection of a ROS increment in our ccRCC cells treated with TGF-β1 could confirm this interpretation.

In 786-O ccRCC cells we noted that Arg expression is downregulated by TGF-β1 stimulation and, conversely, the downregulation of Arg obtained by silencing was able to upregulate TGF-β1 secretion (Fig.4A-B). We observed an upregulation of TGF-β1 secretion and expression in renal tubular cells as well after Arg silencing and in $Arg^{-/-}$ MEF (Torsello B, 2016; Torsello B, 2019), suggesting that an ubiquitary molecular mechanism may be responsible for this mutual modulation. Even in this case a ROS-dependent oxidative stress might be involved in the Arg-dependent upregulation of TGF-β secretion. It has been noted that Arg deficiency attenuates catalase activation with consequent accumulation of ROS (Cao C, 2003). Moreover, ROS

accumulation in the microenvironment can induce TGF-β secretion and activate latent TGF-β (Liu RM, 2010; Gorowiec MR, 2012). Notably, Arg silencing in 786-O ccRCC cells also increased Lox secretion and inhibition of the TGF-β-receptor by SB431542 reversed this effect, suggesting that Arg-dependent modulation of Lox production is mediated by TGF-β signaling activation. Neither PI3K/Akt- nor Smad-dependent TGF-β pathway was modulated by Arg silencing suggesting that the TGF-β-dependent upregulation of Lox production, activated by Arg silencing, was mediated by other non-canonical TGF-β1 pathways not analyzed here (Fig.4C). The acquisition of invasion ability by tumor cells is one of the most important and studied aspects of tumor progression. For this reason, we evaluated the functional role of TGF-β1, Lox and Arg and their interactions in ccRCC cell invasion by a 3D invasion assay performed in collagen, the most abundant extracellular matrix component of bones (Kolb AD, 2019). We observed that the invasive capacity of 786-O ccRCC cells increased after TGF-β1 stimulation and the inhibition of its signaling by SB431542 reversed this effect (Fig.5B). These results are consistent with those obtained by others using a 2D invasion assay in matrigel (Sitaram RT, 2016). Moreover, we observed that Arg silencing in ccRCC cells induced a decrease in their invasion ability as described in breast cancer (Gil-Henn H, 2013), hepatocellular carcinoma (Xing QT, 2014) and melanoma (Ganguly SS,

2012). In these tumors, Arg has been detected in invadopodia, protrusive membrane structures that promote remodeling of the extracellular matrix during tumor invasion (Smith-Pearson PS, 2010; Mader CC, 2011), and it was involved in cytoskeleton rearrangement responsible for their formation (Beaty BT, 2013; Gil-Henn H, 2013). However, we observed that in our cellular model Arg silencing affected invasion ability even in TGF-β1 treated cells (Fig.5B). Since TGF-β1 signaling inhibition reduced invasion of Arg silenced cells too, we argue that Arg and TGF-β1 signaling are equally important in the stimulation of ccRCC invasion. We previously described the decrement of ccRCC cell invasivity induced by Lox silencing, proving the role of Lox as inducer of ccRCC cell invasion (Di Stefano V, 2016). The evaluation of the effect of Lox inhibition by βAPN on invasion ability of TGF-β1 treated 786-O cells will clarify the role of Lox overproduction, induced by TGF-β1 stimulation, on invasive behavior of control and Arg silenced 786-O cells.

We also analyzed the effect of the molecular interactions among TGF-β1, Lox and Arg in ccRCC cells on the formation of premetastatic bone lesions. For the premetastatic niche formation tumor secreted factors capable of modulating the behavior of resident host cells in absence of tumor cells are essential (Cox TR, 2016). We have investigated the role of ccRCC secretome, also containing TGF-β1 and Lox, on *in vitro* osteoblast and osteoclast behavior. Recent reports

demonstrated that Lox secreted by tumor cells has a key role in the formation of premetastatic bone lesions of breast and colon cancer through osteoclast activation and osteoblast inhibition (Cox TR, 2015; Reynaud C, 2017), but untill now no evidence of this Lox role has been shown in ccRCC. Using our *in vitro* model, we showed that ccRCC conditioned media (CM) inhibited osteoblast proliferation, and CM of 786-O cells treated with TGF-β1 further inhibited their growth (Fig.6A). However, the presence of Lox in this CM was only partially responsible for this effect, as shown by its inhibition with 350µM βAPN that, completly reversed the decrease of osteoblast growth induced by the addition in fresh medium of 150ng/ml rLox, a concentration much higher than the one detected in ccRCC cell CM (Fig.6B). Thus, other molecules such as some chemokines and cytokines described as osteoblast inhibitors (Brylka LJ, 2019; Janssens K, 2005) might be secreted in CM by ccRCC cells and induce the observed inhibition of osteoblast growth. Otherwise, the inhibition of TGF-β1 by the addition of SB431542 to CM of ccRCC cells further decreases osteoblast proliferation (Fig.6A) confirming the role of inducer of osteoblast proliferation described by some authors for TGF-β1 (Tang Y, 2009; Janssens K, 2005).

Moreover, 786-O conditioned media slightly increased the osteoclastic differentiation of RAW264.7 cells grown in presence of the RANK-ligand that in our cellular model and

in our experimental conditions, was necessary to induce osteoclastogenesis. Treatment with βAPN efficiently reverted this CM-dependent increment of osteoclastogenesis, suggesting a key role of Lox secreted by ccRCC cells in this process (Fig.6E). However, the increment of Lox secretion induced by TGF-β1 in ccRCC cells did not improve the osteoclastogenesis induced by RANK-ligand, probably because of the TGF-β1 treatment which increased the secretion of Lox, but which might also increase the secretion of other molecules able to inhibit osteoclastogenesis, such as INFs, IL-3, IL-4 and IL-10 (Amarasekara DS, 2018), thus counteracting the effect of Lox increment (Fig.6F). These preliminary data suggest that ccRCC conditioned media, inducing inhibition of osteoblast proliferation and a slight activation of osteoclastogenesis, might create an imbalance between bone formation and bone resorption that favours the development of premetastatic bone lesions. Moreover, the increment of Lox secretion, induced by TGF-β1 in ccRCC cells that further inhibited osteoblast growth, may further impair bone formation. The study of the effects induced by CM of Arg silenced ccRCC cells on osteoblast and osteoclast behavior will clarify the role of the Arg-dependent modulation of ccRCC secretome and particularly of TGF-β1 and Lox secretion on premetastatic bone lesion formation.

Our findings describe the molecular interactions among TGF-β1, Lox and Arg in ccRCC cells and their functional effects on

ccRCC invasion and modulation of osteoblast and osteoclast behavior, improve the current knowledge about the molecular mechanisms of ccRCC progression and may open new targeted therapeutic strategies for ccRCC patients.

Figure Legends:

Figure 1:

Effect of TGF-β1 treatment on Lox expression in ccRCC cells. A: Lox and BMP1 transcripts evaluated by real-time PCR in 786-O cells untreated (NT) or treated with TGF-β1 in the presence of or absence of SB431542 (SB). The relative amount of the different transcripts, calculated as $2^{-\Delta\Delta Ct}$, were represented as fold change compared to the corresponding untreated (NT) sample considered equal to 1. Mean values ± SEM of at least three independent experiments analyzed in duplicate. *p<0.05 (paired Student's t-test). **B**: Lox enzyme evaluated by ELISA assay in conditioned medium of 786-O cells untreated (NT) or treated with TGF-β1 in the presence of or absence of SB431542 (SB). The concentration values were represented as fold change compared to the untreated (NT) sample. Mean values ± SEM of at least three independent experiments analyzed in duplicate. *p<0.05 (paired Student's t-test). **C**: Quantification of Lox and BMP1 transcripts performed by real-time PCR in normal cortex and ccRCC primary cell cultures. Mean values, expressed as $2^{-\Delta Ct}$, ± SEM of at least 8 different cortex and 16 different

ccRCC cultures analyzed in duplicate. *p<0.05 (unpaired Student's t-test). **D**: 1,5x10^5 cells were grown for 48 hours in complete medium, and TGF-β1 and Lox concentrations were quantified in corresponding conditioned medium by ELISA assay. Mean values, expressed as ng/10^5 cells, ± SEM of 5 different cortex and 8 different ccRCC cultures analyzed in duplicate. *p<0.05 (unpaired Student's t-test). **E**: Linear regression analysis between TGF-β1 and Lox concentrations evaluated in ccRCC primary culture conditioned media by ELISA assay.

Figure 2:

Effect of TGF-β1 treatment on Arg expression in ccRCC cells. A: Arg transcript expression evaluated by real-time PCR in normal cortex and ccRCC primary cell cultures. Mean values, expressed as $2^{-\Delta Ct}$, ± SEM of 8 different cortex and 16 different ccRCC cultures analyzed in duplicate. **B**: Representative western blot analysis of Arg and β-actin proteins performed in lysates from matched cortex (C) and ccRCC (T) primary cell cultures taken from three different patients (pt). In the graph, densitometric data expressed as relative OD values of Arg protein bands normalized for corresponding β-actin band. Mean values ± SEM of 13 different cortex and 21 different ccRCC cultures. **C**: Arg transcript expression evaluated by real-time PCR in 786-O cells untreated (NT) or treated with TGF-β1 in the presence

of or absence of SB431542 (SB). The relative amount of the transcript, calculated as $2^{-\Delta\Delta Ct}$, was represented as fold change compared to the untreated sample (NT) considered equal to 1. Mean values ± SEM of at least three independent experiments analyzed in duplicate. **D**: Representative western blot analysis of Arg and β-actin proteins performed in lysates from 786-O cells untreated (NT) and treated with TGF-β1 in the presence of or absence of SB431542 (SB) or MG132. In the graph, Arg band intensities normalized for corresponding β-actin were expressed as fold change compared to the untreated sample (NT). Mean values ± SEM of at least three independent experiments. *$p<0.05$ (paired Student's t-test).

Figure 3:

TGF-β pathways involved in Lox and Arg modulation in ccRCC cells. A: Representative western blot analysis of protein lysates from 786-O cells untreated (NT) or treated with TGF-β1 in presence or absence of Wortmannin (WORT) or SIS3. The protein bands of phospho-Akt (P-Akt), Akt, phospho-Smad3 (P-Smad3) and Smad2/3 are shown. Smad3 specific band was indicated by an arrow. **B**: Lox and BMP1 transcripts evaluated by real-time PCR in 786-O cells untreated (NT) or treated with TGF-β1 in the presence of or absence of Wortmannin (WORT) or SIS3. The relative amount of the different transcripts, calculated as $2^{-\Delta\Delta Ct}$, was

represented as fold change compared to the corresponding untreated (NT) sample considered equal to 1. Mean values ± SEM of at least three independent experiments performed in duplicate. *p<0.05 (paired Student's t-test). **C**: Representative western blot analysis of Arg and β-actin proteins performed in lysates of 786-O cells untreated (NT) or treated with TGF-β1 in the presence of or absence of Wortmannin (WORT) or SIS3. In the graph, Arg band intensities normalized for corresponding β-actin were expressed as fold change compared to the untreated (NT) sample. Mean values ± SEM of at least three independent experiments. *p<0.05. (paired Student's t-test).

Figure 4:

Effect of Arg silencing on TGF-β1 and Lox secretion by ccRCC cells. A: Representative western blot analysis of Arg and β-actin proteins in 786-O cells treated for 48 hours with control (ctrl) or Arg siRNA in the presence of or absence of SB431542 (SB). **B**: TGF-β1 and Lox secreted in conditioned media of control (ctrl siRNA) and Arg silenced (Arg siRNA) 786-O cells in the presence of or absence of SB431542 (SB) evaluated by ELISA assay. Data expressed as fold change compared to the corresponding control (ctrl siRNA) sample. Mean values ± SEM of at least three independent experiments performed in duplicate. *p<0.05. (paired Student's t-test). **C**: Representative western blot of protein

lysates from 786-O cells treated with control (ctrl) siRNA or Arg siRNA in the presence of or absence of SB431542 (SB). The protein bands of phospho-Akt (P-Akt), Akt, phospho-Smad3 (P-Smad3) and Smad2/3 are shown. Smad3 specific band was indicated by an arrow. In the graph the phospho-Akt (P-Akt) band intensity normalized for the corresponding total Akt band, and the phospho-Smad3 (P-Smad3) band intensity normalized for the corresponding total Smad3 band and both were expressed as fold change compared to the corresponding control (ctrl siRNA) sample. Mean values ± SEM of at least three independent experiments.

Figure 5:

Effects of Arg silencing and TGF-β1 treatment on ccRCC cell invasion. A: Representative western blot analysis of Arg and β-actin proteins performed in lysates of 786-O cells treated for 72 hours with control (ctrl) or Arg siRNA. **B**: Representative images of 786-O cell spheroids, obtained using control (ctrl siRNA) or Arg silenced (Arg siRNA) 786-O cells untreated (NT) or treated with TGF-β1 in the presence of or absence of SB431542 (SB), invading collagen in a 3D invasion assay for 48 hours. In the graph was reported the invasion area of the 786-O cell spheroids. Mean values ± SEM of the data obtained with six spheroids for each treatment in three independent experiments. *$p<0.05$. (paired Student's t-test).

Figure 6:

Effect of ccRCC cell conditioned media on osteoblast proliferation and osteoclast differentiation. A: Cell proliferation of MC3T3-E1 osteoblasts treated with conditioned media of 786-O cells untreated (786-O CM) or TGF-β1 treated (786-O TGF-β1 CM) and cultured in the presence of or absence of βAPN or of SB431542 (SB) for 72 hours. M: fresh medium. Mean values ± SEM of three independent experiments performed in duplicate. *$p<0.05$. (paired Student's t-test). **B**: Cell proliferation of MC3T3-E1 osteoblasts treated with rLox with or without βAPN for 72 hours. Mean values ± SEM of two independent experiments performed in duplicate. **C**: Cell proliferation of MC3T3-E1 osteoblasts treated with conditioned media of ccRCC primary cell cultures and grown in the presence of or absence of βAPN or of SB431542 (SB) for 72 hours. Mean values ± SEM of two independent experiments performed in duplicate. **D**: Representative images of TRAP staining performed in RAW264.7 cells grown for 8 days in the presence of fresh medium containing RANK-ligand (M) or of conditioned media of untreated 786-O cells (786-O CM) or of TGF-β1 treated 786-O cells (786-O TGF-β1 CM) containing RANK-ligand and where indicated, βAPN. Bars: 50µm. Insets: 4X digital magnification of $TRAP^+$ multinucleated cells indicated by arrows. **E**: $TRAP^+$ multinucleated osteoclasts obtained after

8 days of treatment with fresh complete medium containing RANK-ligand (M), with or without rLox and βAPN. Data expressed as mean ± SEM of $TRAP^+$ multinucleated cells enumerated in each field. 40 fields at 200X magnification for each well were analyzed in two independent experiments. **F**: $TRAP^+$ multinucleated osteoclasts obtained after 8 days of treatment with fresh complete medium containing RANK-ligand (M) and with CM described in **D.** Data expressed as mean ± SEM of $TRAP^+$ multinucleated cells in each field. 40 fields at 200X magnification for each well were analyzed in at least three independent experiments.

Figure 1

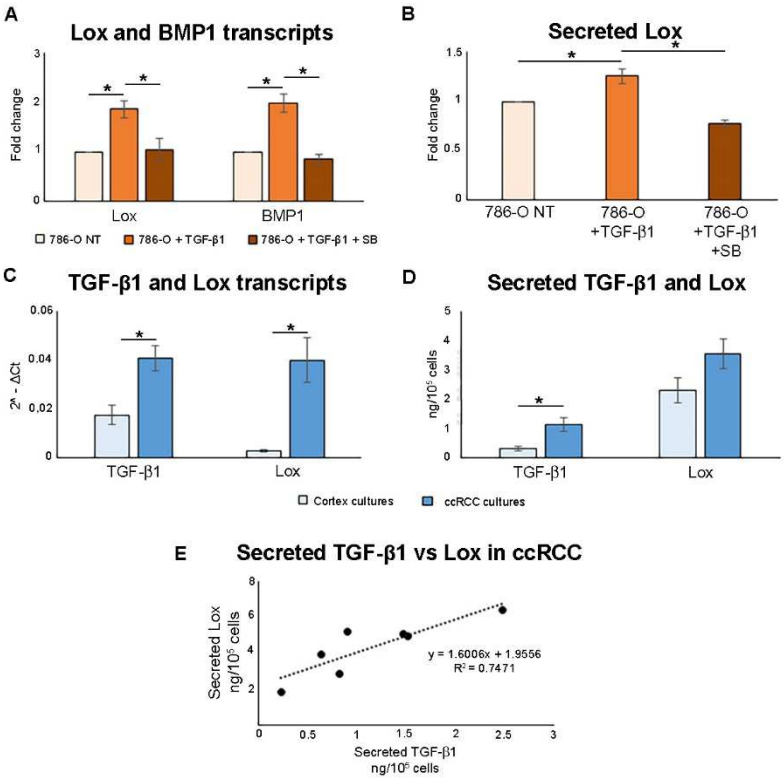
A
Lox and BMP1 transcripts
Fold change
Lox
BMP1
786-O NT
786-O + TGF-β1
786-O + TGF-β1 + SB
B
Secreted Lox
Fold change
786-O NT
786-O +TGF-β1
786-O +TGF-β1 +SB
C
TGF-β1 and Lox transcripts
2^- ΔCt
TGF-β1
Lox
D
Secreted TGF-β1 and Lox
ng/10^6 cells
TGF-β1
Lox
Cortex cultures
ccRCC cultures
E
Secreted TGF-β1 vs Lox in ccRCC
Secreted Lox ng/10^6 cells
y = 1.6006x + 1.9556
R² = 0.7471
Secreted TGF-β1 ng/10^6 cells

Figure 2

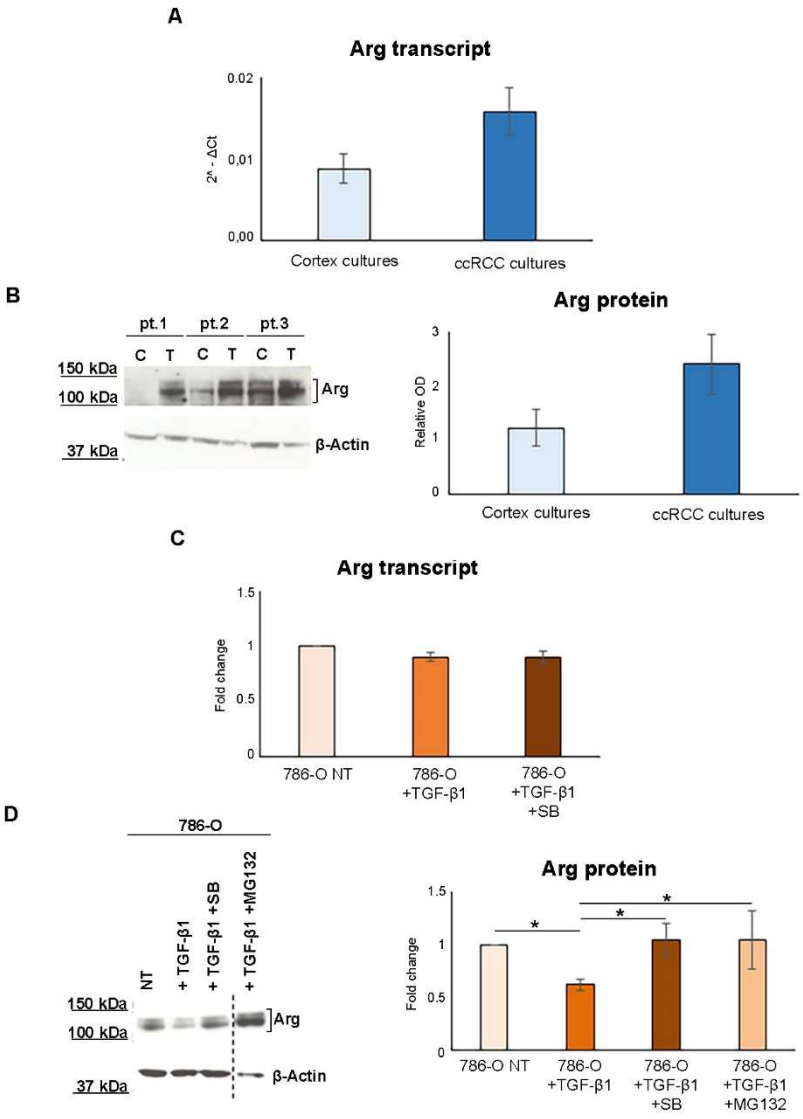
A
Arg transcript
0.02
0,01
0,00
2^- ΔCt
Cortex cultures
ccRCC cultures
B
pt.1
pt.2
pt.3
C T C T C T
150 kDa
100 kDa
37 kDa
Arg
β-Actin
Arg protein
Relative OD
3
2
1
0
Cortex cultures
ccRCC cultures
C
Arg transcript
1.5
1
0.5
0
Fold change
786-O NT
786-O +TGF-β1
786-O +TGF-β1 +SB
D
786-O
NT
+ TGF-β1
+ TGF-β1 +SB
+ TGF-β1 +MG132
150 kDa
100 kDa
37 kDa
Arg
β-Actin
Arg protein
1.5
1
0.5
0
Fold change
*
*
*
786-O NT
786-O +TGF-β1
786-O +TGF-β1 +SB
786-O +TGF-β1 +MG132

Figure 3

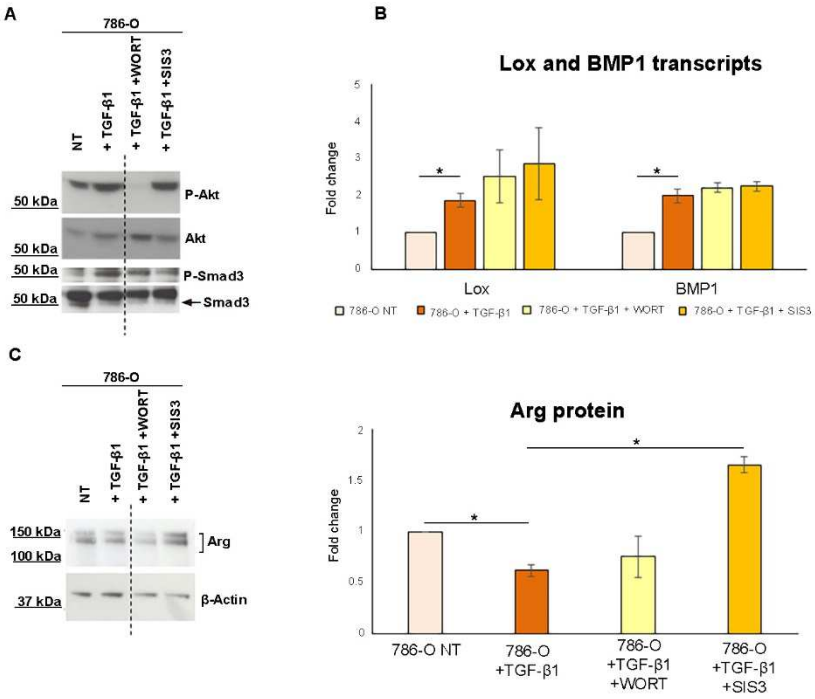
A
786-O
NT
+ TGF-β1
+ TGF-β1 +WORT
+ TGF-β1 +SIS3
50 kDa
P-Akt
50 kDa
Akt
50 kDa
P-Smad3
50 kDa
Smad3
B
Lox and BMP1 transcripts
Fold change
Lox
BMP1
786-O NT
786-O + TGF-β1
786-O + TGF-β1 + WORT
786-O + TGF-β1 + SIS3
C
786-O
NT
+ TGF-β1
+ TGF-β1 +WORT
+ TGF-β1 +SIS3
150 kDa
100 kDa
Arg
37 kDa
β-Actin
Arg protein
Fold change
786-O NT
786-O +TGF-β1
786-O +TGF-β1 +WORT
786-O +TGF-β1 +SIS3

Figure 4

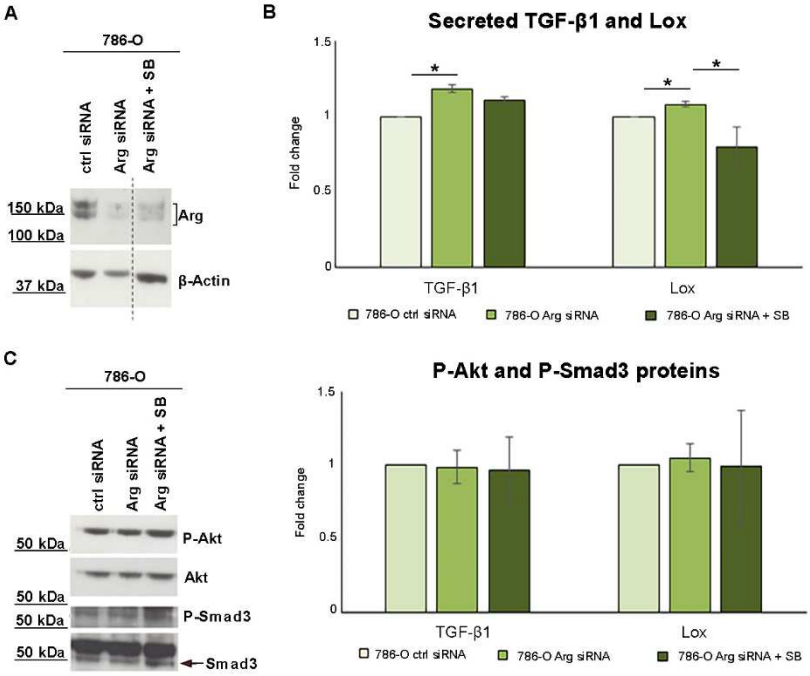
A
786-O
ctrl siRNA
Arg siRNA
Arg siRNA + SB
150 kDa
100 kDa
Arg
37 kDa
β-Actin
B
Secreted TGF-β1 and Lox
Fold change
1.5
1
0.5
0
*
*
*
TGF-β1
Lox
786-O ctrl siRNA
786-O Arg siRNA
786-O Arg siRNA + SB
C
786-O
ctrl siRNA
Arg siRNA
Arg siRNA + SB
50 kDa
P-Akt
50 kDa
Akt
50 kDa
P-Smad3
50 kDa
Smad3
P-Akt and P-Smad3 proteins
Fold change
1.5
1
0.5
0
TGF-β1
Lox
786-O ctrl siRNA
786-O Arg siRNA
786-O Arg siRNA + SB

Figure 5

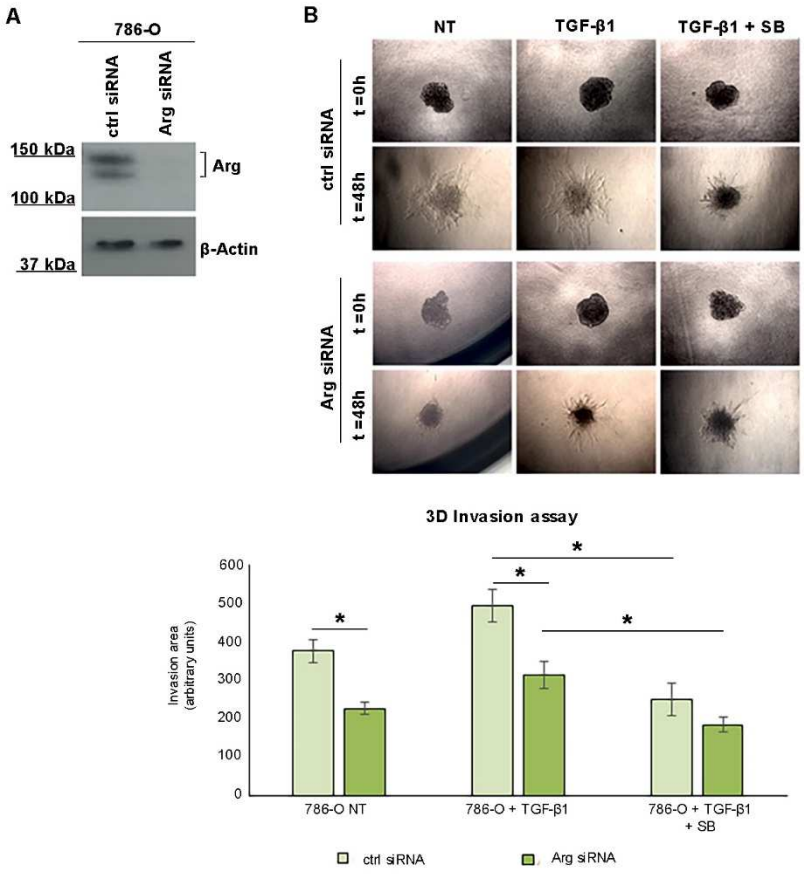
A
786-O
ctrl siRNA
Arg siRNA
150 kDa
100 kDa
Arg
37 kDa
β-Actin
B
NT
TGF-β1
TGF-β1 + SB
ctrl siRNA
t =0h
t =48h
Arg siRNA
t =0h
t =48h
3D Invasion assay
Invasion area (arbitrary units)
600
500
400
300
200
100
0
786-O NT
786-O + TGF-β1
786-O + TGF-β1 + SB
ctrl siRNA
Arg siRNA

Figure 6

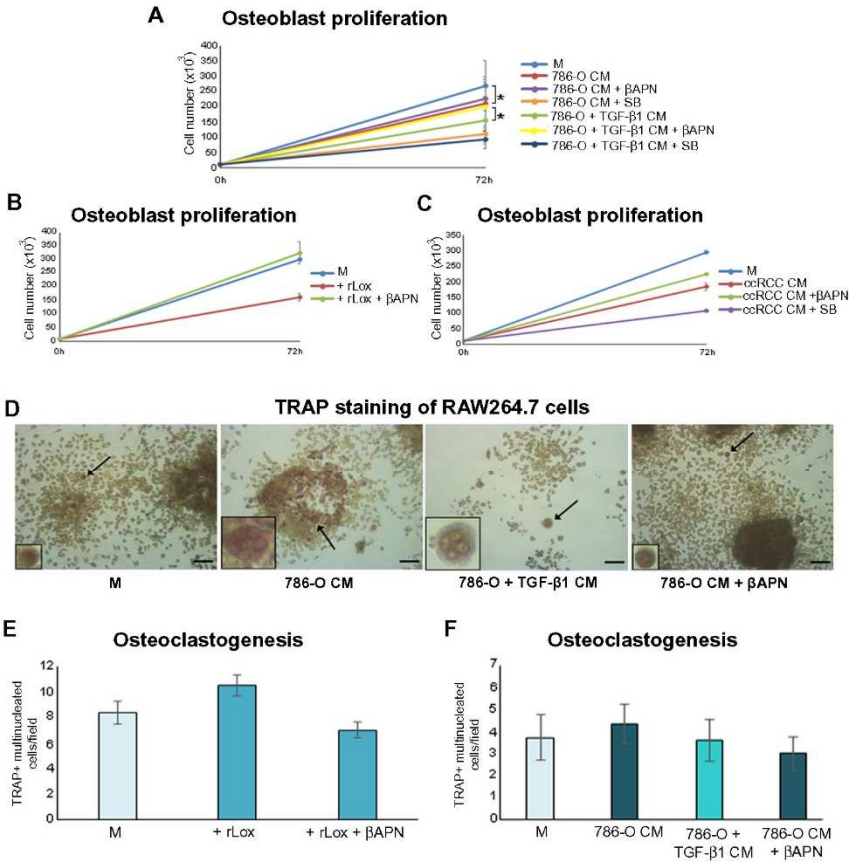
A
Osteoblast proliferation
Cell number (x10³)
M
786-O CM
786-O CM + βAPN
786-O CM + SB
786-O + TGF-β1 CM
786-O + TGF-β1 CM + βAPN
786-O + TGF-β1 CM + SB
0h
72h
B
Osteoblast proliferation
Cell number (x10³)
M
+ rLox
+ rLox + βAPN
C
Osteoblast proliferation
Cell number (x10³)
M
ccRCC CM
ccRCC CM +βAPN
ccRCC CM + SB
D
TRAP staining of RAW264.7 cells
M
786-O CM
786-O + TGF-β1 CM
786-O CM + βAPN
E
Osteoclastogenesis
TRAP+ multinucleated cells/field
M
+ rLox
+ rLox + βAPN
F
Osteoclastogenesis
TRAP+ multinucleated cells/field
M
786-O CM
786-O + TGF-β1 CM
786-O CM + βAPN

References

Amarasekara DS, Yun H, Kim S, Lee N, Kim H and Rho J. Regulation of osteoclast differentiation by cytokine networks. *Immune Netw.* (2018); 18(1):e8.

Ananth S, Knebelmann B, Grüning W, Dhanabal M, Walz G, Stillman IE and Sukhatme VP, Transforming growth factor beta1 is a target for the von Hippel-Lindau tumor suppressor and a critical growth factor for clear cell renal carcinoma. *Cancer Res.* (1999); 59(9):2210-2216.

Baker AM, Bird D, Lang G, Cox TR and Erler JT. Lysyl oxidase enzymatic function increases stiffness to drive colorectal cancer progression through FAK. *Oncogene.* (2013); 32(14):1863-1868.

Barker HE, Cox TR and Erler JT. The rationale for targeting the LOX family in cancer. *Nat Rev Cancer.* (2012); 12(8):540-552.

Beaty BT, Sharma VP, Bravo-Cordero JJ, Simpson MA, Eddy RJ, Koleske AJ and Condeelis J. B1 integrin regulates Arg to promote invadopodial maturation and matrix degradation. *Mol Biol Cell.* (2013); 24(11):1661-1675.

Bianchi C, Torsello B, Angeloni V, Bombelli S, Soldi M, Invernizzi L, Brambilla P and Perego RA. Eight full-length Abelson related gene (Arg) isoforms are constitutively expressed in Caki-1 cell line and cell distribution of two isoforms has been analyzed after transfection. *J Cell Biochem*. (2008); 105(5):1219-1227.

Bianchi C, Bombelli S, Raimondo F, Torsello B, Angeloni V, Ferrero S, Di Stefano V, Chinello C, Cifola I, Invernizzi L, Brambilla P, Magni F, Pitto M, Zanetti G, Mocarelli P and Perego RA. Primary cell cultures from human renal cortex and renal-cell carcinoma evidence a differential expression

of two spliced isoforms of Annexin A3. *Am J Pathol.* (2010); 176(4):1660-1670.

Bianchi C, Meregalli C, Bombelli S, Di Stefano V, Salerno F, Torsello B, De Marco S, Bovo G, Cifola I, Mangano E, Battaglia C, Strada G, Lucarelli G, Weiss RH and Perego RA. The glucose and lipid metabolism reprogramming is grade-dependent in clear cell renal cell carcinoma primary cultures and is targetable to modulate cell viability and proliferation. *Oncotarget.* (2017); 8(69):113502-113515.

Boak AM, Roy R, Berk J, Taylor L, Polgar P, Goldestein RH and Kagan HM. Regulation of lysyl oxidase expression in lung fibroblasts by transforming growth factor-beta1 and prostaglandin E2. *Am J Respir Cell Mol Biol.* (1994); 11(6):751-755.

Boguslawska J, Kedzierska H, Poplawski P, Rybicka B, Tanski Z and Piekielko-Witkowska A. Expression of genes involved in cellular adhesion and extracellular matrix remodelling correlates with poor survival of patients with renal cancer. *J Urol.* (2016); 195(6):1892-1902.

Bradley WD and Koleske AJ. Regulation of cell migration and morphogenesis by Abl-family kinases: emerging mechanisms and physiological contexts. *J Cell Sci*. (2009); 122(19):3441-3454.

Brodaczewska KK, Szczylik C, Fiedorowicz M, Porta C and Czarnecka AM. Choosing the right cell line for renal cell cancer research. *Mol Cancer.* (2016); 15(1):83.

Brylka LJ and Schinke T. Chemokine in physiological and pathological bone remodelling. *Front Immunol.* (2019); 10:2182.

Cai L, Xiong X, Kong X and Xie J. The role of the lysyl oxidases in tissue repair and remodeling: a concise review. *Tissue Eng Regen Med.* (2017); 14(1):15-30.

Cao C, Leng Y and Kufe D. Catalase activity is regulated by c-Abl and Arg in the oxidative stress response. *J Biol Chem.* (2003); 278(32):29667-29675.

Cao C, Li Y, Leng Y, Li P, Ma Q and Kufe D. Ubiquitination and degradation of the Arg tyrosine kinase is regulated by oxidative stress. *Oncogene.* (2005); 24(15):2433-2440.

Cifola I, Bianchi C, Mangano E, Bombelli S, Frascati F, Fasoli E, Ferrero S, Di Stefano V, Zipeto MA, Magni F, Signorini S, Battaglia C and Perego RA. Renal cell carcinoma primary cultures maintain genomic and phenotypic profile of parental tumor tissues. *BMC Cancer.* (2011); 11:244.

Condeelis J and Pollard JW. Macrophages: obligate partners for tumor cell migration, invasion and metastasis. *Cell.* (2006); 124(2):263-266.

Cox TR, Rumney RM, Schoof EM, Perryman L, Hoye AM, Agrawal A, Bird D, Latif NA, Forrest H, Evans HR, Huggins ID, Lang G, Linding R, Gartland A and Erler JT. The hypoxic cancer secretome induces pre-metastatic bone lesions through lysyl oxidase. *Nature.* (2015); 522(7554):106-110.

Cox TR, Gartland A and Erler JT. Lysyl oxidase, a targetable secreted molecule involved in cancer metastasis. *Cancer Res.* (2016); 76(2):188-192.

Di Stefano V, Torsello B, Bianchi C, Cifola I, Mangano E, Bovo G, Cassina V, De Marco S, Corti R, Meregalli C, Bombelli S, Viganò P, Battaglia C, Strada G and Perego RA. Major action of endogenous lysyl oxidase in clear cell renal cell carcinoma progression and collagen stiffness revealed by primary cell cultures. *AM J Pathol.* (2016); 186(9):2473-2485.

Ganguly SS, Fiore LS, Sims JT, Friend JW, Srinivasan D, Thacker MA, Cibull ML, Wang C, Novak M, Kaetzel DM and

Plattner R. c-Abl and Arg are activated in human primary melanomas, promote melanoma cell invasion via distinct pathways, and drive metastatic progression. *Oncogene*. (2012); 31(14):1804-1816.

Gil-Henn H, Patsialou A, Wang Y, Warren MS, Condeelis JS and Koleske AJ. Arg/Abl2 promotes invasion and attenuates proliferation of breast cancer in vivo. *Oncogene*. (2013); 32(21): 2622-2630.

Gorowiec MR, Borthwick LA, Parker SM, Kirby JA, Saretzki GC and Fisher AJ. Free radical generation induces epithelial-to-mesenchymal transition in lung epithelium via a TGF-β1-dependent mechanism. *Free Radic Biol Med.* (2012); 52(6):1024-1032.

Goto Y, Uchio-Yamada K, Anan S, Yamamoto Y, Ogura A and Manabe N. Transforming growth factor-beta1 mediated up-regulation of lysyl oxidase in the kidneys of hereditary nephrotic mouse with chronic renal fibrosis. *Virchows Arch.* (2005); 447(5):859-868.

Hegele A, Varga Z, von Knobloch R, Heidenreich A, Kropf J and Hofmann R. TGFbeta1 in patients with renal cell carcinoma. *Urol. Res.* (2002); 30(2):126-129.

Islam KN, Kayanoki Y, Kaneto H, Suzuki K, Asahi M, Fujii J and Taniguchi N. TGF-beta1 triggers oxidative modifications and enhances apoptosis in HIT cells through accumulation of reactive oxygen species by suppression of catalase and glutathione peroxidase. *Free Radic Biol Med.* (1997); 22(6):1007-1017.

Janssens K, ten Dijke P, Janssens S and Van Hul W. Transforming growth factor-β1 to the bone. *Endocr Rev.* (2005); 26(6):743-774.

Kajdaniuk D, Marek B, Borgiel-Marek H and Kos-Kudla B. Transforming growth factor β1 (TGFβ1) in physiology and

pathology. *Endokrynol Pol.* (2013); 64(5):384-396.

Kolb AD and Bussard KM. The bone extracellular matrix as an ideal milieu for cancer cell metastases. *Cancers (Basel).* (2019); 11(7):pii:E1020.

Kominsky SL, Doucet M, Brady K and Weber KL. TGF-beta promotes the establishment of renal cell carcinoma bone metastasis. *J Bone Miner Res.* (2007); 22(1):37-44.

Kruh GD, Perego R, Miki T and Aaronson SA. The complete coding sequence of arg defines the Abelson subfamily of cytoplasmic tyrosine kinases. *Proc Natl Acad Sci*. (1990); 87(15):5802-5806.

Laczko R, Szauter KM, Jansen MK, Hollosi P, Muranyi M, Molnar J, Fong KS, Hinek A and Csiszar K. Active lysyl oxidase (LOX) correlates with focal adhesion kinase (FAK)/paxillin activation and migration in invasive astrocytes. *Neuropathol Appl Neurobiol.* (2007); 33(6):631-643.

Lee S, Solow-Cordero DE, Kessler E, Takahara K and Greenspan DS. Transforming growth factor-beta regulation of bone morphogenetic protein-1/procollagen C-proteinase and related proteins in fibrogenic cells and keratinocytes. *J Biol Chem.* (1997); 272(30):19059-19066.

Liu RM and Gaston Pravia KA. Oxidative stress and glutathione in TGF-beta-mediated fibrogenesis. *Free Radic Biol Med.* (2010); 48(1):1-15.

Liu X, Hu H and Yin JQ. Therapeutic strategies against TGF-beta signaling pathway in hepatic fibrosis. *Liver Int.* (2006); 26(1):8-22.

Mader CC, Oser M, Magalhaes MA, BravoCordero JJ, Condeelis J, Koleske AJ and Gil-Henn H. An EGFR-Src-Arg-cortactin pathway mediates functional maturation of invadopodia and breast cancer cell invasion. *Cancer*

Res.(2011); 71(5):1730-1741.

Mitropoulos D, Kiroudi A, Christelli E, Serafetinidis E, Zervas A, Anastasiou I and Dimopoulos C. Expression of transforming growth factor beta in renal cell carcinoma and matched non-involved renal tissue. *Urol. Res.* (2004); 32(5):317-322.

Motzer RJ, Escudier B, Gannon A and Figlin RA. Sunitinib: ten years of successful clinical use and study in advanced renal cell carcinoma. *Oncologist.* (2017); 22(1):41-52.

Naber HP, Wiercinska E, Ten Dijke P and van Laar T. Spheroid assay to measure TGF-β-induced invasion. *J Vis Exp.* (2011); (57):pii:3337.

Parsons M, Kessler E, Laurent GJ, Brown RA and Bishop JE. Mechanical load enhances procollagen processing in dermal fibroblasts by regulating levels of procollagen C-proteinase. *Exp Cell Res.* (1999); 252(2):319-331.

Payne SL, Fogelgren B, Hess AR, Seftor EA, Wiley EL, Fong SF, Csiszar K, Hendrix MJ and Kirschmann DA. Lysyl oxidase regulates breast cancer cell migration and adhesion through a hydrogen peroxide-mediated mechanism. *Cancer Res.* (2005); 65(24):11429-11436.

Perego R, Ron D and Kruh GD. Arg encodes a widely expressed 145 kDa protein-tyrosine kinase. *Oncogene.* (1991); 6(10):1899-1902.

Perego RA, Corizzato M, Bianchi C, Eroini B and Bosari S. N-and C-terminal isoforms of Arg quantified by Real-Time PCR are specifically expressed in human normal and neoplastic cells, in neoplastic cell lines, and in HL-60 cell differentiation. *Mol Carcinog*. (2005); 42(4):229-239.

Petejova N and Martinek A. Renal cell carcinoma: Review of etiology, pathophysiology and risk factors. *Biomed Pap Med*

Fac Univ Palacky Olomouc Czech Repub. (2016); 160(2):183-194.

Pickup M, Novitskiy S and Moses HL. The roles of TGFβ in the tumour microenvironment. *Nat Rev Cancer.* (2013); 13(11):788-799.

Raimondi A, Randon G, Sepe P, Claps M, Verzoni E, de Braud F and Procopio G. The evaluation of response to immunology in metastatic renal cell carcinoma: open challenges in the clinical practice. *Int J Mol Sci.* (2019); 20(17):pii:E4263.

Reynaud C, Ferreras L, Di Mauro P, Kan C, Croset M, Bonnelye E, Pez P, Thomas C, Aimond G, Kamoub AE, Brevet M and Clézardin P. Lysyl oxidase is a strong determinant of tumor cell colonization in bone. *Cancer Res.* (2017); 77(2):268-278.

Roy R, Polgar P, Wang Y, Goldstein RH, Taylor L and Kagan HM. Regulation of lysyl oxidase and cyclooxygenase expression in human lung fibroblasts: interactions among TGF-beta, IL-1beta and prostaglandin E. *J Cell Biochem.* (1996); 62(3):411-417.

Sethi A, Mao W, Wordinger RJ and Clark AF. Transforming growth factor-beta induces extracellular matrix protein cross-linking lysyl oxidase (LOX) genes in human trabecular meshwork cells. *Invest Ophthalmol Vis Sci.* (2011); 52(8):5240-5250.

Sethi A, Wordinger RJ and Clark AF. Gremlin utilizes canonical and non-canonical TGFβ signaling to induce lysyl oxidase (LOX) genes in human trabecular meshwork cells. *Exp Eye Res.* (2013); 113:117-127.

Sitaram RT, Mallikarjuna P, Landström M and Ljungberg B. Transforming growth factor-β promotes aggressiveness and invasion of clear cell renal cell carcinoma. *Oncotarget.*

(2016); 7(24):35917-35931.

Sjölund J, Boström AK, Lindgren D, Manna S, Moustakas A, Ljungberg B, Johansson M, Fredlund E and Axelson H. The notch and TGF-β signaling pathways contribute to the aggressiveness of clear cell renal cell carcinoma. *PLoS One.* (2011); 6(8):e23057.

Smith-Pearson PS, Greuber EK, Yogalingam G and Pendergast AM. Abl kinases are required for invadopodia formation and chemokine-induced invasion. *Journal of Biological Chemistry*. (2010); 285:40201-40211.

Song W, He D, Chen Y, Yeh CR, Hsu I, Huang Q, Zhang X, Chang LS, Zuo L, Chen J, Doersch KM, Chang C, Li L and Yeh S. Targeting newly identified ERβ/TGF-β1/SMAD3 signals with the FDA-approved anti-estrogen Faslodex or on ERβ selective antagonist in renal cell carcinoma. *Mol Oncol.* (2018); 12(12):2055-2071.

Sturrock A, Cahill B, Norman K, Huecksteadt TP, Hill K, Sanders K, Karwande SV, Stringham JC, Bull DA, Gleich M, Kennedy TP and Hoidal JR. Transforming growth factor-beta1 induces Nox4 NAD(P)H oxidase and reactive oxygen species-dependent proliferation in human pulmonary artery smooth muscle cells. *Am J Physiol Lung Cell Mol Physiol.* (2006); 290(4):L661-L673.

Tang Y, Wu X, Lei W, Pang L, Wan C, Shi Z, Zhao L, Nagy TR, Peng X, Hu J, Feng X, Van Hul W, Wan M and Cao X. TGF-beta1-induced migration of bone mesenchymal stem cells couples bone resorption with formation. *Nat Med.* (2009); 15(7):757-765.

Torsello B, Bianchi C, Meregalli C, Di Stefano V, Invernizzi L, De Marco S, Bovo G, Brivio R, Strada G, Bombelli S and Perego RA. Arg tyrosine kinase modulates TGF-β1 production in human renal tubular cells under high-glucose conditions. *J Cell Sci.* (2016); 129(15):2925-2936.

Torsello B, De Marco S, Bombelli S, Chisci E, Cassina V, Corti R, Bernasconi D, Giovannoni R, Bianchi C and Perego RA. The 1ALCTL and 1BLCTL isoforms of Arg/Abl2 induce fibroblast activation and extra cellular matrix remodelling differently. *Biol Open.* (2019); 8(3):1-9.

Trackman PC. Diverse biological functions of extracellular collagen processing enzymes. *J Cell Biochem.* (2005); 96(5):927-937.

Umer M, Mohib Y, Atif M and Nazim M. Skeletal metastasis in renal cell carcinoma: a review. *Ann Med Surg (Lond).* (2018); 27:9-16.

Voloshenyuk TG, Landesman ES, Khoutorova E, Hart AD and Gardner JD. Induction of cardiac fibroblast lysyl oxidase by TGF-β1 requires PI3K/Akt, Smad3, and MAPK signaling. *Cytokine.* (2011); 55(1):90-97.

Vuong L, Kotecha RR, Voss MH and Hakimi AA. Tumor microenvironment dynamics in clear-cell renal cell carcinoma. *Cancer Discov.* (2019); 9(10):1349-1357.

Xing QT, Qu CM and Wang G. Overexpression of Abl2 predicts poor prognosis in hepatocellular carcinomas and is associated with cancer cell migration and invasion. *Onco Targets Ther.* (2014); 7;881-885.

You W, Hong Y, He H, Huang X, Tao W, Liang X, Zhang Y and Li X. TGF-β mediates aortic smooth muscle cell senescence in Marfan syndrome. *Aging (Albany NY).* (2019); 11(11):3574-3584.

Chapter 5

Summary, Conclusions and Future Perpectives

Summary

The ccRCC is the most frequent malignant neoplasm of the kidney and despite the recent introduction of molecular therapies in clinical practice, it still remains a therapy-resistant tumor (Alonso AH, 2015). About 25-30% of clear cell Renal Cell Carcinoma (ccRCC) patients show an advanced stage of disease at the time of diagnosis, and about 30% of these patients have metastasis affecting bones (Umer M, 2018). An involvement of TGF-β1 in promoting ccRCC aggressiveness, invasion and bone metastasis has been described (Kominsky SL, 2007; Sitaram RT, 2016). We showed that even the extracellular matrix modifying enzyme lysyl oxidase (Lox) promotes cell migration and invasion and was overexpressed in ccRCC (Di Stefano V, 2016). In breast and colon cancer Lox has a key role in formation of premetastatic bone lesions through osteoclast activation and osteoblast inhibition (Cox TR, 2015; Reynaud C, 2017). We demonstrated that TGF-β1 production in human renal tubular cells was modulated by Arg tyrosine kinase (Torsello B, 2016), known to induce invasion and metastasis of breast and prostate cancer cells through cytoskeleton rearrangement (Beaty BT, 2013; Gil-Henn H, 2013). As described in chapter 3 (Torsello B, 2019), we have also evidenced a differential role of two Arg isoforms, 1ALCTL and 1BLCTL, in modulation of fibroblast activation, an important aspect of tumor microenvironment involved in tumor invasion

and progression. However, little is currently known about the molecular mechanism involved in ccRCC progression and bone metastasis formation. To shed light on these mechanisms is mandatory to identify candidate targets for novel molecular therapies that lower the risk of skeletal complications. Based on these premises, we investigated the existence of molecular interactions among TGF-β1, Lox and Arg in ccRCC cells and their functional involvement in the modulation of invasion and osteoblast and osteoclast behavior responsible for premetastatic bone lesion formation. This study has been performed using ccRCC cell line (786-O) and primary cell cultures established from normal renal cortex and ccRCC human samples. These primary cultures maintain, in the first passages, the phenotypic and molecular characteristics of the corresponding tissue (Perego RA, 2005; Bianchi C, 2010; Cifola I, 2011) and, as described in chapter 2 (Bianchi C, 2017) its metabolic profile. For this reason they represent a reproducible and well-characterized cellular model of ccRCC suitable for studying the molecular interactions among TGF-β1, Lox and Arg and for functional studies dealing with some aspects of ccRCC progression.

TGF-β1 treatment of ccRCC 786-O cell line upregulated Lox expression and secretion and even the expression of the Lox activating enzyme BMP1. The presence of TGF-β1-receptor inhibitor SB431542 reversed these effects suggesting that TGF-β1 and its signaling are involved in the modulation of

Lox production in 786-O ccRCC cells. The molecular link between TGF-β1 and Lox has been evidenced analyzing the level of these two targets, both upregulated in ccRCC compared to normal cortex primary cell cultures, and in ccRCC conditioned media in which we observed that TGF-β1 secretion is positively and significantly correlated with Lox. TGF-β1 stimulation of 786-O cells was associated with a significant decrease of Arg protein level but did not affect its transcript. Specific inhibition of the Smad-dependent TGF-β pathway by SIS3 and of proteasome activity by MG132 reversed the downregulation of Arg protein induced by TGF-β1, suggesting that this canonical TGF-β1 signalling was involved in modulation of Arg protein stability. The evaluation of the ubiquitination level of Arg after TGF-β1 treatment will probably confirm the involvement of TGF-β1 signaling in Arg protein stability.

We observed that Arg expression in ccRCC cells was downregulated by TGF-β1 stimulation but Arg silencing induced an increase of TGF-β1 and Lox secretion, reversed by SB431542 treatment, suggesting that Arg-dependent modulation of Lox production was mediated by TGF-β signaling activation. Overall, these data showed that in ccRCC cells Arg modulates Lox production by secretion of TGF-β1 that, in turn, modulates Arg protein stability through a Smad-dependent pathway. To investigate the role of the molecular interactions among TGF-β1, Lox and Arg on

ccRCC cell invasion, we used Arg silenced 786-O cells in an *in vitro* 3D invasion assay in a collagen matrix. Arg silencing decreased cell invasion in the presence of TGF-β1 treatment and TGF-β1 signalling inhibition with SB431542 reduced cell invasion in Arg silenced cells. These data suggested that Arg and TGF-β1 signalling were both important in ccRCC cell invasion induction. The evaluation of the effect of Lox inhibition by βAPN on the invasion ability of TGF-β1 treated 786-O cells will clarify the role of Lox overproduction induced by TGF-β1 stimulation on invasive behavior of control and Arg silenced 786-O cells. To investigate the role of the molecular interactions among TGF-β1, Lox and Arg on the formation of premetastatic bone lesions we analyzed the effect of ccRCC cell secretome on osteoblast proliferation and osteoclast activation.

Treatment with 786-O conditioned media (CM) inhibited MC3T3-E1 osteoblast proliferation and CM of TGF-β1 treated 786-O cells further inhibited this proliferation. Lox inhibitor βAPN partially reversed these effects suggesting that other molecules secreted by ccRCC cells may be responsible for the observed inhibition of osteoblast proliferation.

Moreover, 786-O conditioned media slightly increased the osteoclastic differentiation of RAW264.7 cells grown in the presence of the RANK-ligand. Treatment with βAPN efficiently reverted this CM dependent increment of

osteoclastogenesis, suggesting a key role of Lox secreted by ccRCC cells in osteoclastogenesis. However, the increment of Lox secretion induced by TGF-β1 in ccRCC cells did not improve the osteoclastogenesis induced by RANK-ligand, probably because TGF-β1 treatment increased the secretion by 786-O cells of Lox and of other molecules able to inhibit osteoclastogenesis and thus to counteract the effect of Lox increment. These preliminary data suggested that ccRCC conditioned media, inducing inhibition of osteoblast proliferation and a slight activation of osteoclastogenesis, might create an imbalance between bone formation and bone resorption that favours the development of premetastatic bone lesions.

Conclusion and application to translational medicine

Studies performed in different tumors evidenced that TGF-β1, Lox and Arg are involved in tumor progression and metastasis (Mitropoulos D, 2004; Kominsky SL, 2007; Cox TR, 2015; Reynaud C, 2017; Gil-Henn H, 2013; Di Stefano V, 2016; Torsello B, 2019). My PhD work, performed in *in vitro* models of ccRCC, has shown that Arg induced Lox production by secretion of TGF-β1 that in turn, modulates Arg protein stability through a Smad-dependent pathway. These complex interactions among TGF-β1, Lox and Arg are involved in modulation of ccRCC cell invasion and osteoblast and osteoclast behavior that favours the development of

premetastatic bone lesions. The definition of these complex molecular interactions among an intracellular protein with tyrosine kinase activity able to modulate cytoskeleton, such as Arg, and two secreted factors involved in extracellular matrix structure modulation, may help to shed light on the molecular mechanisms of ccRCC invasion and metastatization. In fact, metastatization is a complex systemic process that involves not only primary tumor cells, but also non-malignant cells residing in the tumor microenvironment, which provide an enormous repertoire of both soluble and insoluble signals facilitating the development of metastasis. In particular, it has been shown that the secreted factors (secretome) from tumor cells are able to modulate the behavior of host cells present in secondary organs in the absence of cancer cells. This leads to the remodeling of local environment creating permissive niches (premetastatic niches) that later cancer cells can colonize and thus, form metastasis (Cox TR, 2016). The identification and characterization of molecular interactions among TGF-β1, Lox and Arg and their functional effects on the metastatic process may also have a clinical relevance, providing molecular prognostic markers and targets for preventive therapeutic interventions. This is particularly important in ccRCC because, despite great progress in the treatment, its metastatic disease is not curable and treatment options remain palliative.

Future perspectives

Having shown that neither Smad-dependent nor PI3K/Akt-dependent TGF-β1 pathways are involved in TGF-β-dependent upregulation of Lox production in ccRCC cells, we will investigate the involvement of other non-canonical TGF-β1 pathways, such as the MAPK-dependent one, in this modulation. Moreover, the putative role of oxidative stress in Arg protein degradation induced by TGF-β1 treatment and upregulation of TGF-β1 secretion induced by Arg silencing will be investigated.

Using CRISP/CAS9 gene editing we are going to produce an Arg knockout ccRCC cell model to evaluate the specific role of the eight different Arg isoforms in TGF-β1 secretion.

Furthermore, we will complete the studies on the role of TGF-β1, Lox and Arg interactions on ccRCC progression:

1. evaluating the role of Lox overproduction induced by TGF-β1 stimulation on invasive behavior of Arg silenced 786-O cells by using Lox inhibition with βAPN;
2. analyzing the effects induced by CM of Arg silenced ccRCC cells on osteoblast and osteoclast behavior, in order to clarify the role of Arg-dependent modulation of ccRCC secretome and particularly of TGF-β1 and Lox secretion on premetastatic bone lesion formation.

Moreover, since modeling bone metastasis microenvironment with 3D cultures may be important to

develop anti-cancer strategies, we are going to use 3D collagen-based scaffold functionalized with hydroxyapatite (Liverani C, 2019) as a reliable 3D *in vitro* model for studying the role of TGF-β1, Lox and Arg interactions in pathogenesis of ccRCC bone metastasis.

References

Alonso AH, García MC and Enguita CG. Is there a role for systemic targeted therapy after surgical treatment for metastases of renal cell carcinoma? *World J Nephrol.* (2015); 4:254-262.

Beaty BT, Sharma VP, Bravo-Cordero JJ, Simpson MA, Eddy RJ, Koleske AJ and Condeelis J. B1 integrin regulates Arg to promote invadopodial maturation and matrix degradation. *Mol Biol Cell.* (2013); 24(11):1661-1675.

Bianchi C, Bombelli S, Raimondo F, Torsello B, Angeloni V, Ferrero S, Di Stefano V, Chinello C, Cifola I, Invernizzi L, Brambilla P, Magni F, Pitto M, Zanetti G, Mocarelli P and Perego RA. Primary cell cultures from human renal cortex and renal-cell carcinoma evidence a differential expression of two spliced isoforms of Annexin A3. *Am J Pathol.* (2010); 176(4):1660-1670.

Bianchi C, Meregalli C, Bombelli S, Di Stefano V, Salerno F, Torsello B, De Marco S, Bovo G, Cifola I, Mangano E, Battaglia C, Strada G, Lucarelli G, Weiss RH and Perego RA. The glucose and lipid metabolism reprogramming is grade-dependent in clear cell renal cell carcinoma primary cultures and is targetable to modulate cell viability and proliferation. *Oncotarget.* (2017); 8(69):113502-113515.

Cifola I, Bianchi C, Mangano E, Bombelli S, Frascati F, Fasoli E, Ferrero S, Di Stefano V, Zipeto MA, Magni F, Signorini S, Battaglia C and Perego RA. Renal cell carcinoma primary cultures maintain genomic and phenotypic profile of parental tumor tissues. *BMC Cancer.* (2011); 11:244.

Cox TR, Rumney RM, Schoof EM, Perryman L, Hoye AM, Agrawal A, Bird D, Latif NA, Forrest H, Evans HR, Huggins ID, Lang G, Linding R, Gartland A and Erler JT. The hypoxic cancer secretome induces pre-metastatic bone lesions

through lysyl oxidase. *Nature.* (2015); 522(7554):106-110.

Cox TR, Gartland A and Erler JT. Lysyl oxidase, a targetable secreted molecule involved in cancer metastasis. *Cancer Res.* (2016); 76(2):188-192.

Di Stefano V, Torsello B, Bianchi C, Cifola I, Mangano E, Bovo G, Cassina V, De Marco S, Corti R, Meregalli C, Bombelli S, Viganò P, Battaglia C, Strada G and Perego RA. Major action of endogenous lysyl oxidase in clear cell renal cell carcinoma progression and collagen stiffness revealed by primary cell cultures. *AM J Pathol.* (2016); 186(9):2473-2485.

Gil-Henn H, Patsialou A, Wang Y, Warren MS, Condeelis JS and Koleske AJ. Arg/Abl2 promotes invasion and attenuates proliferation of breast cancer in vivo. *Oncogene*. (2013); 32(21): 2622-2630.

Kominsky SL, Doucet M, Brady K and Weber KL. TGF-beta promotes the establishment of renal cell carcinoma bone metastasis. *J Bone Miner Res.* (2007); 22(1):37-44.

Liverani C, De Vita A, Minardi S, Kang Y, Mercatali L, Amadori D, Bongiovanni A, La Manna F, Ibrahim T and Tasciotti E. A biomimetic 3D model of hipoxia-driven cancer progression. *Sci Rep.* (2019); 9(1):12263.

Mitropoulos D, Kiroudi A, Christelli E, Serafetinidis E, Zervas A, Anastasiou I and Dimopoulos C. Expression of transforming growth factor beta in renal cell carcinoma and matched non-involved renal tissue. *Urol. Res.* (2004); 32(5):317-322.

Perego RA, Corizzato M, Bianchi C, Eroini B and Bosari S. N-and C-terminal isoforms of Arg quantified by Real-Time PCR are specifically expressed in human normal and neoplastic cells, in neoplastic cell lines, and in HL-60 cell differentiation. *Mol Carcinog*. (2005); 42(4):229-239.

Reynaud C, Ferreras L, Di Mauro P, Kan C, Croset M, Bonnelye E, Pez P, Thomas C, Aimond G, Kamoub AE, Brevet M and Clézardin P. Lysyl oxidase is a strong determinant of tumor cell colonization in bone. *Cancer Res.* (2017); 77(2):268-278.

Sitaram RT, Mallikarjuna P, Landström M and Ljungberg B. Transforming growth factor-β promotes aggressiveness and invasion of clear cell renal cell carcinoma. *Oncotarget.* (2016); 7(24):35917-35931.

Torsello B, Bianchi C, Meregalli C, Di Stefano V, Invernizzi L, De Marco S, Bovo G, Brivio R, Strada G, Bombelli S and Perego RA. Arg tyrosine kinase modulates TGF-β1 production in human renal tubular cells under high-glucose conditions. *J Cell Sci.* (2016); 129(15):2925-2936.

Torsello B, De Marco S, Bombelli S, Chisci E, Cassina V, Corti R, Bernasconi D, Giovannoni R, Bianchi C and Perego RA. The 1ALCTL and 1BLCTL isoforms of Arg/Abl2 induce fibroblast activation and extra cellular matrix remodelling differently. *Biol Open.* (2019); 8(3):1-9.

Umer M, Mohib Y, Atif M and Nazim M. Skeletal metastasis in renal cell carcinoma: a review. *Ann Med Surg (Lond).* (2018); 27:9-16.

Publications

1. Barbara Torsello, Cristina Bianchi, Chiara Meregalli, Vitalba Di Stefano, Lara Invernizzi, **Sofia De Marco**, Giorgio Bovo, Rinaldo Brivio, Guido Strada, Silvia Bombelli and Roberto A. Perego.
   "Arg tyrosine kinase modulates TGF-β1 production in human renal tubular cells under high-glucose conditions".
   J Cell Sci. (2016); 129(15):2925-2936.
   doi: 10.1242/jcs.183640.

2. Vitalba Di Stefano, Barbara Torsello, Cristina Bianchi, Ingrid Cifola, Eleonora Mangano, Giorgio Bovo, Valeria Cassina, **Sofia De Marco**, Roberta Corti, Chiara Meregalli, Silvia Bombelli, Paolo Viganò, Cristina Battaglia, Guido Strada and Roberto A. Perego.
   "Major action of endogenous lysyl oxidase in clear cell renal cell carcinoma progression and collagen stiffness revealed by primary cell cultures".
   Am J Pathol. (2016); 186(9):2473-2485.
   doi: 10.1016/j.ajpath.2016.05.019.

3. Bianchi Cristina, Meregalli Chiara, Bombelli Silvia, Di Stefano Vitalba, Salerno Francesco, Torsello Barbara, **De Marco Sofia**, Bovo Giorgio, Cifola Ingrid, Mangano Eleonora, Battaglia Cristina, Strada Guido, Lucarelli Giuseppe, Weiss Robert H and Perego Roberto A.
   “The glucose and lipid metabolism reprogramming is grade-dependent in clear cell renal cell carcinoma primary cultures and is targetable to modulate cell viability and proliferation”.
   Oncotarget. (2017); 8(69):113502-113515.
   doi: 10.18632/oncotarget.23056.

4. Silvia Bombelli, Chiara Meregalli, Carla Scalia, Giorgio Bovo, Barbara Torsello, **Sofia De Marco**, Massimiliano Cadamuro, Paolo Viganò, Guido Strada, Giorgio Cattoretti, Cristina Bianchi and Roberto A. Perego.
   "Nephrosphere-derived cells are induced to multilineage differentiation when cultured on human decellularized kidney scaffolds".
   Am J Pathol. (2018); 188(1):184-195.
   doi: 10.1016/j.ajpath.2017.09.012.

5. Barbara Torsello, **Sofia De Marco**, Silvia Bombelli, Elisa Chisci, Valeria Cassina, Roberta Corti, Davide Bernasconi, Roberto Giovannoni, Cristina Bianchi, and Roberto A Perego.
   "The 1ALCTL and 1BLCTL isoforms of Arg/Abl2 induce fibroblast activation and extra cellular matrix remodelling differently".
   Biol Open (2019); 8(3):1-9.
   doi: 10.1242/bio.038554.